2006

Wheel loader powertrain modeling for real-time vehicle dynamic simulation

Matthew Michael Tinker
University of Iowa

WHEEL LOADER POWERTRAIN MODELING FOR REAL-TIME VEHICLE DYNAMIC SIMULATION

by

Matthew Michael Tinker

A thesis submitted in partial fulfillment
of the requirements for the Master of
Science degree in Mechanical Engineering
in the Graduate College of
The University of Iowa

July 2006

Thesis Supervisor: Professor Lea-Der Chen

Graduate College
The University of Iowa
Iowa City, Iowa

CERTIFICATE OF APPROVAL

_____

MASTER'S THESIS

_____

This is to certify that the Master's thesis of

Matthew Michael Tinker

has been approved by the Examining Committee
for the thesis requirement for the Master of Science
degree in Mechanical Engineering at the July 2006 graduation.

Thesis Committee: _____
Lea-Der Chen, Thesis Supervisor

_____
Weidong Pan

_____
Shaoping Xiao

ACKNOWLEDGMENTS

I would like to thank my advisor, Professor Lea-Der Chen, for giving me the opportunity to carry out this research.

This research would not have been possible without financial support from Caterpillar Incorporated, and intellectual support from both Caterpillar engineers and the researchers at National Advanced Driving Simulator (NADS). I would particularly like to thank Rob Vail from Caterpillar and Weidong Pan from the NADS for their guidance.

I would like to thank the engineers and researchers who have developed the dynamic software for the National Advanced Driving Simulator. This research is an extension of their work, and could not have been carried out without their efforts.

Finally, I would like to thank my Parents for their support during my college years and God for giving meaning to my time.

TABLE OF CONTENTS

LIST OF TABLES

Table

LIST OF FIGURES

Figure

CHAPTER 1

INTRODUCTION

1.1 Purpose

This thesis documents the development of the engine, powertrain, and braking portion of a computer based dynamic model of the Caterpillar 980G Series II Medium Wheel Loader (980G SII MWL). The purpose of the vehicle model is to facilitate the realistic motion, visual, and audio simulation of the 980G SII MWL operator environment in the National Advanced Driving Simulator (NADS). The potential use of the NADS as an operator in the loop virtual prototyping tool motivated this project.

1.2 Background

1.2.1 Motivation for Virtual Prototyping

Virtual prototyping is the practice of modeling and testing a device in a virtual environment. When a manned vehicle is the device being designed, the operator-machine interaction must be considered. A driving simulator is a tool that allows operators to drive a vehicle in a virtual environment. Because less time and money are required to build a computer based model of a machine than to build a physical prototype, operator related design problems can be addressed earlier in the design process. This reduces the cost and time required to design a new machine.

1.2.2 Project Goals and Thesis Goals

The value of a driving simulator as a virtual prototyping tool is based on the idea that a person driving the simulator will feel as though they were driving the actual machine. For a driver to perceive a simulation is realistic, they must receive motion, visual, and audio sensory cues that are realistic in nature. The cues must also accurately represent the vehicle being evaluated. Two things are required for a driving simulation to be realistic. First, the simulator must be capable of reproducing realistic motion, visual,

and audio cues. Second, some logic must be in place that tells the physical parts of the simulator—the motors, hydraulic cylinders, projectors, speakers, etc.—what signals they should be sending.

The primary goal of the 980G SII project is to demonstrate the physical capabilities of the NADS. The results from this demonstration will be used to evaluate the NADS potential as virtual prototyping tool for future projects. The goal of this thesis is to develop some of the logical aspects of the simulation—the 980G SII engine, powertrain, and brake models—which are required for the evaluation to take place.

1.2.3 Driving Simulator Operation

This section describes how the physical and virtual parts of the NADS work together to simulate a driving maneuver. The physical components are shown in Figure 1 [1]. The interaction between the driver, the physical simulator components, and virtual components is shown in Figure 2.

The operation of the simulator may be thought of as a loop, beginning and ending with the driver. The driver is seated in a cab inside a large, movable, dome. A driving scene is projected on the inner walls of the dome, and speakers are present inside the dome.

Figure 1. National Advanced Driving Simulator [1]

The driver is asked to perform a task, and moves the controls—steering wheel, brake pedal, accelerator pedal, etc.—to elicit a response from the "vehicle." The positions of the controls are sent to the computer based vehicle model. These control inputs are used by the vehicle model to calculate the state of the vehicle at the next instant in time. The motion, visual, and sound system of the simulator then are updated to reflect the current state of the vehicle as would be perceived by the driver. The decisions made by the driver in terms of how to actuate the controls at the next instant in time are influenced by the simulated vehicle feedback. The simulation loop continues forward in time, repeating hundreds of times each second, until the driving task is completed.

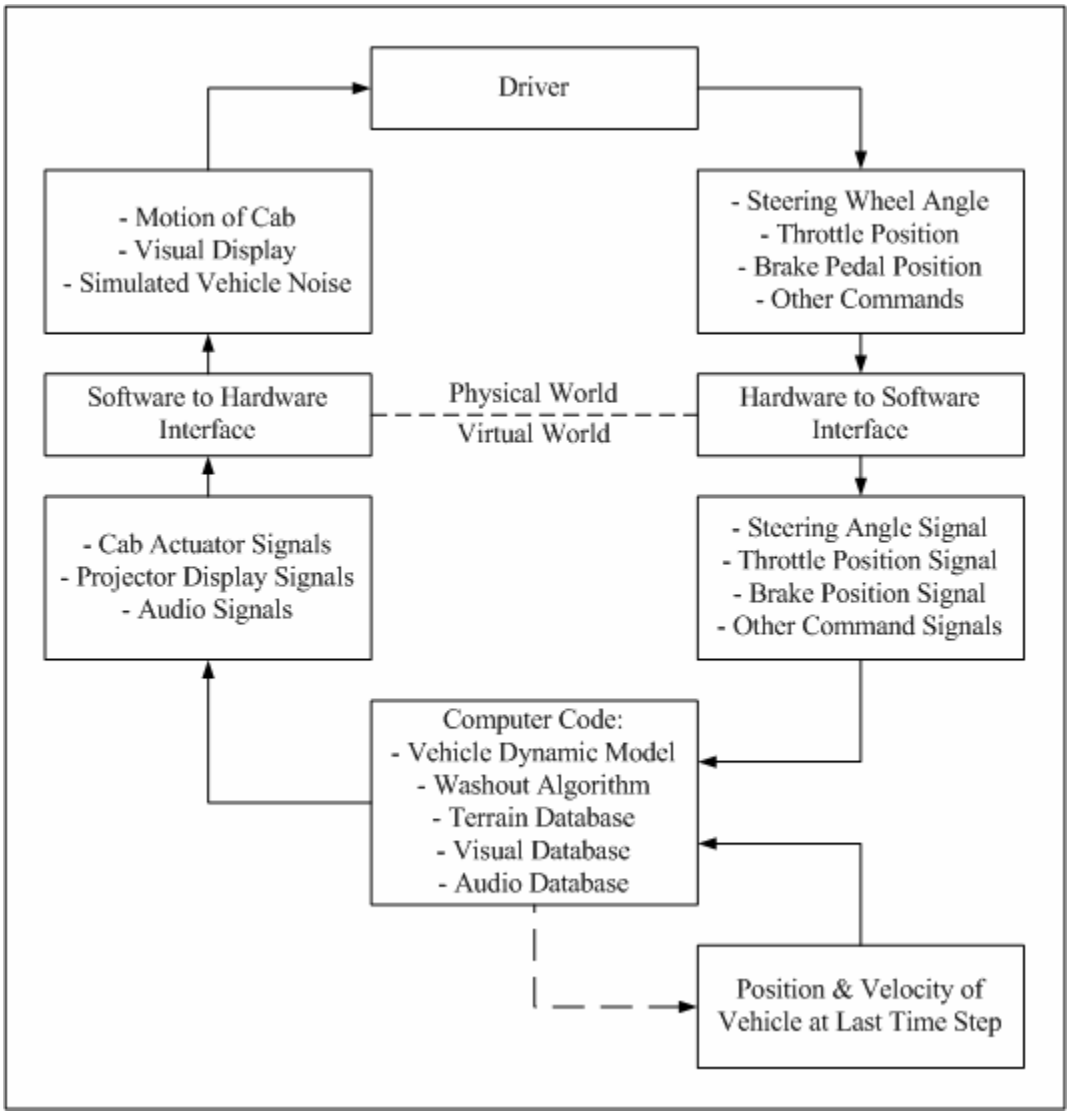

Figure 2. Driving Simulator Operation

1.3 Modeling Considerations

The models discussed in this report will be judged primarily on their ability to reliably simulate the motion of the 980G SII MWL. From a practical standpoint, the models should be accurate enough that any further increase in accuracy will not be perceptible to the operator residing in the NADS dome. One limitation placed on the models is that they must be solvable in real time. Generally speaking, the time required to

solve the models increases with the complexity of the models. It is not feasible to allocate a certain amount of processor time to each vehicle sub-system model, nor is the solution of the models the only function which takes processor time. Thus, the general practice adopted when modeling for real time simulation is to only include as much fidelity as is needed to realistically calculate the desired output.

Other limiting factors are lack of available vehicle subsystem models which are suited for real time simulation, or if suitable models are available, lack of data required to implement the models. In either case there is a cost/benefit relationship associated with the time and effort required to develop alternative modeling techniques. The objective taken in modeling the 980G SII MWL powertrain was to create/implement models which will lead to the most accurately simulated cab motion, subject to the limitations of real-time solvability, availability of data, and new model development time vs. project deadline.

1.4 Outline

Chapter 2 provides an overview of the engine, powertrain, and braking system models. Chapters 3 and 4 discuss the engine and torque converter models. Both of these chapters have the same format. They begin with an overview of how the real system works. Then different methods which have been used to model the system are described. A method is selected and the model is detailed.

Chapters 5 through 7 are focused on the transmission model. Chapter 5 gives a short description of how the transmission operates, and discusses the motivation for creating a new model. Chapter 6 is focused on the dynamic aspects of the transmission model. Chapter 7 describes the clutch model.

A new approximate transfer case model is developed in Chapter 8, which allows a locked transfer case to be modeled in a robust manner using estimated data. Chapter 9

describes the relatively straightforward models used for the differentials, final drives, service brakes, and parking brake.

Chapter 10 compares the simulated vehicle behavior with test data recorded from the actual machine. Chapter 11 gives a summary of the results, assessment of the models, and recommendations for future work.

CHAPTER 2

SYSTEM OVERVIEW

2.1 Engine, Powertrain, and Braking Systems

This chapter gives an overview of the engine, powertrain, and braking system models used in the 980G SII MWL vehicle model. On the actual machine these systems work to generate, transmit, and control the amount of torque applied to the vehicle's wheels. The engine produces torque through the combustion of a fuel air mixture. Some of this torque is used to drive pumps for the hydraulic system, some is used to power engine accessories, and the rest is transmitted through the powertrain to the wheels. Using the most exclusive definition, a powertrain consists of the torque transmitting elements between the engine and wheels. In the case of the 980G SII MWL, the powertrain then includes the torque converter, the transmission, a transfer case, front and rear drive shafts, front and rear differentials, front and rear sets of axle shafts, and four final drive gears sets – one for each wheel. The purpose of the powertrain is to decouple the engine rotation from the vehicle's wheels, vary the direction and magnitude of the torque transmitted by the engine to the wheels, and distribute the torque to the wheels. The 980G SII MWL uses one service brake per wheel, each mounted inboard of the final drive gear set. It is also equipped with an auxiliary parking brake.

2.2 Engine, Powertrain, and Brake Model Overview

The primary function of the engine, powertrain, and brake model is to calculate the wheel torque. Figure 3 shows the individual subsystem models which compose the engine, powertrain and brake system models. Chapters 3 through 9 describe these subsystem models in depth. It is informative to look at how these models interact before examining each one in detail.

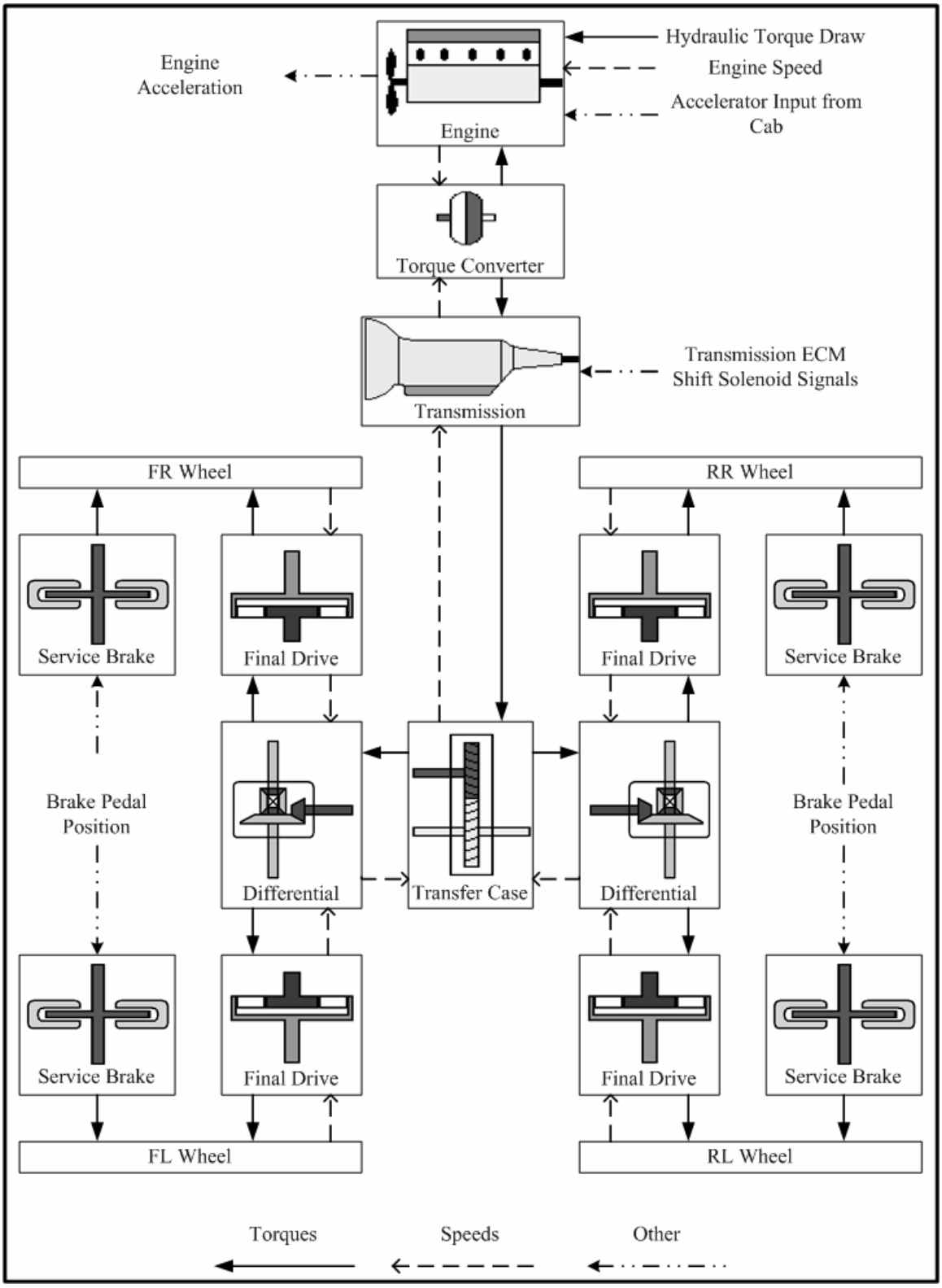

Figure 3. Engine, Powertrain, and Brake Model Internal Structure

The torque converter model is the central element in the engine and powertrain structure. It receives speed values and returns torque values. The engine and final drives may be thought of as two opposing ends of the powertrain. At the beginning of each time step the speeds at the "ends" are known, and by the end of the time step the toques at the "ends" will need to have been determined. Thus data flows in a "speed" path from the engine to the torque converter, and a separate "speed" path from the final drives to the torque converter. These speed paths meet at the torque converter, and follow "torque" paths back to their origins. There is a short forward and return path beginning and ending with the engine, and a longer forward and return path beginning and ending at the final drives.

The engine's crankshaft speed is input to the engine model from the integration code. It is equal to the torque converter impeller speed. The torque converter model accepts the turbine and impeller speeds, and returns the torque acting at the turbine and impeller. The impeller torque is applied to the engine`s crankshaft, representing the torque absorbed to propel the vehicle. The engine model sums this torque with the other torques acting on the engine. The torque required to power the hydraulic pumps is calculated by the hydraulic model. The torque required to by the engine accessories is calculated in the engine model. The engine torque produced from combustion is formulated using an engine map. The combustion torque is a function of engine speed and a fuel rack input—which reflects the operator's actuation of the accelerator pedal. The total torque acting on the engine is divided by the mean effective inertia of the rotating assembly to yield the engine's angular acceleration. This acceleration is then passed out to the integrator, which will calculate the engine speed at the next time step.

The other speed/torque path begins at the final drives, goes though powertrain to the torque converter, then returns back through the powertrain to the final drives. The wheel speeds are input from the vehicle dynamic model. These are used to calculate the speeds of the solidly connected driveline members using algebraic equations, up to the

transmission. When the transmission is not shifting, an algebraic equation is used to relate the transmission output shaft speed to the input shaft speed, which is identical to the torque converter turbine speed. The turbine torque is passed back through the transmission model. When the transmission is in gear, the output shaft torque is an algebraic function of the turbine torque, with some efficiency losses. The transmission output shaft torque is then passed back through the remaining powertrain models to the wheels.

The brake model does not interact with the other models presented in this paper, and communicates only with the wheel models and the brake signal from the vehicle cab. If the driver is activating the brakes, the maximum available brake torque is passed to the wheel models, separate from the powertrain torque originating from the engine.

CHAPTER 3

ENGINE

3.1 Engine Operation

The 980G SII MWL is equipped with a six cylinder 14.6 liter turbocharged compression ignition engine. The engine operates using a four stroke process, represented in Figure 4 [2]. Filtered air is compressed by the turbocharger's impeller and passed through an intercooler before it enters the intake manifold. During the intake stroke the piston moves down the cylinder, drawing in air from the intake manifold through the intake valve. After the piston reaches the bottom dead center, it begins to move up the cylinder for the compression stroke. The intake valve will close slightly after the piston begins to move upward. As the piston nears top dead center, fuel is injected into the cylinder. The elevated temperature and pressure of the compressed air cause the fuel-air mixture to ignite and burn, further increasing the pressure and temperature in the cylinder. The high pressure forces the piston downward during the power stroke. The force exerted on the piston is transferred to the crankshaft through the connecting rod. This force causes a torque on the crankshaft due to the offset connection between the connecting rod and the crankshaft's center of rotation. Once the piston has reached bottom dead center, it begins to travel upward for the exhaust stroke. The exhaust valve opens allowing the burned gasses to leave the cylinder. The exhaust gasses leaving the cylinder are routed through the turbocharger's turbine, and the torque exerted on the turbine from the exhaust is used to power the turbocharger's impeller. The amount of power which is produced in a compression ignition engine is controlled by the amount of fuel which is delivered. The maximum amount of fuel which is delivered for a certain accelerator position is regulated by the fuel governor.

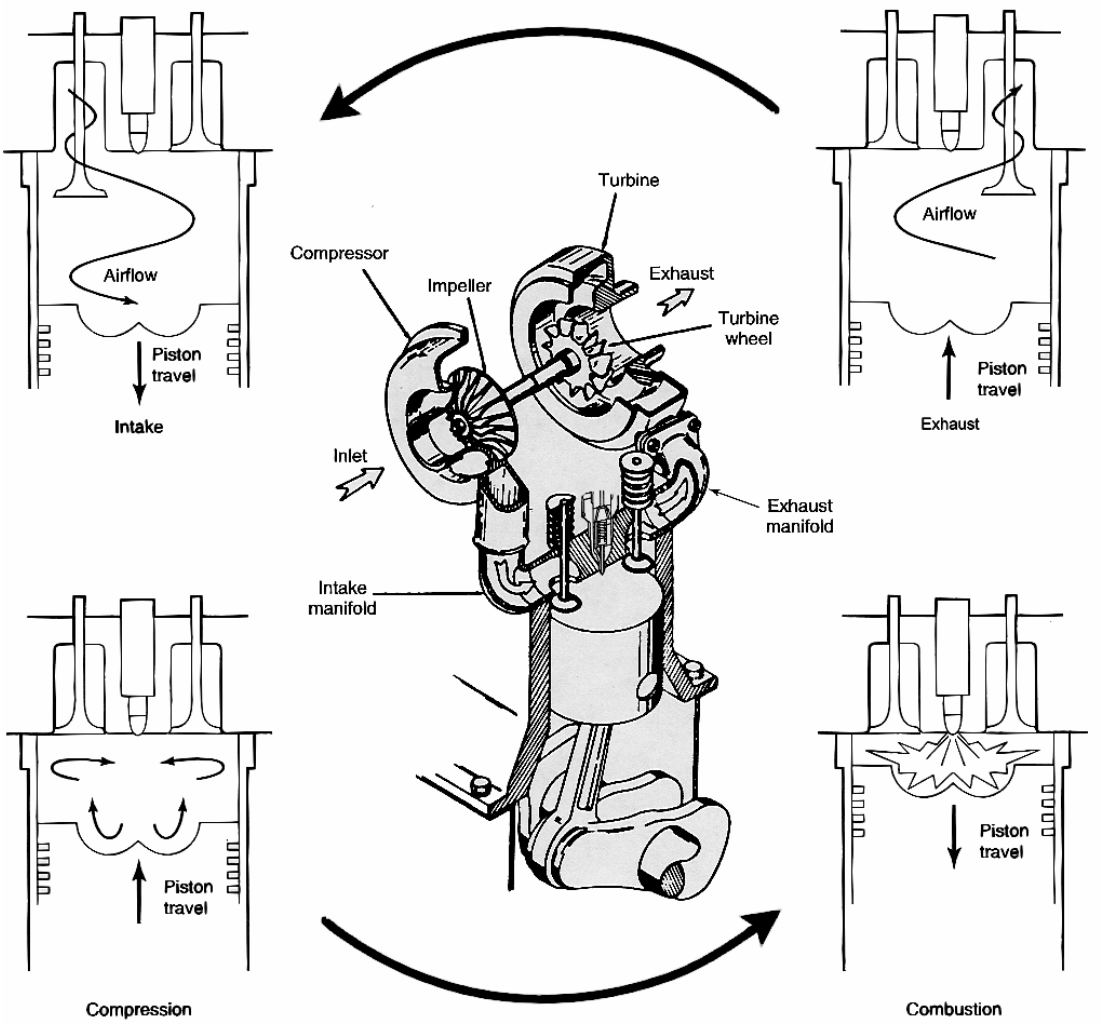

Figure 4. Representation of Four Stroke Turbocharged CI Engine Cycle [2]

3.2 Engine Modeling Methods

Engine models vary in fidelity and may be theoretically based, empirically based or some combination of the two. The physical processes that take place in an engine are quite complex. Due to this complexity, engine models which rely heavily on theory are limited in scope for practical reasons. Engine models used in vehicle dynamic simulations are usually based more on empirical data.

Assanis and researchers [3] have combined empirical data with physical relationships in order to create a library of parametric engine component models. Because individual components, such as cylinders, are modeled separately, various engine configurations can be tested. This method of modeling could be used for parametric studies or when empirical data is not available. If empirical engine torque measurements are available, a mean torque model can be used. The basic mean torque model uses an engine map to relate the combustion torque to engine speed and fuel rack position, and a constant inertia to represent the rotating assembly. This type of model neglects transient aspects of engine operation, but has been found adequate in a number of vehicle dynamic simulation studies [4, 5].

Variations of this model are formed by including torque correction factors based on the calculations of engine component models. This is done for two reasons. One is to increase the realism of the model by including transient or other effects which are not accounted for with the steady state torque data. Ciesla and Jennings [6] added a correction factor based on the difference between the instantaneous equivalence ratio and the expected steady state equivalence ratio. The instantaneous equivalence ratio is influenced by the turbocharger, intercooler, intake manifold and exhaust manifold models. Lags in response are accounted for by applying this correction factor to the steady state combustion torque from the engine map. Past vehicle models validated for use in the NADS have augmented the mean torque model with a first order time lag on the fuel rack or throttle input to account for fuel system lags and possibly induction delay.

Another reason for including additional component models is to study particular engine or drive train behavior. Tsangarides and Tobler [7] augmented measured steady state torque data with considerations for torque variations due to individual cylinder pressure fluctuations and inertial torque due to the reciprocating piston mass. This was done for the purpose of studying torque converter damping characteristics. Spark Ignition (SI) engine models for control studies include correction factors which account for

air/fuel ratio, idle air control valve operation, exhaust gas recirculation valve operation, spark timing, and various other factors influenced by the control strategy. These factors need to be included for the model to serve its intended purpose, and do not necessarily increase the accuracy of the model.

3.3 Engine Model

3.3.1 Engine Model Discussion

An engine map was used to model the torque production along with a first order time lag to account for fuel system delays. This type of model has been used successfully and validated in the NADS simulation environment.

The benefit of using an engine map is that the low frequency torque can be captured with good accuracy and minimal complexity. One limitation is high frequency torque pulsations are not captured. However, excluding these should not be directly or indirectly (through their effect on other vehicle subsystem models) noticeable to the driving simulator operator. Another limitation of using an engine map, which is a limitation common to all empirical models, is that the model cannot be used to gauge the effect of changing engine parameters. However, the purpose of this present study is to simulate a stock 980G, not to compare different engine designs. Thus, an engine map based model is adequate for the present study.

The benefit of using a set time lag to account for transient engine operation is that it is simple and does not required additional data. The time lag is set based on measured vehicle test data. This lag is applied to the accelerator pedal position and serves partly to simulate fuel system delays and partly to filter the pedal position signal. It does not address turbo lag, as such a lag would be based on engine speed, not accelerator pedal position.

3.3.2 Engine Model Formulation

The engine torque production at a given fuel rack position and steady state engine speed is found by interpolating the data in the engine map table*. The torque values found in an engine map are measured from actual engine tests. They implicitly include intake and exhaust pumping losses, mechanical friction losses, thermal losses, etc. Typically the engine accessories—fan, alternator, etc.—are not installed when the engine is tested, so the torque loss from powering these components must be considered separately. The engine map torque is formulated as shown in Equation 1 [8]:

$$T_{E\_Map} = f_{Int}[\dot{\theta}_E, FR_{Map}, EngMap] \tag{1}$$

where T_{E_Map} is the engine map torque, f_{Int} is an interpolation function, $\dot{\theta}_E$ is the engine speed, FR_{Map} is the delayed fuel rack position, and $EngMap$ is a three dimensional array of constant values, which contains the engine torque measured at specific engine speed and per cent fuel rack positions. The accessory torque is formulated as shown in Equation 2, which is similar to the standard NADS formula [8]:

$$T_{E\_Acc} = c_{Acc\_1} + c_{Acc\_2}\dot{\theta}_E + c_{Acc\_3}\dot{\theta}_E^2 + f[\dot{\theta}_E, OtherVars] \tag{2}$$

where c_{Acc_1}, c_{Acc_2}, c_{Acc_3} are constant values, and the term $f[\dot{\theta}_E, OtherVars]$ is included to account for any accessory torques which are not functions of engine speed alone. In the present model only the first two terms are used. The accelerator delay is formulated with a first order time lag using the Equation 3 [8]:

$$\frac{d}{dt}FR_{Map} = \frac{FR_{Acc} - FR_{Map}}{t_{FR}} \tag{3}$$

where FR_{Acc} is the fuel rack position corresponding to the immediate accelerator pedal position and t_{FR} is the first order time lag constant. This equation is integrated to get the fuel rack value used in the engine map interpolation. The future speed of the engine is

* Torque curves and a governor model may also be used to achieve the same outcome.

found by taking the time integral of the engine's current acceleration. The current engine acceleration is formulated using Newton's second law applied to rotational motion. All the torques acting on the engine's rotating assembly are collected and divided by the mean effective inertia of the engine's rotating assembly to yield the acceleration. The engine acceleration is formulated as shown in Equation 4 [8]:

$$\ddot{\theta}_E = \frac{T_{E\_net}}{J_E} \tag{4}$$

In the above equation $\ddot{\theta}_E$ is the engine acceleration, J_E is the mean effective inertia of the rotating assembly, and T_{E_net} is the net torque acting on the rotating assembly, which is calculated by Equation 5 (similar to the formula given in [8]):

$$T_{E\_net} = T_{E\_Map} - T_{TC\_I} - T_{E\_Acc} - T_{E\_Hyd} \tag{5}$$

where T_{TC_I} is the torque absorbed from the torque converter impeller, which may be thought of as the torque supplied to drive the vehicle, and T_{E_Hyd} is the torque draw on the engine from the hydraulic pumps.

CHAPTER 4

TORQUE CONVERTER

4.1 Torque Converter Operation

The torque converter functions a damper, a torque transmission device, and a torque multiplication device. Figure 5 below [9] shows a representation of a three element (turbine, impeller, and reactor or stator) torque converter. The impeller element is connected to the engine crankshaft. The turbine is connected to the transmission input shaft, and the stator (or reactor) is connected to the transmission housing with a one way clutch.

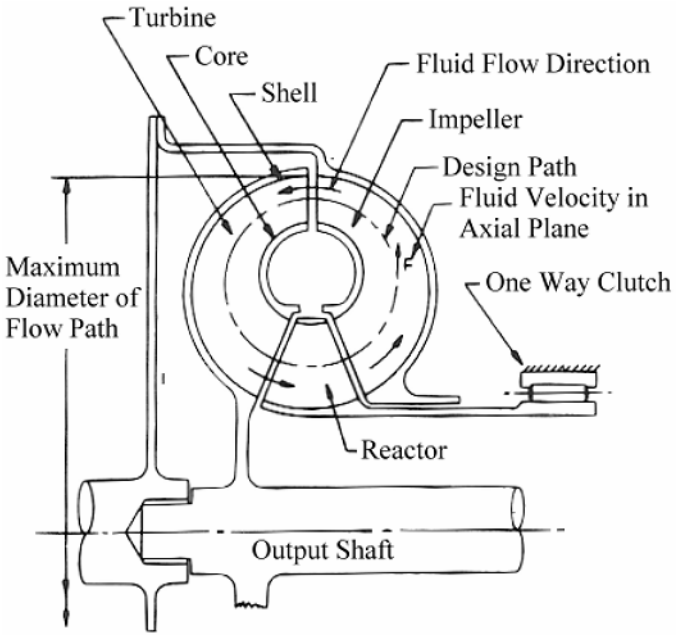

Figure 5. Torque Converter Side View [9]

Torque converter operation is summarized as follows. When the impeller is turning faster than the turbine, for instance when the vehicle is accelerated from a stationary position, the centrifugal force of the fluid turning under the influence of the impeller will cause the pressure at the outer radius of the impeller to be greater than the pressure at the outer radius of the turbine. This results in flow from the impeller to the turbine at the outer radius of their interface. The fluid will have gained momentum as it traveled outward through the impeller, since its absolute velocity increases as it travels away from the axis of rotation. The momentum imparted on the fluid as it travels through the impeller is analogous to the engine torque absorbed by the torque converter. The fluid exiting the impeller enters the turbine and moves radially inward through the turbine. Its velocity and thus momentum are decreased in the process. The momentum lost by the fluid is imparted on the blades of the turbine and is analogous to the torque sent to the transmission input shaft.

The fluid then passes from the turbine to the stator. When the stator's one way clutch is locked, the stator redirects the flow path between the turbine and impeller, imparting a greater net momentum on the turbine element. In this case, the torque supplied to the transmission is greater than the torque absorbed from the engine. The additional torque is equal to the reaction torque which holds the stator`s one way clutch fixed. In cases when the stator is freewheeling, the turbine and impeller torque relationship is near 1:1, with some deviation due to leakage, stator clutch drag, and other losses.

The torque converter is overrun when the turbine is turning faster than the impeller, causing a reversal in the aforementioned flow direction. In this instance the vehicle is transmitting torque to the engine. If the stator is freewheeling, the torque transmitted from the turbine to the impeller will again be near 1:1, but typically the converter will experience greater losses when overrunning since the element blade angles are optimized for flow in the other direction.

4.2 Torque Converter Modeling Methods

4.2.1 Overview of Torque Converter Models

The primary purpose of the torque converter model in the current project is to provide input and output torque and speed relationships. There are a number of torque converter models in use, ranging in complexity and application. Computational Fluid Dynamics (CFD) software has been used to model toque converters for design and analysis purposes [10]. These models are complex and are not practical for real time simulation. Less complicated "dynamic" torque converter models use a differential equation for each torque converter element and one also to account for the inertia of the working fluid. The more computationally intensive equations, such as those characterizing fluid frictional and shock losses, are simplified using empirical relations. Static torque converter models are the least complex. They function by extrapolating empirical data to cover the entire range of torque converter operation. Both a dynamic model and static model were investigated for use in this project.

4.2.2 Static Torque Converter Model

The steady state performance of a particular torque converter is a function of four variables; input speed, output speed, input torque, output torque [11]. The performance is typically represented using the following Equations 6-8 [11]:

$$SR = \frac{\omega_{Out}}{\omega_{In}} \tag{6}$$

$$TR = \frac{T_{Out}}{T_{In}} \tag{7}$$

$$K = \frac{\omega}{\sqrt{T}} \tag{8}$$

where SR is the speed ratio, ω_{Out} is the output speed, ω_{In} is the input speed, TR is the torque ratio, T_{Out} is the output torque, T_{In} is the input torque, and K is the capacity

factor, which can be expressed in terms of either the input or output values. A description of the capacity factor is as follows, "The K factor is a parameter representing the relationship of torque and speed for a converter of a particular size and blading…It is useful for the expeditious computation of converter performance for different torque and speed conditions and can be used for either input or output conditions." [11]

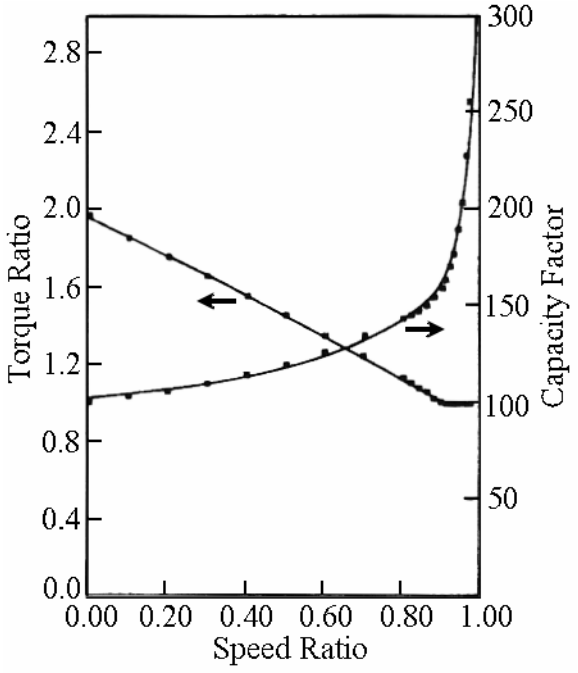

Figure 6. Torque Converter Steady State Performance [12]

Static models usually are based on Equations 6-8, using the input capacity factor for Equation 8. Data for the torque ratio and input capacity factor as functions of speed ratio are found from test results specific to the torque converter which is to be modeled, for example, as illustrated in Figure 6 [12]. The benefit of organizing the equations in

terms of the speed ratio, torque ratio, and input capacity factors is that the performance is generally found to be independent of the individual speeds and loads [12]. Torque converter modelers have used polynomial fits or lookup tables to reference the test data.

4.2.3 Dynamic Torque Converter Model

The dynamic torque converter model investigated for this study was presented in detail by Hrovat and Tobler [13]. A full discussion of this model is beyond the scope of this thesis. The model is given in Appendix A for reference, and a brief discussion of model's principles is included there. The model may be summarized as follows:

> During operation above the coupling point, the present torque converter model contains four energy storage elements characterized by the fluid inertia and by the impeller, turbine and stator mechanical inertia. As a consequence, the torque converter dynamics are described by four first-order nonlinear differential equations in four state variables. These state variables are the velocities corresponding to each of the above inertias. The three equations for the mechanical inertias follow from the application of the moment-of-momentum equation, whereas the equation corresponding to the fluid inertia will be obtained from the power balance for the torque converter system. For operation below the coupling point, only three first order differential equations will result since the stator is held identically zero by the action of a one-way clutch. [13]

One of the problems associated with using a dynamic model is that it is difficult to obtain the data needed to implement the model. The Hrovat and Tobler model is attractive because it presents a clever method to estimate hard to obtain model parameters, such as blade angles, element inlet and exit radii, and fluid friction and shock loss factors. The inlet and exit radii and blade angles are referenced at the fluid design path—the path of mean effective flow. If specification drawings are available for the torque converter, the blade geometry may be known; however it is difficult to know where the actual design path will be in operation. Further, tests would almost necessarily need to be performed in order to determine the shock loss coefficients and flow factor. To overcome this problem, Hrovat and Tobler have used a calibration procedure. The steady state torque converter governing equations can be realized by setting the transient terms

to zero in the state equations. An optimization code can then be executed to calibrate the estimated parameters by minimizing the least squares error between steady state test data and the steady state model predictions.

4.2.4 Torque Converter Model Comparison

The principal advantage the dynamic model has over the static model is that the effects of the fluid inertia are included. Pan and Moskwa [14] limit the applicability of the static model to conditions with speed changes of less than 4 Hz. Ishihara and Emori [15] state that the fluid inertia effects are negligible when the frequency of external disturbances is less than one pulse per two impeller revolutions, and have found this threshold to be about the same for torque converters of various designs.

The fluid inertia effects may be important in this present study because a dynamic transmission model is used. In previous NADS automatic transmission models, torque converter speed ratio blends were used during shifts. Thus, the torque converter speed changes were bounded. Torque converter element speed changes in the present model are dictated by the transmission dynamics and may be rapid. A number of modelers have used a static torque converter model with a dynamic transmission model [5, 14, & 16]. However, Pan and Moskwa stated that the static torque converter model was the limiting factor in further enhancement in their transmission simulation [14].

There are two main drawbacks to using a dynamic torque converter model. One is that the parameters needed to create the model are not always available. However, this problem may be overcome by estimating the hard to determine parameters using the optimization technique developed by Hrovat and Tobler. The second problem with the dynamic model is that it is more complicated than the static model. The Hrovat and Tobler model results in four coupled nonlinear differential equations, and the equations must be changed when the flow changes directions or the stator changed from locked to freewheeling. Pan and Moskwa [14] stated that real time simulation applications are

severely limited by the heavy calculation demanded by the dynamic model, citing a private communication with Tobler.

One method to sidestep the computational difficulties is to account for the fluid inertia effects by including time lags in a static torque converter model. This has been done by Ciesla and Jennings [6] and Tugcu, et al. [17]. Tugcu and coworkers state that the parameters used in the time lags must be determined experimentally.

4.3 Torque Converter Model

4.3.1 Proposed Torque Converter Model

The modeling method that was attempted for this current study is outlined as follows:

1. Perform the optimization process outlined by Hrovat and Tobler to determine the parameters needed to formulate the dynamic torque converter model
2. Run the dynamic model offline and use the results to formulate parameters for time lags to account for the transient fluid behavior
3. Implement the static model with the addition of the time lags

Assuming that time lags can adequately capture the effects of the fluid inertia, this method overcomes the problems associated with formulating the dynamic model, and simulating transient effects for real time. This process was unsuccessfully attempted for the 980G torque converter. A problem arose in the optimization process, where no reasonable convergence was attained. The steady state test data provided for the 980G indicated that the stator was locked for speed ratios of 0-0.85, freewheeling for speed ratios of 0.85-1, and locked for speed ratios greater than 1. This inconsistency was the reason the optimization technique would not converge. Further study of this discrepancy is underway; however a static model was used in this study. A few simulations were run

with different lag constants for the sake of investigation. The values used covered the frequency ranges where the fluid inertia effects are reported to have influence [14 & 15]. Including these lags did not discernibly influence the simulated vehicle performance.

4.3.2 Torque Converter Model Formulation

The static model used in this study was provided by Caterpillar. The model's equations are similar to the standard NADS static model equations, except reference impeller and turbine torques are interpolated as a function of the speed ratio, as opposed to reference impeller capacity factor and torque ratio parameters. These equations were used because they were recommended by the same source which provided the test data. The torque converter impeller and turbine torques are found with Equations 9-11 below:

$$SR = \frac{\dot{\theta}_{TC\_T}}{\dot{\theta}_{TC\_I}} \tag{9}$$

$$T_{TC\_T} = T_{TC\_T}[SR]\left(\frac{\dot{\theta}_{TC\_I}}{\dot{\theta}_{Test}}\right)^2 \tag{10}$$

$$T_{TC\_I} = T_{TC\_I}[SR]\left(\frac{\dot{\theta}_{TC\_I}}{\dot{\theta}_{Test}}\right)^2 \tag{11}$$

where SR is the speed ratio, $\dot{\theta}_{TC\_T}$ is the torque converter turbine speed which is equal to the transmission input shaft speed, $\dot{\theta}_{TC\_I}$ is the speed of the torque converter impeller which is equal to the engine speed, $\dot{\theta}_{Test}$ is the speed of the torque converter impeller which was used during testing, T_{TC_T} is the torque converter turbine torque, $T_{TC\_T}[SR]$ is the torque converter turbine torque interpolated from test data as a function of the speed ratio, T_{TC_I} is the torque converter impeller torque, and $T_{TC\_I}[SR]$ is the torque converter impeller torque interpolated from test data as a function of the speed ratio.

CHAPTER 5

TRANSMISSION

5.1 Transmission Operation

The 980G is equipped with an automatic transmission which has four forward and four reverse gears of operation. The transmission's internal gears are arranged in a planetary configuration. A single planetary gear set consists of a sun gear, multiple planet gears which ride in a carrier, and one ring gear. An example of a planetary gear set is shown in Figure 7 [18]. The sun, planet carrier, or ring gear may be used as the input (or output) connection point to the gear set. Torque is transmitted between any two of these bodies by constraining the motion of the third body—holding it stationary or fixing it to another body. When multiple planetary gear sets are linked together with operable clutches, many possible overall input/output ratios can be achieved with relatively few gear sets, and in a compact area. The 980G transmission has a total of five planetary gear sets. A layout of the 980G transmission is shown in Figure 8 [19]. The operating gear is set by engaging one of the transmission's two directional clutches, and one of the transmission's four speed clutches.

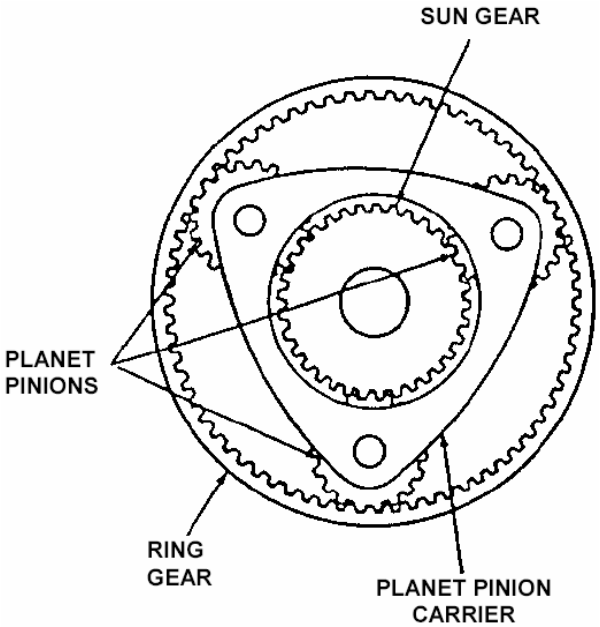

Figure 7. Planetary Gear Set [18]

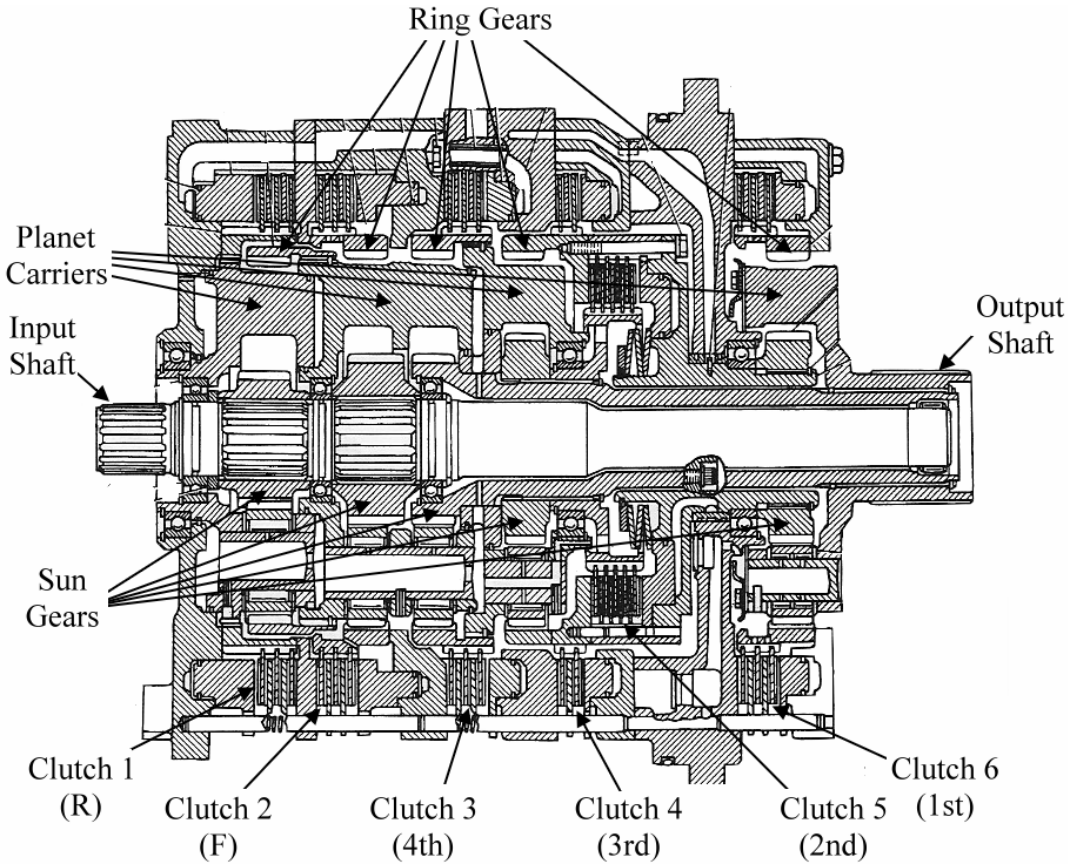

Figure 8. 980G Transmission Side View [19]

The driver can choose manual or automatic shift modes. In automatic mode the transmission's Electronic Control Module (ECM) decides when to shift based on the operating conditions. In manual mode the driver selects the gear of operation using upshift/downshift buttons located on the steering grip. The driver may also neutralize the transmission in braking situations by depressing the left brake pedal. Once a decision to shift has been made, the transmission ECM will coordinate the shift through signals to the appropriate solenoids. Each solenoid actuates a valve which allows fluid into the hydraulic circuits responsible for supplying each clutch piston chamber with pressure. As the pressure acting on the clutch piston increases, it will overcome the force of the clutch return springs, and force the clutch friction disks into contact with the separator plates. The clutch friction disks and separator plates are connected to separate bodies within the transmission. The friction induced torque between the clutch friction disks and separator plates will slow then stop the relative motion of the bodies to which each are connected. As long as the reaction torque between the bodies to which the friction disks and separator plates are attached is less than the clutch torque available, the bodies will undergo no relative motion and are effectively locked together. Through selective locking and unlocking of various clutches, connected to various planetary gear set components, the desired overall transmission gear reduction ratio is attained.

5.2 New Transmission Model Considerations

The functions which must be simulated by this transmission model are different than the functions which have been simulated by past NADS automatic transmission models. In past NADS automatic transmission models, the shift logic was contained within the model. This allowed the transmission model to know what the next gear of operation would be at the onset of a shift, and also allowed the transmission model to know beforehand the nature of each shift. The transmission model used in this study will interface with the vehicle's transmission ECM. The ECM has control over the shifting

process. The only information available to the model is the shift solenoid signals at each instant in time. The benefits of using the actual transmission ECM is that it allows for a more realistic simulation and the full functionality of the transmission controller is available to the operator, e.g., manual or automatic shift modes can used and the transmission neutralizer pedal is functional with no additional modeling required effort or hardware.

The second unique aspect of this transmission model is that it must be able to simulate directional shifts—where the moving vehicle is shifted directly from a forward gear into a reverse gear or vice versa. In past NADS automatic transmission models, only sequential shifts were simulated. During clutch-to-clutch shifts it is valid to assume small changes in vehicle speed during the shift. This assumption allows the use of a torque converter speed ratio blend function to specify the torque converter impeller speed during a shift. It is also valid to assume a continuous transmission torque ratio during clutch-to-clutch shifts. This allows the use of torque ratio curves to model the transmission output torque during a shift. Neither of these assumptions are valid for directional shifts.

The 980G project required the creation of a transmission model which is more representative of the physical transmission. This equates to modeling the clutch torque in response to the transmission ECM signals, and calculating the torque converter impeller speed and transmission output shaft torque using a dynamic transmission model. The transmission dynamic model is discussed next in Chapter 6, and the clutch torque model is discussed in Chapter 7.

CHAPTER 6

TRANSMISSION DYNAMIC MODEL

6.1 Transmission Dynamic Model Overview

6.1.1 Introduction

This chapter is focused on the dynamic transmission model. The dynamics of the transmission will change depending on which clutches are locked; therefore many sets of similar equations are used in the model. This section describes the equations which are required to model the transmission, and the logical aspect of the transmission model. The assumptions/idealizations used in the model are also discussed. The required equations are then derived in the following sections of this chapter.

6.1.2 Transmission Degrees of Freedom

Figure 9 shows a representation of the transmission. There are five planetary gears sets each having a sun gear (S1-S5), a planet carrier (C1-C5), planet gears (P1-P5), and a ring gear (R1-R5). There are six clutches (CL1-CL6). Clutch 1 and clutch 2 are referred to as directional clutches because they control whether the transmission is in a forward or reverse gear of operation. Clutches 3-6 are termed speed clutches because they influence the overall transmission ratio for a particular gear of operation. A single planetary gear set has two degrees of freedom. The five planetary gear sets in the 980G transmission would have ten degrees of freedom were they not connected to one another. The attachments between S1-S2, R1-C2-C3, S3-S4-C5, R3-C4, and R4-S5 impose a total of seven constraints. The velocity of the output shaft is set by the wheels, and is treated as a driving constraint. This results in the transmission having two degrees of freedom at most. When two clutches are locked, a speed clutch and a directional clutch, the transmission will have no unconstrained coordinates. In this case the transmission will be kinematically driven. The speed of the input shaft will be an algebraic function of the

output shaft speed. The output shaft torque will also be formulated with an algebraic equation. The transmission will be dynamically driven when less than one speed clutch and one directional clutch are locked. In these cases differential equations must be used to determine the speeds of the independent transmission bodies. The rotation of the input shaft is always selected as one independent coordinate. The possible second independent coordinate is selected as the rotation of the R1-C2-C3 body, which will be referred to as the intermediate body.

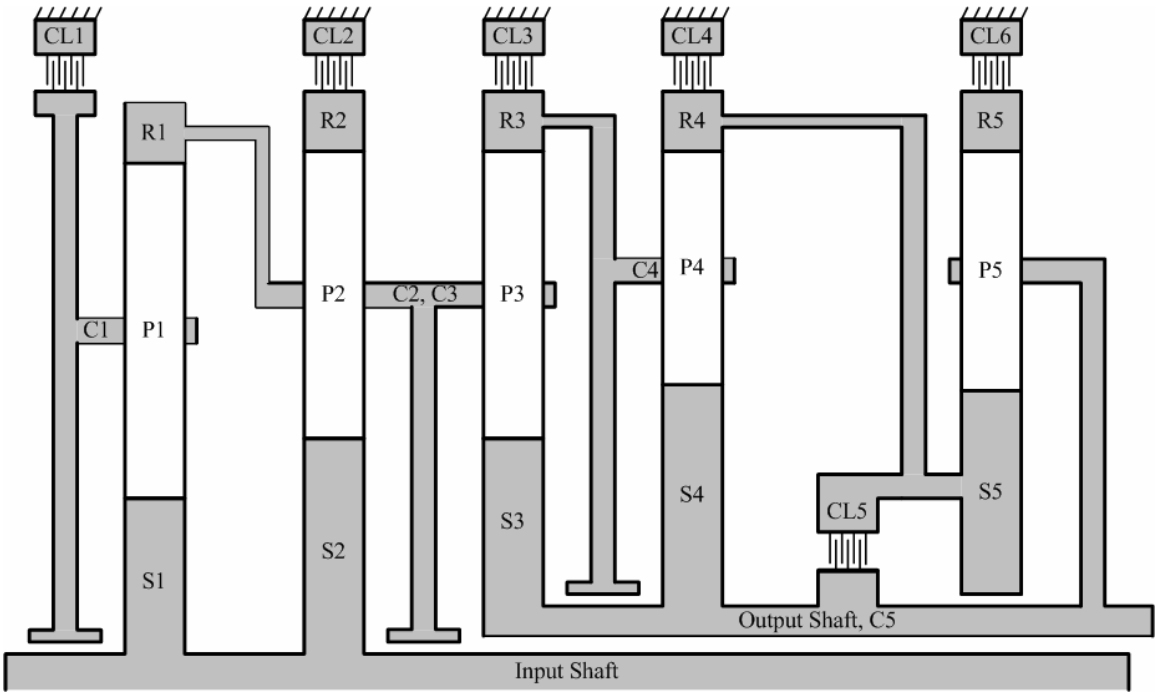

Figure 9. Transmission Representation

6.1.3 Transmission Modes and Logic

There are fifteen different probable kinematic configurations or *modes* [20]; eight for each gear of operation, six for cases when only one clutch is locked, and one when no clutches are locked. Thus fifteen sets of equations are required to account for all operating modes. The locked clutches for each mode are given in Table 1.

Table 1. Transmission Clutch Configurations

Mode	Locked Clutches	Gear
1	C1 & C3	4th Reverse
2	C1 & C4	3rd Reverse
3	C1 & C5	2nd Reverse
4	C1 & C6	1st Reverse
5	C2 & C3	4th Forward
6	C2 & C4	3rd Forward
7	C2 & C5	2nd Forward
8	C2 & C6	1st Forward
9	C1	--
10	C2	--
11	C3	Neutral
12	C4	--
13	C5	--
14	C6	--
15	None	--

When modeled in this manner all 144 possible shifts can be simulated. There is no limit to the number of clutches which can be exerting torque at any time. The only situations not accounted for are when two directional clutches, two or more speed clutches, or more than three total clutches are locked. These cases represent situations where the transmission is holding the input shaft stationary, holding the vehicle

stationary, or holding both the input shaft and vehicle stationary. It was assumed that these situations would not need to be simulated.

Logic is used to determine whether a clutch is slipping or locked. If the reaction torque at a locked clutch is greater than that clutch's torque capacity, the clutch will unlock. If the relative velocity across an unlocked clutch changes sign, and its torque capacity is less than the reaction torque would be if the clutch was to become locked, then the clutch will become locked. A velocity sign change is used as opposed to a near zero velocity condition because of fixed simulation step size.

6.1.4 Transmission Model Assumptions

The following assumptions and idealizations were used in the current transmission model:

1. The transmission gears and shafts are assumed rigid.
2. The gears are assumed to have no backlash.
3. The inertia of the planet gears associated with their rotation about a planet carrier is neglected.
4. Only the inertias of the input shaft body and intermediate body are considered.
5. The inertias of the transmission bodies are assumed to be inconsequential in the calculation of the clutch reaction torque for the purpose determining whether a clutch should lock or unlock.
6. The output shaft is idealized as having infinite inertia compared to the input shaft and internal bodies.

Idealization 4 is motivated by the fact that no values were available for the inertias of the transmission's internal bodies. It is assumed that any gains in accuracy from including these inertias would be slight considering the time required to estimate the inertias, the error in the estimated values, and the increased model complexity.

Assumption 5 is a practical simplification. It is due to the fact that the torque from the torque converter and the clutch torque capacities are dominant over any transmission body inertial torque. The nature of this assumption is that it is either right or wrong, as opposed to having a partial effect on the calculations in the transmission model.

Assumption 6 is based on the idea that the inertia of the transmission bodies are slight compared to the inertia of the wheels and the effective inertia of the vehicle transmitted through the wheels. This assumption results in the transmission being modeled with a set gear ratio when it is not shifting. The effective inertia of a body increases with the square of the gear ratio through which it is connected. Although the local inertia of the transmission input shaft, for example, may be small compared to the effective inertia of the vehicle, the effective inertia of the transmission input shaft may not be negligible when there is a large gear reduction between the transmission and the wheels. For this reason the assumption is questionable, but it should not have a major impact considering the intended use of the vehicle model. This assumption is discussed further in Chapter 8 in association with the transfer case model.

6.2 Equation Derivation Options

There are a number of methods which may be used to derive the transmission's equations of motion. The bond graph method and the lever analogy are attractive because they are accompanied by visual references. Of the two, the lever method is more intuitive. The lever method is also advantageous because once the lever diagrams have been drawn, the equations of motion, speed relationships, and clutch reaction torque equations can be formulated easily.

The drawback to using the lever method is that it requires the modeler to use some degree of reasoning in its application, so there is a chance for error in the application of the rules, which is a concern for one who is not experienced in its use. For this reason, both the embedding technique and the lever method were used to derive the

transmission's equations of motion. The results from the embedding technique were used to verify those of the lever method. The embedding technique is a very efficient and systematic way of generating the equations of motion; however it does not give the speeds of the dependent coordinates or the clutch reaction torques needed for the clutch switching logic.

The rest of this chapter details how the transmission model is formulated. The next section describes how the transmission kinematics are set up using the lever analogy. Following this, the transmission equations of motion are derived for three modes using the lever analogy. The equations of motion for these three modes are also derived using the embedding technique for comparison. This derivation can be found in Appendix B.

6.3 The Lever Analogy for Transmission Kinematics

6.3.1 Applying the Lever Analogy

This section describes how the lever analogy is used to represent the transmission kinematics. First the lever method is described, and the levers are set up for the 980G transmission. The resultant lever diagrams are checked by comparing the speed ratios derived using the levers with the speed ratios given by Caterpillar. Finally the levers are used to formulate the relative angular velocity at each clutch in terms of the input shaft speed, intermediate body speed, and output shaft speed—the possible independent coordinates and driven coordinate. The lever diagrams created in this section will be used in following sections where the transmission dynamics are considered.

The lever analogy takes advantage of the similarities between a lever and a planetary gear set to represent the torque and speed relationships in a visually intuitive manner. The first step in the method is to replace each gear set with a lever, with pivot points located proportional to the number of teeth on the sun and ring gears. With reference to the earlier Figure 9, the Figure 10 shows the transmission gear sets replaced by levers.

The kinematic rules for using the lever method are:

1. The distance between the ring and carrier is set equal to $K * n_s$, and the distance between the carrier and the sun is set as $K * n_r$, where n_s is the number of teeth on the sun gear, n_r is the number of teeth on the ring gear and K is a constant [21]. To simplify the notation, both lever distances are divided by n_s, so that the distance between the ring and carrier is set equal to K, and the distance between the carrier and sun is set equal to $K * e$, with $e = n_r / n_s$.

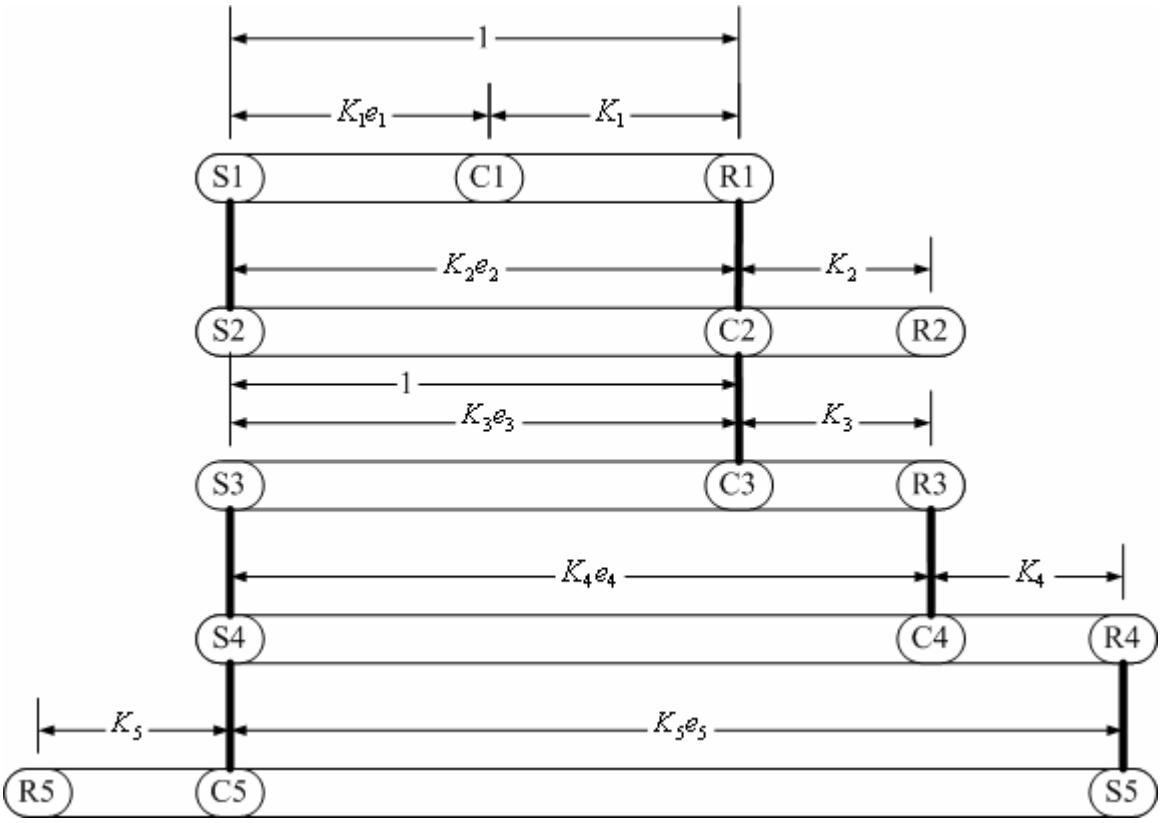

Figure 10. Initial Lever Diagram

2. When there are two interconnections between gear sets, the gear sets are combined into a single lever [21].
3. The distance between a gear set combination input and output is set equal to 1 [22].

Solving to eliminate the lever constants and combining the levers using rule 2, Figure 11 is formed. Here the clutches are also represented symbolically.

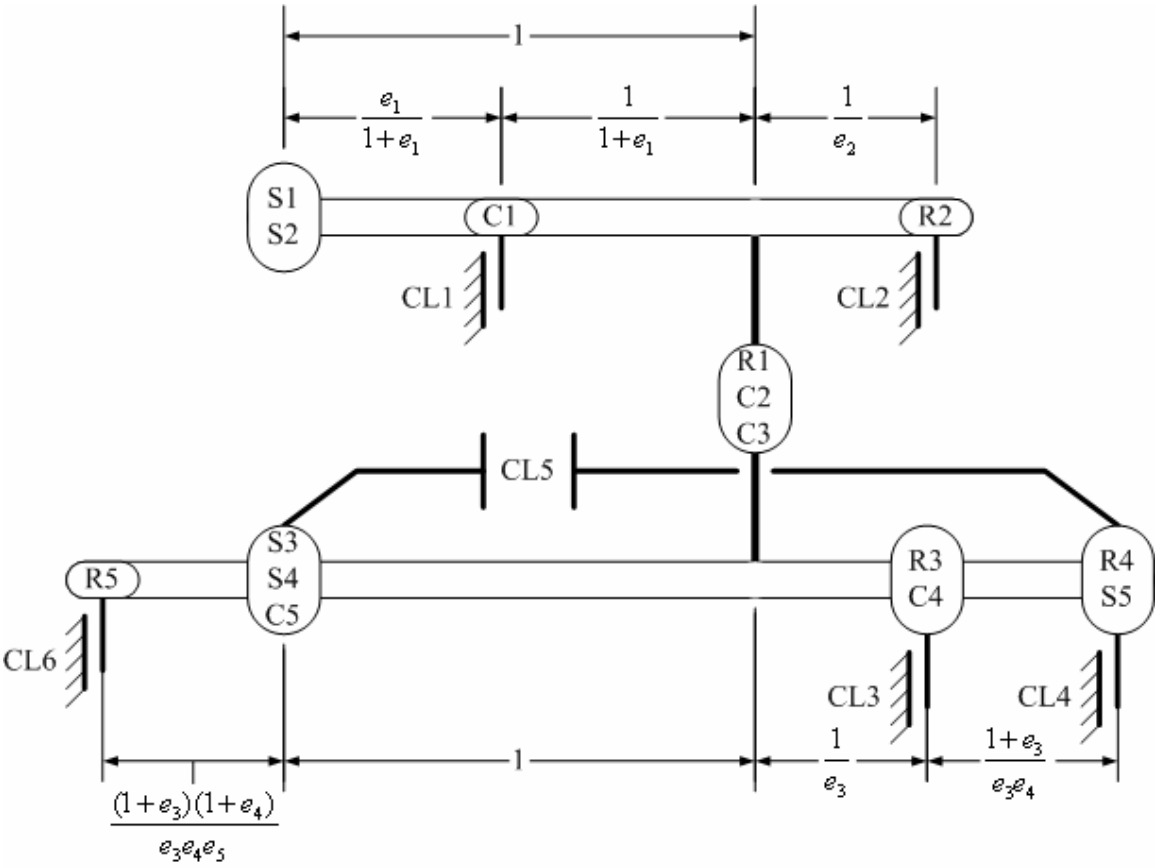

Figure 11. Combined Lever Diagram

When using the lever analogy, torques are represented by forces on the lever, and the lever displacements relative to the reaction points represent the angular velocities [21]. To test the lever analogy factors, speed relationships for each gear are derived next. The lever configuration corresponding to first gear reverse, with clutch 1 and clutch 6 locked is shown in the Figure 12. For brevity, the gear set elements are labeled with numbers, shown in Table 2.

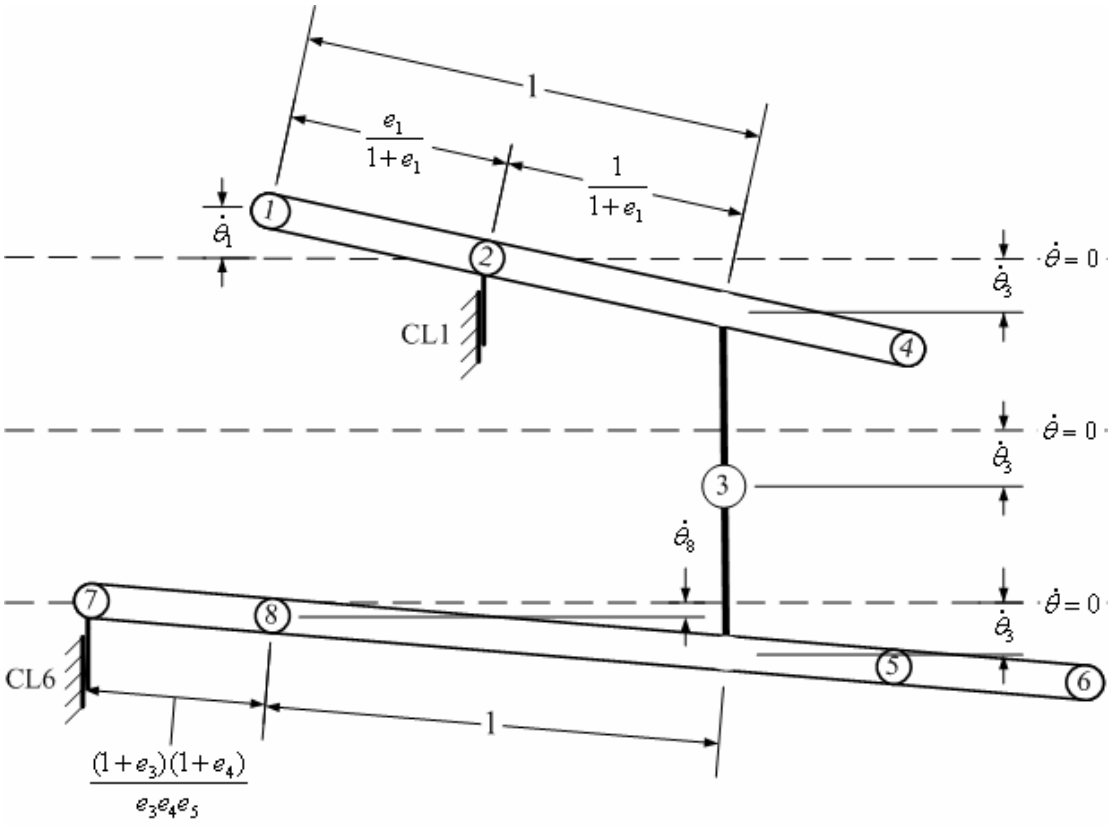

Figure 12. Lever Diagram for First Gear Reverse (Mode 4)

Table 2. Numeric Labels for Gear Set Elements

Body Number	Gear Set Label	Alternative Name
1	S1, S2	Input Shaft
2	C1	
3	R1, C2, C3	Intermediate Body
4	R2	
5	R3, C4	
6	R4, S5	
7	R5	
8	S3, S4, C5	Output Shaft

In Figure 12, the dashed lines represent the local reference locations where the angular velocity is zero. With clutch 1 and clutch 6 locked, bodies 2 & 7 are fixed to the transmission housing, with zero velocity. The angular velocities of all other bodies are related through the lever geometries. The transmission gear ratios can be solved for dividing the input shaft velocity, $\dot{\theta}_1$, by the output shaft velocity, $\dot{\theta}_8$. First the input shaft velocity and output shaft velocity are solved for in terms of the velocity of the intermediate body, $\dot{\theta}_3$, as shown below:

$$\dot{\theta}_1 \frac{1}{1+e_1} = -\dot{\theta}_3 \frac{e_1}{1+e_1}$$

$$\dot{\theta}_3 \frac{(1+e_3)(1+e_4)}{e_3 e_4 e_5} = \dot{\theta}_8 \left(1 + \frac{(1+e_3)(1+e_4)}{e_3 e_4 e_5} \right)$$

The above equations are then combined to eliminate $\dot{\theta}_3$, yielding the first gear reverse ratio, shown in Equation 12.

$$\text{1st Gear Reverse}: \frac{\dot{\theta}_1}{\dot{\theta}_8} = -e_1 \frac{e_3 e_4 e_5 + (1+e_3)(1+e_4)}{(1+e_3)(1+e_4)} \tag{12}$$

The remaining total transmission ratios can be calculated in the same manner, using the lever values from Figure 11 and transmission clutch map from Table 1. When

calculated in this manner, the following overall transmission ratios for the remaining gears of operation are:

$$\text{2nd Gear Reverse}: \frac{\dot{\theta}_1}{\dot{\theta}_8} = -e_1 \tag{13}$$

$$\text{3rd Gear Reverse}: \frac{\dot{\theta}_1}{\dot{\theta}_8} = -\frac{e_1(1+e_3+e_4)}{1+e_3+e_4(1+e_3)} \tag{14}$$

$$\text{4th Gear Reverse}: \frac{\dot{\theta}_1}{\dot{\theta}_8} = -\frac{e_1}{1+e_3} \tag{15}$$

$$\text{1st Gear Forward}: \frac{\dot{\theta}_1}{\dot{\theta}_8} = \frac{(1+e_2)(1+e_4+e_3(1+e_4(1+e_5)))}{(1+e_3)(1+e_4)} \tag{16}$$

$$\text{2nd Gear Forward}: \frac{\dot{\theta}_1}{\dot{\theta}_8} = 1+e_2 \tag{17}$$

$$\text{3rd Gear Forward}: \frac{\dot{\theta}_1}{\dot{\theta}_8} = \frac{(1+e_2)(1+e_3+e_4)}{1+e_3+e_4(1+e_3)} \tag{18}$$

$$\text{4th Gear Forward}: \frac{\dot{\theta}_1}{\dot{\theta}_8} = \frac{1+e_2}{1+e_3} \tag{19}$$

The number of teeth on the sun and ring gears are given in Table 3 along with their e ratios. In order to check that the lever diagram has been set up correctly, the e values from Table 3 were substituted into Equations 12-19 to find the transmission overall gear ratio for each gear of operation. The ratios found using the lever analogy are compared to those given by Caterpillar for this transmission in Table 4. The values in Table 4 indicate that the levers have been set up correctly.

Table 3. Teeth Numbers for the 980G Transmission Gears

Gear Set	n_s	n_r	e
1	32	88	11/4
2	42	90	15/7
3	42	90	15/7
4	51	90	30/17
5	50	90	9/5

Table 4. Transmission Gear Ratios

Gear	From Levers Exact	From Levers Approximate	From Caterpillar Spec. Sheet
1F	1844/329	5.604863	5.6048
2F	22/7	3.142857	3.1428
3F	584/329	1.775076	1.7751
4F	1	1.000000	1.0000
1R	-461/94	-4.904255	-4.9042
2R	-11/4	-2.750000	-2.7500
3R	-73/47	-1.553191	-1.5532
4R	-7/8	-0.875000	-0.8750

6.3.2 Transmission Kinematic Model

The clutch relative velocity equations can be formulated from the lever diagrams in a similar manner. These are given in the following Equations 20-25 in terms of the two possible independent coordinates and the driven coordinate. When all clutches are slipping, the speeds of the input shaft and intermediate body are found by integrating their acceleration equations. These integrated speeds can be used, along with the speed of the output shaft, in Equations 20-25 to find the clutch relative speeds. In cases when one clutch is locked, the input shaft body is selected as the independent body, and its speed is

found through integration of its acceleration. The speed of the intermediate body is defined in terms of either the input shaft speed or output shaft speed by setting the appropriate clutch speed to zero. The remaining equations may then be solved for the remaining dependent clutch relative speeds. In cases when two clutches are locked, both clutch speeds are set equal to zero in the appropriate equations. The result can be used to define the input shaft speed and the intermediate body speed in terms of the output shaft speed. Equations 20-25 can then be solved for the dependent clutch relative speeds. The clutch relative angular velocities are denoted as ω_{CL1} - ω_{CL6} for clutches 1-6. This notation is used to emphasize these are relative angular velocities.

$$\omega_{CL1} = \frac{1}{1+e_1}\dot{\theta}_1 + \frac{e_1}{1+e_1}\dot{\theta}_3 \tag{20}$$

$$\omega_{CL2} = -\frac{1}{e_2}\dot{\theta}_1 + \frac{1+e_2}{e_2}\dot{\theta}_3 \tag{21}$$

$$\omega_{CL3} = \frac{1+e_3}{e_3}\dot{\theta}_3 - \frac{1}{e_3}\dot{\theta}_8 \tag{22}$$

$$\omega_{CL4} = \frac{(1+e_3)(1+e_4)}{e_3 e_4}\dot{\theta}_3 - \frac{1+e_3+e_4}{e_3 e_4}\dot{\theta}_8 \tag{23}$$

$$\omega_{CL5} = \frac{(1+e_3)(1+e_4)}{e_3 e_4}\dot{\theta}_3 - \frac{1+e_3+e_4+e_3 e_4}{e_3 e_4}\dot{\theta}_8 \tag{24}$$

$$\omega_{CL6} = -\frac{(1+e_3)(1+e_4)}{e_3 e_4 e_5}\dot{\theta}_3 + \frac{e_3 e_4 e_5 + (1+e_3)(1+e_4)}{e_3 e_4 e_5}\dot{\theta}_8 \tag{25}$$

6.4 The Transmission Dynamic Model Formulation

6.4.1 Required Equations for Dynamic Model

For each operating mode, equations must be derived for: the input shaft speed and output shaft torque, the clutch relative velocities in terms of the output shaft velocity and any independent coordinates, and the clutch reaction torque at a locked clutch. The clutch

reaction torque equations for a certain mode will be the same as the potential reaction torque equations if the transmission were to change into that mode*. Therefore, the reaction torque equations only need to be derived for modes where the clutches are locked.

One of the difficulties associated with deriving the equations for each mode is the troubleshooting/debugging that is required to catch simple algebra and sign errors. In the following section the lever analogy is used to derive the equations for mode 15, when no clutches are locked. The same method could be used to derive the equations for all modes. However, after spending some time deriving equations with the lever analogy, certain patterns become evident which can be exploited to generate the equations in a systematic manner. After the next example, a method is presented for systematically deriving the equations for the remaining modes. The method is carried out by modifying the equations derived for mode 15 (when no clutches are locked) by adding clutch constraints.

6.4.2 Transmission Dynamics using the Lever Analogy: Mode 15

The clutch slip velocities are given by Equations 20-25 for the case when no clutches are locked. Also, there is no need to calculate the potential clutch reaction torques, because those equations will be the same as the reaction torque equations found when deriving the equations for modes 9-14. The procedure for using the lever analogy to derive the transmission equations of motion is to attach masses representing the rotational inertia of the elements which connect to the gear set. Force and moment balance equations are then solved to yield the dynamic equations [21]. When all clutches are slipping, the dynamic lever diagram is shown in Figure 13.

* See assumption 5 in Section 6.1.4.

The gray circles in Figure 13 represent bodies which have inertia values*. The upward dimension is positive angular velocity, and clockwise rotation is positive. The rotational dimension has units in the form of angular velocity/gear ratio. When all clutches are slipping, equations are needed for the motion of body 1, body 3, and the output shaft torque. Equations 26-28 are found by performing force balances on the upper lever, body 3, and lower lever.

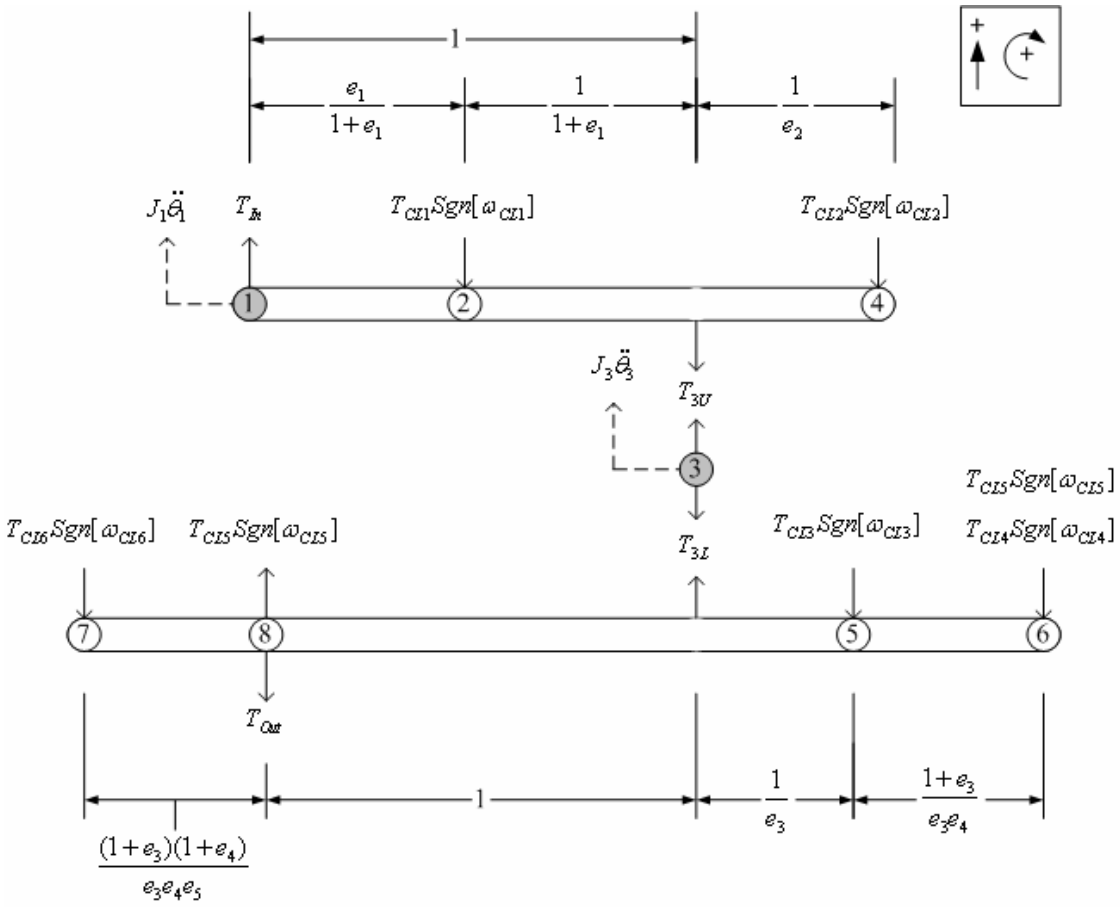

Figure 13. Dynamic Levers

* See idealizations 4 an 6 in Section 6.1.4.

$$J_1\ddot{\theta}_1 = T_{In} - T_{CL1}\,\mathrm{sgn}[\omega_{CL1}] - T_{3U} - T_{CL2}\,\mathrm{sgn}[\omega_{CL2}] \tag{26}$$

$$J_3\ddot{\theta}_3 = T_{3U} - T_{3L} \tag{27}$$

$$T_{Out} = T_{3L} - T_{CL3}\,\mathrm{sgn}[\omega_{CL3}] - T_{CL4}\,\mathrm{sgn}[\omega_{CL4}] - T_{CL6}\,\mathrm{sgn}[\omega_{CL6}] \tag{28}$$

where J_1 and J_3 are the inertias of body 1 and 3, $\ddot{\theta}_1$ and $\ddot{\theta}_3$ are the angular accelerations of body 1 and 3, T_{CL1} through T_{CL6} are the torque capacities of clutches 1 through 6, ω_{CL1} through ω_{CL6} are the relative angular velocities at clutches 1 through 6, T_{3U} is the reaction torque between body 3 and the upper lever, T_{3L} is the reaction torque between body 3 and the lower lever, T_{In} is the torque applied to the input shaft, and T_{Out} is the torque at the output shaft. The reaction torques, T_{3U} and T_{3L}, are solved for by performing moment balances on the upper and lower lever. A moment balance on the upper lever about body 1 (Equation 29), and a moment balance on the lower lever about body 8 (Equation 30) yield:

$$0 = T_{3U} + \frac{e_1}{1+e_1}T_{CL1}\,\mathrm{sgn}[\omega_{CL1}] + \left(1+\frac{1}{e_2}\right)T_{CL2}\,\mathrm{sgn}[\omega_{CL2}] \tag{29}$$

$$\begin{aligned} 0 = -T_{3L} &+ \frac{1+e_3}{e_3}T_{CL3}\,\mathrm{sgn}[\omega_{CL3}] + \left(1+\frac{1}{e_3}+\frac{1+e_3}{e_3e_4}\right)T_{CL4}\,\mathrm{sgn}[\omega_{CL4}] \\ &+ \left(1+\frac{1}{e_3}+\frac{1+e_3}{e_3e_4}\right)T_{CL5}\,\mathrm{sgn}[\omega_{CL5}] - \frac{(1+e_3)(1+e_4)}{e_3e_4e_5}T_{CL6}\,\mathrm{sgn}[\omega_{CL6}] \end{aligned} \tag{30}$$

Solving the above equations for the reaction torques, and substituting the reaction torques into Equations 26-28 yields Equations 31-33 in terms of the desired variables.

$$J_1\ddot{\theta}_1 = T_{In} - \frac{1}{1+e_1}T_{CL1}\,\mathrm{sgn}[\omega_{CL1}] + \frac{1}{e_2}T_{CL2}\,\mathrm{sgn}[\omega_{CL2}] \tag{31}$$

$$\begin{aligned} J_3\ddot{\theta}_3 = &-\frac{e_1}{1+e_1}T_{CL1}\,\mathrm{sgn}[\omega_{CL1}] - \frac{1+e_2}{e_2}T_{CL2}\,\mathrm{sgn}[\omega_{CL2}] \\ &-\frac{1+e_3}{e_3}T_{CL3}\,\mathrm{sgn}[\omega_{CL3}] - \frac{(1+e_3)(1+e_4)}{e_3e_4}T_{CL4}\,\mathrm{sgn}[\omega_{CL4}] \\ &-\frac{(1+e_3)(1+e_4)}{e_3e_4}T_{CL5}\,\mathrm{sgn}[\omega_{CL5}] + \frac{(1+e_3)(1+e_4)}{e_3e_4e_5}T_{CL6}\,\mathrm{sgn}[\omega_{CL6}] \end{aligned} \tag{32}$$

$$T_{Out} = \frac{1}{e_3} T_{CL3} \operatorname{sgn}[\omega_{CL3}] + \frac{1+e_3+e_4}{e_3 e_4} T_{CL4} \operatorname{sgn}[\omega_{CL4}] + \frac{(1+e_3)(1+e_4)}{e_3 e_4} T_{CL5} \operatorname{sgn}[\omega_{CL5}] - \frac{(1+e_3)(1+e_4)+e_3 e_4 e_5}{e_3 e_4 e_5} T_{CL6} \operatorname{sgn}[\omega_{CL6}] \quad (33)$$

6.4.3 Transmission Dynamics Systematically: Mode 9

A unique set of equations is required for each transmission mode. One method of obtaining these equations is to draw a lever diagram for each transmission mode. The constraints that are imposed by locking a clutch are reflected in the new lever diagram, and not considered explicitly in the formulation of the equations. Because the levers are drawn for each mode, this method helps one visualize the dynamics of a particular mode. However, if many different modes must be considered, this method becomes tedious and errors in the derivation are more likely. Using the results from the general case, when all clutches are slipping, the mode equations can be derived in a systematic manner by making logical substitutions. This is done in the following examples.

When clutch 1, a directional clutch, is locked, the velocity of the intermediate body is found by setting ω_{CL1} equal to zero in Equation 20, as shown in Equation 34.

$$\omega_{CL1} = 0 = \frac{1}{1+e_1}\dot{\theta}_1 + \frac{e_1}{1+e_1}\dot{\theta}_3 \rightarrow \dot{\theta}_3 = -\frac{1}{e_1}\dot{\theta}_1 \quad (34)$$

With the speed of the input shaft known from integration of the input shaft acceleration from the last time step, and the output shaft speed known, Equation 34 can be used with Equations 20-25 to solve for the clutch relative slip velocities. The approximate* reaction torque at clutch 1 is found by replacing clutch 1 torque term equal to a reaction torque

* See idealization 5 in Section 6.1.4.

variable, $T_{CL1}\,\mathrm{sgn}[\omega_{CL1}] = T_{RCL1}$, and setting the inertia of the input shaft body equal to zero in Equation 31. The reaction torque is then solved for as shown in Equation 35.

$$T_{RCL1} = (1+e_1)T_{In} + \frac{(1+e_1)}{e_2}T_{CL2}\,\mathrm{sgn}[\omega_{CL2}] \tag{35}$$

The intermediate body acceleration is related to the acceleration of the input body by taking the derivative of Equation 34, shown in Equation 36.

$$\ddot{\theta}_3 = -\frac{1}{e_1}\ddot{\theta}_1 \tag{36}$$

Equations 31 and 32 are combined to eliminate the common clutch 1 torque term, and the acceleration of the intermediate body from Equation 36 is substituted into the resultant equation to yield the acceleration of body 1 in terms of known values, shown in Equation 37.

$$\begin{aligned}\ddot{\theta}_1 = \frac{e_1}{(e_1^2 J_1 + J_3)}\Bigg(& e_1 T_{In} + \frac{1+e_1+e_2}{e_2}T_{CL2}\,\mathrm{sgn}[\omega_{CL2}] + \frac{1+e_3}{e_3}T_{CL3}\,\mathrm{sgn}[\omega_{CL3}] \\ & \frac{(1+e_3)(1+e_4)}{e_3 e_4}T_{CL4}\,\mathrm{sgn}[\omega_{CL4}] + \frac{(1+e_3)(1+e_4)}{e_3 e_4}T_{CL5}\,\mathrm{sgn}[\omega_{CL5}] \\ & -\frac{(1+e_3)(1+e_4)}{e_3 e_4 e_5}T_{CL6}\,\mathrm{sgn}[\omega_{CL6}]\Bigg)\end{aligned} \tag{37}$$

The output shaft torque equation is the same as Equation 33.

6.4.4 Transmission Dynamics Systematically: Mode 4

When clutch 1 and clutch 6 are locked, the velocity of the input shaft and intermediate body are solved for in terms of the output shaft velocity by setting the clutch 1 and clutch 6 relative speeds equal to zero in Equations 20 and 25 (Equations 38-40).

$$\begin{aligned}\omega_{CL1} = 0 &= \frac{1}{1+e_1}\dot{\theta}_1 + \frac{e_1}{1+e_1}\dot{\theta}_3 \\ &\rightarrow \dot{\theta}_1 = -e_1\dot{\theta}_3\end{aligned} \tag{38}$$

$$\omega_{CL6} = 0 = -\frac{(1+e_3)(1+e_4)}{e_3 e_4 e_5}\dot{\theta}_3 + \frac{e_3 e_4 e_5 + (1+e_3)(1+e_4)}{e_3 e_4 e_5}\dot{\theta}_8$$
$$\rightarrow \dot{\theta}_3 = \frac{e_3 e_4 e_5 + (1+e_3)(1+e_4)}{(1+e_3)(1+e_4)}\dot{\theta}_8 \tag{39}$$

$$\dot{\theta}_1 = -e_1 \frac{e_3 e_4 e_5 + (1+e_3)(1+e_4)}{(1+e_3)(1+e_4)}\dot{\theta}_8 \tag{40}$$

With the output shaft velocity known, Equation 40 can be solved for the input shaft velocity, and Equations 38 and 39 along with Equations 21-25 completely define the clutch slip velocities. It is noted that Equation 40 for the input shaft speed in terms of the output shaft speed may be rearranged to form Equation 12, which is the overall gear ratio for this mode. The reaction torque at clutch 1 will be the same as that given in Equation 25. The reaction torque at clutch 6 is found by combining Equations 31 and 32 to eliminate the clutch 1 torque term, replacing the clutch 6 torque term with a reaction torque variable, setting the inertias of the input shaft body and intermediate body equal to zero*, and solving for the clutch 6 reaction torque variable. Carrying out these substitutions one obtains Equation 41.

$$T_{RCL6} = \frac{e_1 e_3 e_4 e_5}{(1+e_3)(1+e_4)}T_{In} + \frac{(1+e_1+e_2)e_3 e_4 e_5}{e_2(1+e_3)(1+e_4)}T_{CL2}\,\mathrm{sgn}[\omega_{CL2}]$$
$$+\frac{e_4 e_5}{1+e_4}T_{CL3}\,\mathrm{sgn}[\omega_{CL3}] + e_5 T_{CL4}\,\mathrm{sgn}[\omega_{CL4}] + e_5 T_{CL5}\,\mathrm{sgn}[\omega_{CL5}] \tag{41}$$

The output shaft torque is found by combining Equations 31-33 to eliminate the clutch 1 and clutch 6 torque terms. Employing the infinite output shaft inertia assumption, the inertias of the input shaft body and intermediate body are set equal to zero. Carrying out these substitutions, Equation 42 for the output shaft torque is obtained.

* See idealization 5 in Section 6.1.4.

$$T_{Out} = -\frac{e_1((1+e_3)(1+e_4)+e_3e_4e_5)}{(1+e_3)(1+e_4)}T_{In}$$
$$-\frac{(1+e_1+e_2)((1+e_3)(1+e_4)+e_3e_4e_5)}{e_2(1+e_3)(1+e_4)}T_{CL2}\,\mathrm{sgn}[\omega_{CL2}] \quad (42)$$
$$-\frac{1+e_4(1+e_5)}{1+e_4}T_{CL3}\,\mathrm{sgn}[\omega_{CL3}]-(1+e_5)T_{CL4}\,\mathrm{sgn}[\omega_{CL4}]-e_5T_{CL5}\,\mathrm{sgn}[\omega_{CL5}]$$

It is noted that in the absence of any dragging clutches, the output torque in Equation 42 is the same as the input torque times the overall gear ratio, from Equation 12.

6.5 Implementation

The transmission equations for each of the modes with one or more clutches locked were derived systematically using Equations 20-25, the derivatives of Equations 20-25, and Equations 31-33, as was done in Sections 6.4.2 and 6.4.3. The general equations were entered into *Mathematica*® along with the specific conditions for each mode, and the equations required to define each mode were solved in symbolic form. They were then transferred into the FORTRAN code for simulation. The embedding technique was used to verify the acceleration and output torque equations for each mode. This again was done systematically in *Mathematica*®. Examples of the equation derivation using the embedding technique for the three modes presented in the text are shown in Appendix B.

The output torque variable, T_{Out}, is multiplied by an efficiency term before being passed to the transfer case model. The input shaft speed is passed to the torque converter model. The torque converter model returns the turbine torque, which is identical to the input torque variable, T_{In}, discussed in this chapter.

The execution of the transmission model code is summarized as follows. When two clutches are locked (modes 1-8) the reaction torque at each clutch is compared with torque capacity at each clutch. If the reaction toque exceeds the torque capacity for one or both clutches, the relative velocity sign is set equal to the sign of the clutch reaction toque. The mode is changed to reflect the clutch or clutches that have unlocked, and the

code associated with the new mode is executed before continuing to the next time step. When one clutch is locked (mode 9-14) the reaction torque is checked in the same manner as described above. The input shaft velocity is always selected as an independent coordinate when the transmission is dynamically driven. After the transmission input shaft velocity is solved for, a velocity sign change is checked for at the appropriate clutches. If a speed clutch is locked, all directional clutches are tested and if a directional clutch is locked, all speed clutches are tested. If a velocity sign change takes place, a comparison is made between the clutch`s toque capacity and the equivalent reaction torque at the clutch were it to become locked. If the toque capacity is less than the equivalent reaction torque, the transmission model will change modes to reflect the locked clutch and the new mode equations will be executed before continuing on to the next time step. If no clutches are locked (mode 15) a velocity sign change is monitored for each clutch. If a clutch has a velocity sign change and the equivalent reaction torque is less than the torque capacity, that clutch will lock and the transmission will execute the equations associated with the new mode before continuing on to the next time step.

CHAPTER 7

CLUTCH TORQUE

7.1 Overview

The dynamic transmission model discussed in Chapter 6 requires the clutches` torque capacities to completely characterize the transmission operation. The torque capacity is the amount of torque the clutch can transmit/withstand. The actual torque at a clutch will be equal to the torque capacity when the clutch is slipping, but less than the torque capacity (equal to the reaction torque) when the clutch is locked. The torque capacity will vary primarily with the pressure acting at the clutch piston. To complete the transmission model from Chapter 6, a relationship between the transmission ECM signals and clutch pressures, and a relationship between the clutch pressures and the clutch torques

7.2 Clutch Pressure from Transmission ECM Signals

Little information was available about the relationship between the transmission solenoid signals and the clutch pressure. It was not known at the time of this research whether the transmission ECM was meant to control proportional solenoids or on/off solenoids*. The solenoid signals were not measured during the validation tests. For the present model, the solenoid signals were assumed to be on/off and predefined clutch pressure profiles are used. The pressure profiles were set for each clutch so the overall vehicle model would simulate axle torques and fore/aft accelerations similar to the measurements taken during vehicle tests. The off-going clutch pressure was set to decrease very quickly, and the on-coming clutch pressure is responsible for dictating the dynamic behavior of the shift. This was done to ensure the operator in the loop simulation

* Solenoid traces measured shortly before the pilot run of the project were on/off in nature.

would be predictable. Since solenoid signals were not available for reference, erratic behavior could occur if the on-coming and off-going clutch signals overlap more than expected, causing an unrealistic clutch tie-up condition. Thus, the model tends to err on the side of unrealistically high flair, which is a more predictable condition than unrealistically high tie-up. The fore/aft acceleration peaks can be simulated for clutch to clutch shifts through steep on-coming pressure profiles. This approach, however, does not capture the characteristic shapes of the acceleration and torque graphs corresponding to the typical torque and inertia phases of the shift. However, the peak cab fore/aft acceleration, the wheel speeds, and other values important for simulating the cab motion are still captured well. The results will be presented in Chapter 10. Since the main objective of this current project is to evaluate the realism of the NADS for simulating construction equipment, the objective can be satisfied by using these idealized pressure curves as long as they can reproduce the desired cab motion. The task of creating a transmission hydraulic model which is more physically representative of the real system is left for a future study.

7.3 Clutch Torque Modeling Methods

The 980G transmission uses wet clutches. Each clutch has multiple friction plates and separator plates which run in the presence of automatic transmission fluid. The torque developed across a wet clutch is a combination of hydrodynamic torque and asperity contact torque. The hydrodynamic torque is due to the transmission fluid residing between the separator and friction plates, essentially a viscous damping torque. It is proportional to the relative velocity across the clutch plates and inversely proportional to their separation. The asperity contact torque is due to the friction between the clutch plates. It is mainly a function of clutch activation pressure. Figure 14 shows the hydrodynamic torque, asperity torque, and the total torque across an automobile clutch during a typical engagement [23]. The graph is from a simulation; however it is similar to

measured results [23]. The simulation graph is shown because the asperity and hydrodynamic torques are represented separately.

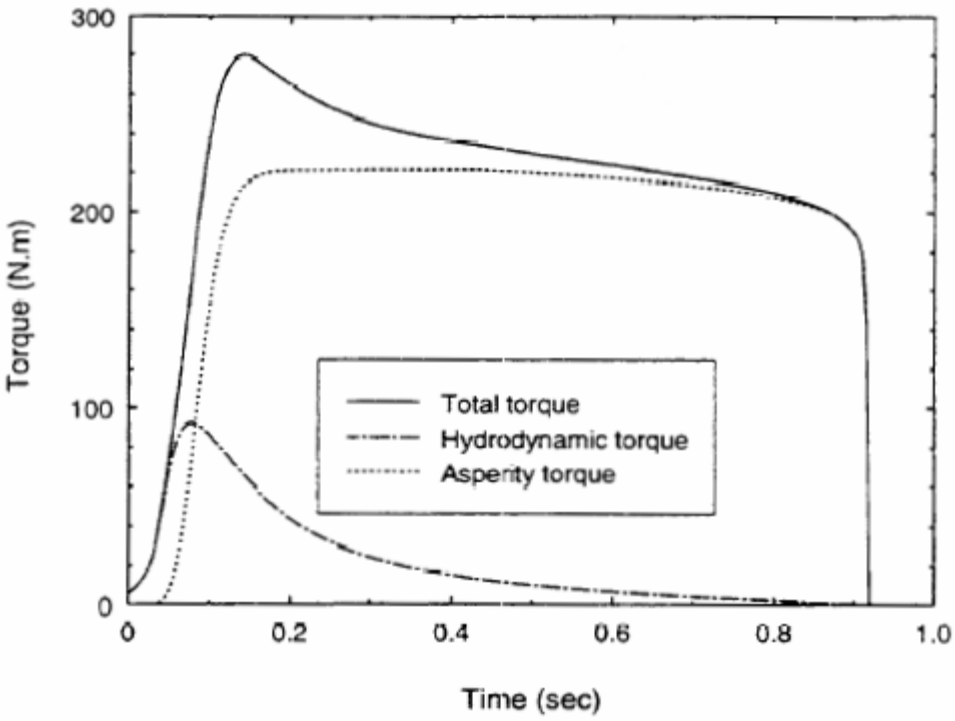

Figure 14. Wet Clutch Torque Simulation for Typical Automobile [23]

Figure 14 shows that the hydrodynamic torque initially makes a substantial contribution to the total torque. The hydrodynamic torque will lead the asperity torque because it is effective before the clutch disks make contact. The relative velocity across the clutch is high at first, and the increase in hydrodynamic torque reflects the decrease in plate separation distance. As engagement continues, the hydrodynamic torque falls off to a small percentage of total torque. This is due to the rapidly decreasing clutch relative

velocity, and also reflects that less fluid contact area is available as the clutch asperity contacts takes over a greater percentage of the disk area. Some of the hydrodynamic torque decrease is also attributed a fluid viscosity which decreases with increasing temperature.

Berger et al. [24] has developed a clutch torque model that accounts for both the hydrodynamic and asperity torque during the engagement of a wet clutch. In Berger`s formulation the hydrodynamic torque is similar to the toque developed across flat annular rotating disks separated by a fluid. The effect of surface roughness on hydrodynamic torque is accounted for using the average flow model method developed by Patir and Cheng [26, 27]. The asperity contact torque is formulated in terms of the portion of the load the contacting asperities support—the other portion of the load is supported by fluid pressure. Asperity geometry, statistical distribution, and plate modulus of elasticity are parameters which are used to relate the separation distance to asperity load. The key term needed to solve for hydrodynamic and asperity torque is the plate separation distance, or fluid film thickness. The film thickness is solved for with a modified version of the Reynolds equation, and flow factors to account for surface roughness [26, 27].

Berger and coworkers reported versions of this model with varying degrees of complexity. One version well suited for real-time applications simplifies the modified Reynolds equation into a first order differential equation [25]. The simplified model can obtain solutions on the order of seconds, and the results are in agreement with the finite element model, which requires a computational time on the order of hours [25].

Yang et al. [22] and Davis et al. [29] extended the simplified Berger model to include thermal effects during the engagement process. However, including thermal effects requires the simultaneous solution of the Reynolds equation and energy equation, which makes the thermal models less favorable for real-time simulation. Davis et al. [29] reported that typical simulations of one second require six to seven seconds of CPU

time*. They reported that the thermal model generally predicts longer engagement times and less peak torque than the isothermal model and the thermal model correlates better with experimental results.

The hydrodynamic torque is often neglected when modeling clutch engagement for the purpose of transmission controller development or gross vehicle dynamic simulation. None of the vehicle dynamic oriented transmission models cited in this thesis considered hydrodynamic torque. However, it should be noted that the influence of hydrodynamic torque will vary depending on the particular clutch being modeled. And most of the vehicle dynamic oriented transmission models do not even specify whether wet or dry clutches are used, though they most likely use wet clutches. Research done on the 980G transmission indicates that the hydrodynamic torque can be neglected. A transmission analysis at Caterpillar stated that, in the models used for transmission controller assessment, hydrodynamic torque is neglected due to the large clutch grooves which effectively channel the fluid away from between the clutch disks [30]. Models such as Berger's do account for grooved clutch disks, however they also assume the clutch disks are submerged in fluid. The clutch disks in a heavy duty construction vehicle, such as the wheel loader being modeled, are not submerged in transmission fluid. Doing so would reduce the transmission efficiency and result in extremely high transmission fluid temperatures [31].

7.4 Clutch Torque Model

The asperity contact torque developed at a clutch may be formulated assuming a uniform pressure distribution and using an empirically measured coefficient of friction. The torque transmitted across a slipping clutch is given in Equation 43 [18]:

$$T_{CL} = F_C f r_m n_s \tag{43}$$

* In the year 2000.

where, T_{CL} is the clutch torque capacity, F_C is the clamping force, f is the coefficient of friction, r_m is the mean radius of the clutch, and n_s is the number of torque transmitting surfaces, which is twice the number of friction disks. The mean radius of the clutch is found using Equation 44 [18]:

$$r_m = \frac{d_o^3 - d_i^3}{3(d_o^2 - d_i^2)} \tag{44}$$

where d_o is the outside diameter of the clutch disk and d_i is the inside diameter of the clutch disk. The clamping force in Equation 43 is found by taking the hydraulic pressure times the area of the clutch piston and subtracting clutch spring force. Depending on the friction material and the transmission fluid, the friction coefficient may increase or decrease with sliding velocity [23]. It is known that the 980G clutch friction coefficient will decrease sliding velocity. However, a constant coefficient of friction is used in this model because the clutch pressure profiles are set to reproduce measured vehicle performance. Changes in clutch torque due to variations in the friction coefficient are implicitly accounted for in the clutch pressure curves.

CHAPTER 8

TRANSFER CASE

8.1 Transfer Case Operation and Modeling Methods

The transfer case distributes the transmission output torque to the front and rear drive shafts and also includes a gear reduction. The transfer case model is responsible for calculating the speed of the transmission output shaft and the drive shaft torque distribution. Previous four wheel drive vehicles modeled for the NADS used open differential or bias differential transfer case models. In these instances, the front and rear drive shafts are independent bodies, and the torque distribution can be calculated in a straightforward manner. The transfer case in the 980G, however, is locked—meaning that the front and rear drive shafts are directly connected. Because the front and rear drive shafts are note independent, it is more difficult to determine their torque distribution.

One option is to assume the transfer case can be represented with the currently available open differential model. In an open differential, the transmission output shaft torque is multiplied by the transfer case gear ratio then distributed equally between the drive shafts. Under most operating conditions reasonable results could be obtained by using a 1:1 front to rear torque distribution. However, using an open differential to model a locked transfer case will cause unrealistic results when there is high powertrain torque and a large difference in the traction available at the front and rear wheels. This will be demonstrated in Section 8.3.

Another option is to include the drive shaft compliance and model the transfer case as an independent body. This is done in off-line vehicle dynamic simulations, where the powertrain inertias and compliances are included to increase the fidelity of the vehicle model. In this current study, torque oscillations due to driveshaft compliance are not a source of concern. The motivation for modeling the transfer case as an inertial body and the drive shafts as compliant would primarily be to determine the proper drive shaft

torque distribution. An attempt was made to model the transfer case in this manner. Figure 15 represents the transfer case and drive shafts. The equation of motion for the rotational coordinate of the transfer case is given by Equation 45:

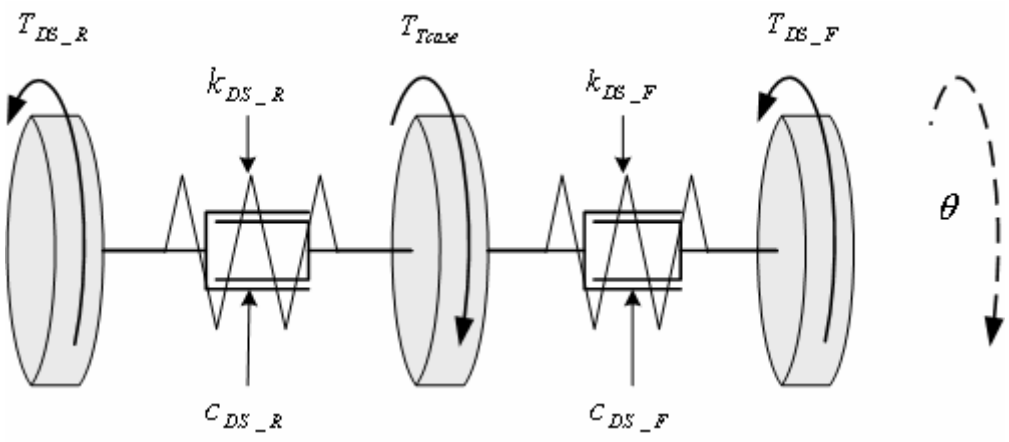

Figure 15. Transfer Case and Drive Shafts Representation

$$\ddot{\theta}_{TCase} = \frac{1}{J_{TCase}}\Big(T_{TCzse} - (\theta_{TCase} - \theta_{DS\_F})k_{DS\_F} - (\dot{\theta}_{TCase} - \dot{\theta}_{DS\_F})c_{DS\_F} - (\theta_{TCase} - \theta_{DS\_R})k_{DS\_R} - (\dot{\theta}_{TCase} - \dot{\theta}_{DS\_R})c_{DS\_R}\Big) \tag{45}$$

where θ_{TCase}, θ_{DS_F}, and θ_{DS_R} are the rotational coordinates of the transfer case, front drive shaft, and rear drive shaft, J_{TCase} is the transfer case/transmission output shaft equivalent inertia, k_{DS_F} and k_{DS_R} are the spring constants of the front and rear drive shafts, and c_{DS_F} and c_{DS_R} are the damping constants of the front and rear drive shafts. T_{TCase} is the torque at the transfer case, with $T_{TCase} = T_{TR\_O}N_{TCase}$, where N_{TCase} is the transfer case gear ratio, and T_{TR_O} is the transmission output shaft torque. Equation 45 is

integrated once to determine the transfer case velocity, and again to determine the transfer case position. The torque at the front and rear drive shafts are found using Equations 46 and 47:

$$T_{DS\_F} = (\theta_{TCase} - \theta_{DS\_F})k_{DS\_F} + (\dot{\theta}_{TCase} - \dot{\theta}_{DS\_F})c_{DS\_F} \quad (46)$$

$$T_{DS\_R} = (\theta_{TCase} - \theta_{DS\_R})k_{DS\_R} + (\dot{\theta}_{TCase} - \dot{\theta}_{DS\_R})c_{DS\_R} \quad (47)$$

where T_{DS_F} and T_{DS_R} are the torques at the front and rear drive shafts.

The inertia of the transfer case/transmission output shaft, and the spring values for the drive shafts were based on scaled measurements taken from a 980G parts manual using digital calipers. A material density and modulus of rigidity for mild steel were used. The damping values were assumed as five per cent of the critical damping constants for the system. Equations 45-47 were implemented into the 980G SII model, and solved using a fourth order Runge-Kutta integration method. The step size was reduced until no discernable changes were seen by further reduction of the step size. Unfortunately, this method did not yield reasonable results most likely due to error in the estimated inertia, spring, and damping values.

8.2 Approximate Transfer Case Model

Equations 45-47 could have been used in the present model had more accurate inertia, spring, and damping values been available. If this present study was concerned with the torque oscillations due to the drive shafts compliance, then this option would have been investigated further. However, this was not the case, and only the torque distribution is needed here. These considerations led to the development of an approximate transfer case model which is discussed in this section.

Neglecting the inertia of the transfer case body, Equation 45 can be re-arranged as shown in Equation 48.

$$T_{TCase} = (\theta_{TCase} - \theta_{DS\_F})k_{DS\_F} + (\dot{\theta}_{TCase} - \dot{\theta}_{DS\_F})c_{DS\_F} + (\theta_{TCase} - \theta_{DS\_R})k_{DS\_R} + (\dot{\theta}_{TCase} - \dot{\theta}_{DS\_R})c_{DS\_R} \quad (48)$$

The key part of the approximate model is that the rotation of the transfer case is constrained to satisfy static equilibrium. Equation 48 is then separated to yield algebraic functions for the transfer case position and velocity, shown in Equations 49 and 50.

$$T_{TCase} = (\theta_{TCase} - \theta_{DS\_F})k_{DS\_F} + (\theta_{TCase} - \theta_{DS\_R})k_{DS\_R}$$
$$\rightarrow \theta_{TCase} = \frac{T_{TCase} + \theta_{DS\_F}k_{DS\_F} + \theta_{DS\_R}k_{DS\_R}}{k_{DS\_F} + k_{DS\_R}} \quad (49)$$

$$0 = (\dot{\theta}_{TCase} - \dot{\theta}_{DS\_F})c_{DS\_F} + (\dot{\theta}_{TCase} - \dot{\theta}_{DS\_R})c_{DS\_R}$$
$$\rightarrow \dot{\theta}_{TCase} = \frac{\dot{\theta}_{DS\_F}c_{DS\_F} + \dot{\theta}_{DS\_R}c_{DS\_R}}{c_{DS\_F} + c_{DS\_R}} \quad (50)$$

Substituting Equations 49 and 50 into Equations 46 and 47, one obtains the front and rear drive shaft torque as shown in Equations 51 and 52.

$$T_{DS\_F} = \frac{k_{DS\_F}}{k_{DS\_F} + k_{DS\_R}}T_{TCase} - \frac{k_{DS\_F}k_{DS\_R}}{k_{DS\_F} + k_{DS\_R}}(\theta_{DS\_F} - \theta_{DS\_R}) - \frac{c_{DS\_F}c_{DS\_R}}{c_{DS\_F} + c_{DS\_R}}(\dot{\theta}_{DS\_F} - \dot{\theta}_{DS\_R}) \quad (51)$$

$$T_{DS\_R} = \frac{k_{DS\_R}}{k_{DS\_F} + k_{DS\_R}}T_{TCase} + \frac{k_{DS\_F}k_{DS\_R}}{k_{DS\_F} + k_{DS\_R}}(\theta_{DS\_F} - \theta_{DS\_R}) + \frac{c_{DS\_F}c_{DS\_R}}{c_{DS\_F} + c_{DS\_R}}(\dot{\theta}_{DS\_F} - \dot{\theta}_{DS\_R}) \quad (52)$$

Though the torque distribution is approximate, the net torque satisfies the property given in Equation 53, found by adding the two above equations and simplifying the result:

$$T_{TCase} = T_{DS\_F} + T_{DS\_R} \quad (53)$$

As shown in Equation 53, the total torque from the transmission will always be sent through the driveline to the wheels. The spring and damping values are only important insofar as they bias the torque. So, even if the spring and damping values are estimated

poorly, the total torque will still be reasonable. There is no need to estimate the transfer case inertia or integrate for the position or velocity of the transfer case, as the transfer case position and velocity are found using algebraic equations.

To gain some physical understanding of the above equations, consider a case when the spring and damping constants for the front and rear drives shafts are equal. The speed of the transfer case, Equation 50, reduces to Equation 54,

$$\dot{\theta}_{TCase} = \frac{\dot{\theta}_{DS\_F}}{2} + \frac{\dot{\theta}_{DS\_R}}{2} \tag{54}$$

This is the speed relationship for an open differential. The front and rear drive shaft torques in Equations 51 and 52 can be reduced to the form shown in Equations 55 and 56.

$$T_{DS\_F} = \frac{T_{TCase}}{2} - \frac{k}{2}(\theta_{DS\_F} - \theta_{DS\_R}) - \frac{c}{2}(\dot{\theta}_{DS\_F} - \dot{\theta}_{DS\_R}) \tag{55}$$

$$T_{DS\_R} = \frac{T_{TCase}}{2} + \frac{k}{2}(\theta_{DS\_F} - \theta_{DS\_R}) + \frac{c}{2}(\dot{\theta}_{DS\_F} - \dot{\theta}_{DS\_R}) \tag{56}$$

Figure 16 shows the symbolic representation of these equations. When the spring and damping values are the same for the front and rear, the approximate model physically corresponds to an open differential transfer case driving the front and rear differentials, with an independent spring-damper link acting between the front and rear differentials.

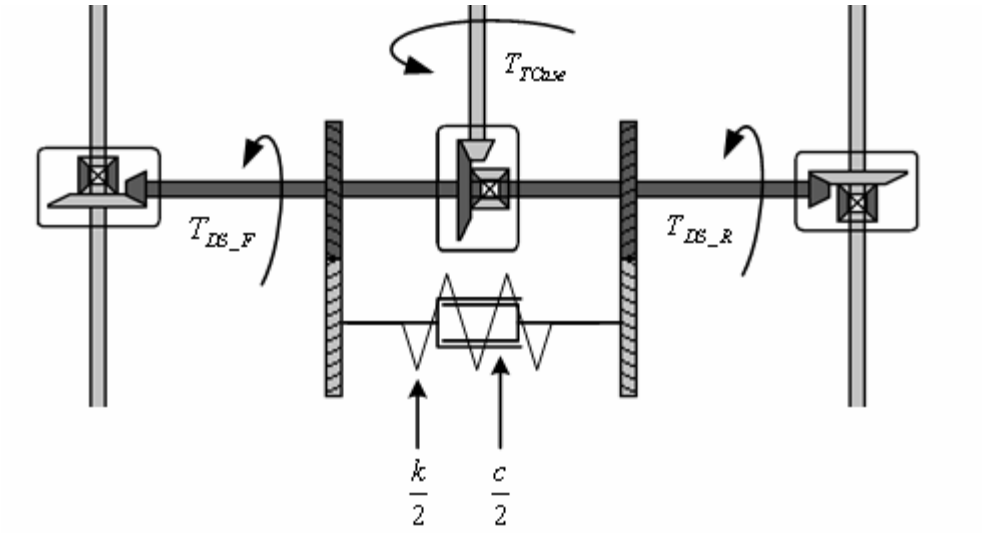

Figure 16. Symbolic Representation of Approximate Transfer Case Model

8.3 The Need for a Locked Transfer Case Model

It was stated earlier that in most situations modeling a locked transfer case as an open differential will yield reasonable results, but when there is high powertrain torque and a large difference in the traction available at the front and rear tires, an open differential model is inadequate. This is the case during full throttle shift reversals. The following figures, Figures 17 and 18, show comparisons between the measured and simulated front right wheel RPM during a full throttle shift from first gear reverse to first gear forward.

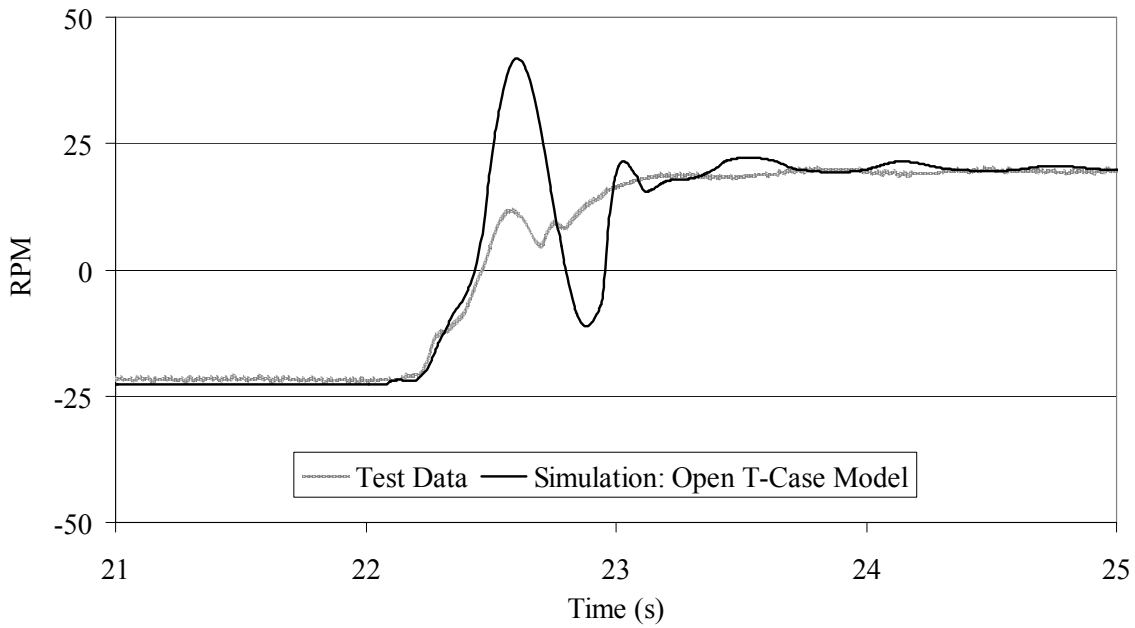

Figure 17. Front Right Wheel RPM for Shift Reversal with Open Transfer Case Model

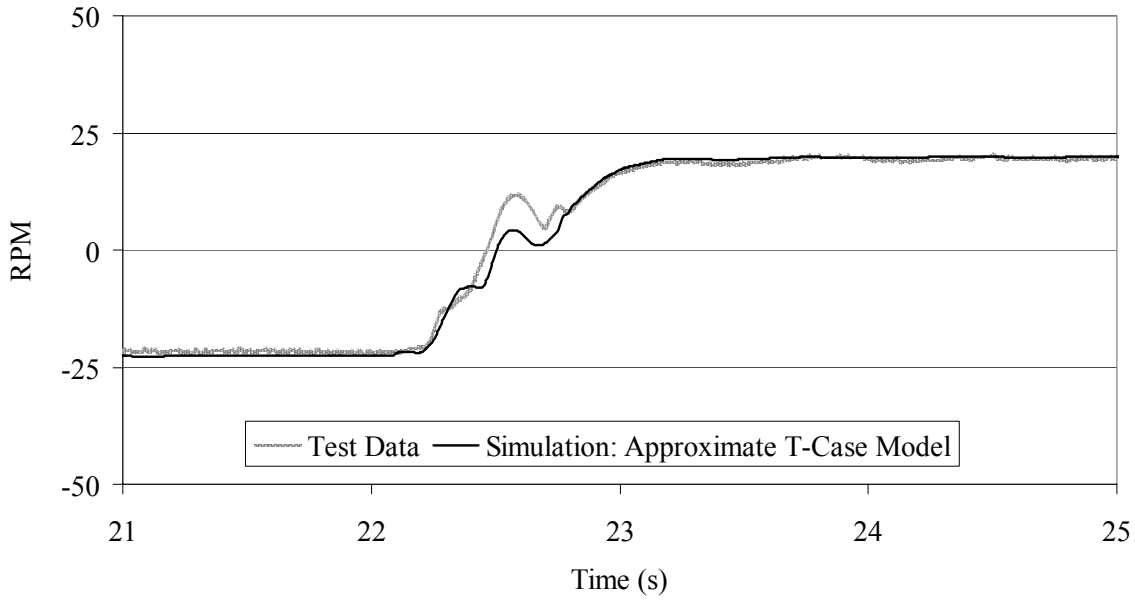

Figure 18. Front Right Wheel RPM for Shift Reversal with Approximate Transfer Case Model

The simulation results shown in Figure 17 are from the 980G vehicle model when an open differential type transfer case model is used. The simulation results shown in Figure 18 are from an identical simulation except the approximate transfer case model from Section 8.2 is used. When shifting from reverse to forward, the front tires experience a reduction in normal force and the rear tires experience an increase in the normal force. This will cause the rear tires to have more available traction than the front tires. Since the transfer case on the actual 980G is locked, the rear tires will be receiving more torque than the front tires. The open differential model equally splits the torque under all conditions. The result is that the front tires are given too much torque and they break loose. As the front wheels spin, the average speed of the drive train increases. This in turn raises the speed of the torque converter turbine, causing a reduction in the total torque at all wheels. As the total torque is lowered the acceleration is reduced, which decreases the dynamic weight transfer, giving the front tires more traction. The increase in traction at the front tires, along with the overall powertrain torque reduction, allows the front tires to regain their grip and stop spinning. When this occurs, the powertrain speed is reduced and the cycle begins again. It is seen in Figure 18 that the approximate transfer case model yields more reasonable results.

The following figures, Figures 19 and 20, show the fore/aft acceleration for this same shift when an open differential transfer case and the approximate locked transfer case model are used. In an open differential, the torque available at either side is limited to the amount which can be supported by the side with the least resistance. Figure 19 shows the reduction in total torque limits the maximum acceleration. Also the cyclic increases and decreases in torque as the front wheels spin and regain traction causes a more “jerky” simulated shift. Figure 20 shows that the approximate locked transfer case model yields more reasonable results.

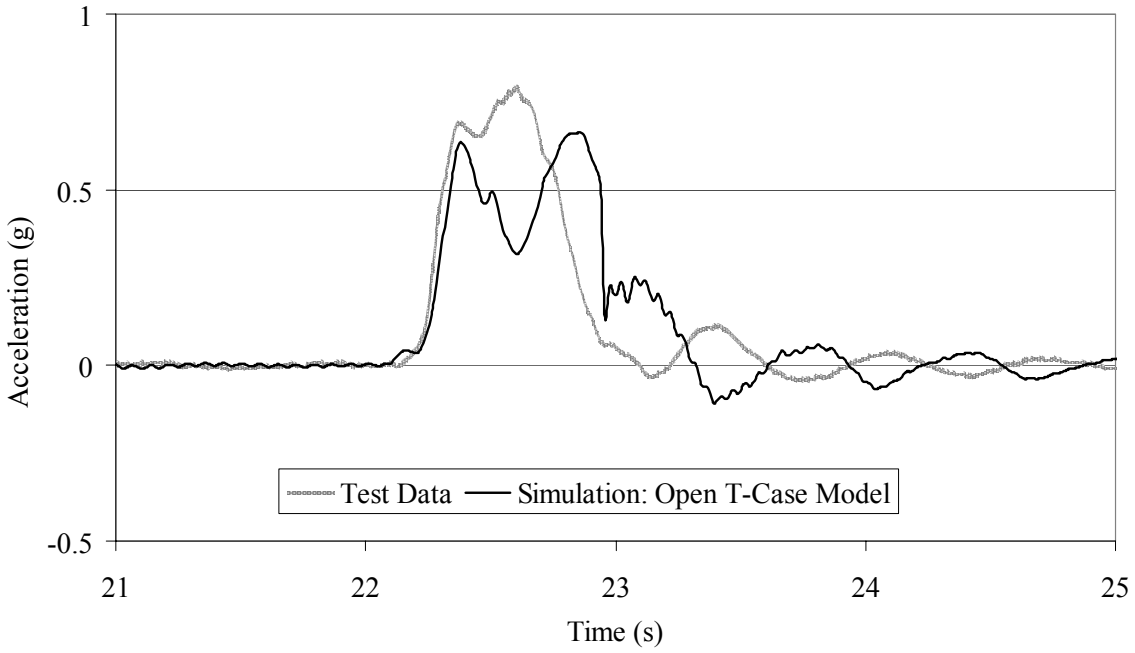

Figure 19. Fore/Aft Acceleration for Shift Reversal with Open Transfer Case Model

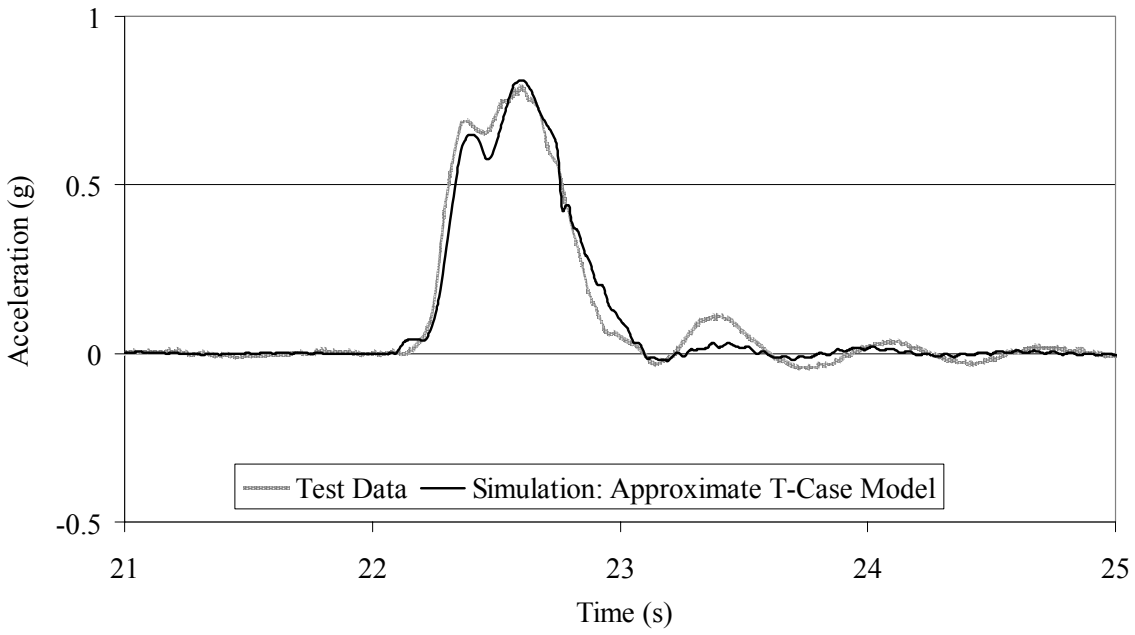

Figure 20. Fore/Aft Acceleration for Shift Reversal with Approximate Transfer Case Model

CHAPTER 9

DIFFERENTIALS, FINAL DRIVES, AND BRAKES

9.1 Differential Description and Model

The front and rear axle housings incorporate a differential, one wet disk brake per wheel, and one final drive planetary gear set per wheel. These are shown in Figure 21.

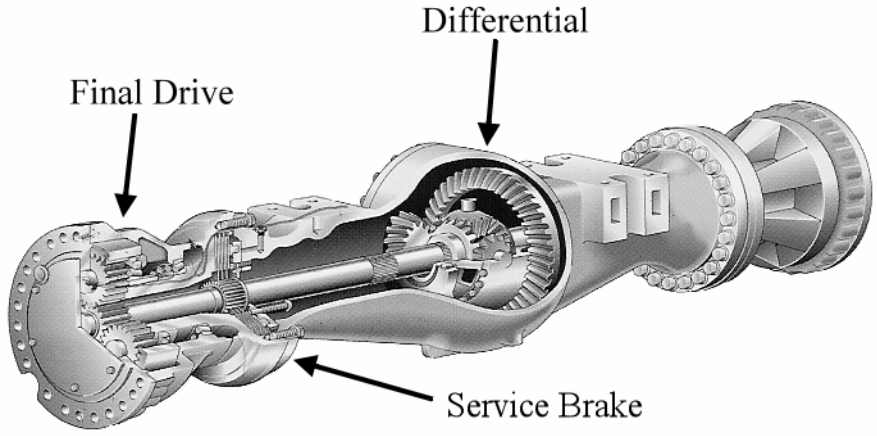

Figure 21. Axle Housing [32]

The differential distributes the drive shaft torque to the axle shafts, and uses a gear reduction to increase the torque in the process. The 980G uses open differentials, which allow the left and right wheels to turn at different speeds. This allows the vehicle to negotiate turns, where the outside wheel must turn faster than the inside wheel. The open differential model is straightforward. Assuming negligible backlash, negligible efficiency losses, and rigid gears, Equations 57-59 characterize the differential's speed and torque relationships.

$$\dot{\theta}_{DS} = \frac{N_{Diff}}{2}(\dot{\theta}_{Ax\_R} + \dot{\theta}_{Ax\_L}) \tag{57}$$

$$T_{Ax\_R} = \frac{1}{2} N_{Diff} T_{DS} \tag{58}$$

$$T_{Ax\_L} = \frac{1}{2} N_{Diff} T_{DS} \tag{59}$$

where $\dot{\theta}_{DS}$, $\dot{\theta}_{Ax\_R}$, and $\dot{\theta}_{Ax\_L}$ are the speeds of the drive shaft, right axle, and left axle, T_{DS}, T_{Ax_R}, T_{Ax_L} are the torques at the drive shaft, right axle, and left axle, and N_{Diff} is the differential gear ratio.

9.2 Final Drive Description and Model

The final drive is simply a gear reduction between the axle shaft and wheel body. Assuming negligible backlash and efficiency losses, Equations 60 and 61 below are used to model the torque and speed relationship of the final drive.

$$\dot{\theta}_{Ax} = N_{FD}\dot{\theta}_{W} \tag{60}$$

$$T_{W} = N_{FD} T_{Ax} \tag{61}$$

where $\dot{\theta}_{Ax}$ and $\dot{\theta}_{W}$ are the angular velocities of the axle shaft and wheel, T_{Ax} and T_{W} are the powertrain torques at the axle and wheel, and N_{FD} is the final drive gear ratio.

9.3 Service Brake Description and Model

The 980G uses wet disk brakes, which are similar to the wet friction clutches used in the transmission. The operator may use either the left or right brake pedal to activate the service brakes. The left pedal activates the transmission neutralizer, causing the transmission to shift into neutral. Because the transmission ECM controls the neutralizer, and the transmission model interfaces with the ECM, there was no need to include the neutralizer as a separate element in the brake model.

In the NADS simulation structure, the brake torque and powertrain axle torque are reported to the wheel body as separate values. The logic that deals with brake lockup

resides in the multi-body dynamic model, so the brake torque calculated in the brake model represents the maximum available brake torque. The brake torque is scaled by the final drive ratio before it is reported to the wheel model because the brakes are mounted inboard the final drives. The torque developed at a brake will vary with the hydraulic pressure acting at that brake. The pressure at each brake is modeled as a linear function of per cent brake pedal displacement. The torque for each brake is shown in Equations 62 and 63:

$$T_{Br} = (N_{FD} F_{B\_Max} f_B r_m n_s) * \%BrakePedal \tag{62}$$

$$F_{B\_Max} = A_B P_{B\_Max} \tag{63}$$

where f_B is the friction coefficient, n_s is the number of friction surfaces (twice the number of brake disks), r_m is the mean radius which was previously defined with Equation 44, F_{B_Max} is the maximum clamping force, A_B is the area behind the brake piston, and P_{B_Max} is the maximum hydraulic brake pressure.

9.4 Parking Brake Description and Model

The parking brake is a drum type shoe brake located on the driveline which is spring applied and hydraulically released. Little information was available on the parking brake. One specification sheet did list the slope holding ability of both the service brakes and the parking brakes. The parking brake torque was estimated based on these slope angles and the calculated service brake torque. Equations 64 and 65 represent equilibrium of forces for the vehicle to be held stationary on a slope.

$$mg \sin[\theta_{SB}] = 4 R_T T_{SB} \tag{64}$$

$$mg \sin[\theta_{PB}] = 4 R_T T_{PB} \tag{65}$$

where m is the mass of the vehicle, g is the acceleration due to gravity, θ_{SB} and θ_{PB} are the slope holding angles for the service brakes and parking brakes, R_T is the tire radius, T_{SB} is the (calculated) maximum service brake torque per wheel, and T_{PB} is the maximum

parking brake torque per wheel. Combining these two equations leads to the estimated parking brake torque, shown in Equation 66.

$$\frac{mg\sin[\theta_{SB}]}{mg\sin[\theta_{PB}]} = \frac{4R_T T_{SB}}{4R_T T_{PB}}$$

$$T_{PB} = T_{SB}\frac{\sin[\theta_{PB}]}{\sin[\theta_{SB}]} \tag{66}$$

CHAPTER 10

SIMULATION RESULTS

10.1 Introduction

The subsystem models discussed in this thesis were created to work with the whole vehicle model for the purpose of driver in the loop simulation using the NADS. This type of simulation is called on-line simulation. During on-line simulation the vehicle model inputs—accelerator pedal position, steering wheel angle, brake pedal position, etc.—will be dictated by the human driver inside the cab. The simulation results presented in this chapter are from off-line simulation. Here the inputs are set in a text file prior to the beginning of the simulation. The purpose of off-line simulation is to test the model and verify that it is working correctly.

In this chapter off-line simulation results from the vehicle model are compared with data measured from the actual vehicle. The test data was measured by Caterpillar engineers for the purpose of validating the NADS vehicle model. The test vehicle was instrumented with sensors which measured both the driver inputs to the controls and the vehicle response. The driver inputs were used to create the off-line model driver input files. The transmission ECM shift solenoid signals which will be received by the model during on-line simulation were not recorded during the vehicle test, but a gear number reading was. This gear number was converted into corresponding clutch on/off signals in the off-line input file. The recorded test data presented in this chapter was filtered to remove any obvious noise and offset to remove any sensor bias if needed.

10.2 Performance of Engine, Powertrain, and Brake Models

A person driving a simulator must perceive a realistic driving environment in order for the simulation to be of value. The value of the engine, powertrain, and brake models lie in how they contribute to the realism of this environment. The following

paragraph discusses the vehicle behavior which is most relevant for the evaluation of the engine, powertrain, and brake models.

The performance the engine, powertrain, and brake models will be most perceptible to the driver through the fore/aft acceleration felt during a shift or brake maneuver and through the effects of the vehicle's top speed under steady state engine/powertrain input conditions. Though the driver will not "feel" the effect of the top speed as they would accelerations during a shift, the speed will perceived visually in the projected driving scene. Also steering changes or road roughness encountered will cause the driver to experience a simulated acceleration which will depend on the vehicle's speed. The engine speed is slightly less critical, and will be evident to the driver through the tachometer display, engine noise, and its effect on the implement operation. Proper calculation of the engine speed is important for determining the correct engine torque from the engine map interpolation. From the driver's perspective, the axle torque is only important insofar as it influences the fore/aft acceleration and the vehicle top speed. Ideally all of the simulated results will match the measured results; however more attention is paid to the performance which will be most prevalent to the driver. The fore/aft acceleration from shifting and braking, and the vehicle's top speed are the two most significant factors which are influenced by the engine, powertrain, and brake models.

10.3 Acceleration Run 1

The first comparison is of straight line acceleration and sequential shifting. The driver gives a full accelerator command and shifts into first gear forward. Once top speed is reached in first gear forward, the driver shifts into second gear forward and continues to hold down the accelerator until top speed is reached in that gear. Once top speed is reached in second gear forward, the driver lets off the accelerator and applies the brake

until the vehicle is stationary. This same maneuver is repeated for first and second reverse gears.

During the test runs the operator applied the left brake pedal to halt the vehicle. However, only the position of the right brake pedal was being recorded. Therefore, there was no way to simulate the same brake pedal inputs in the off-line model simulation. An arbitrary brake input was used in the off-line simulation simply to halt the vehicle so it could take off from a stationary position for the reverse gear part of the test. The simulation results during the braking maneuver are not shown in the figures so the arbitrary brake input does not confuse the comparison. Figures 22 through 27 are discussed after all of the figures for Acceleration Run 1 are shown.

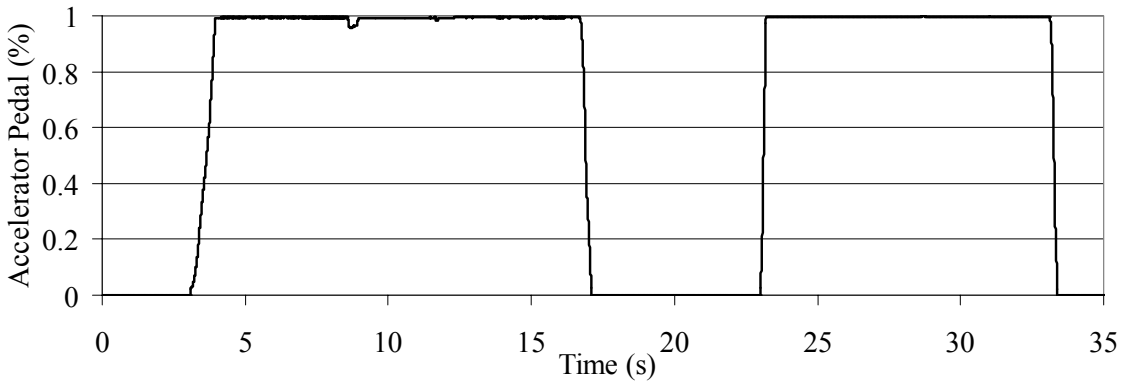

Figure 22. Accelerator Pedal Position for Acceleration Run 1

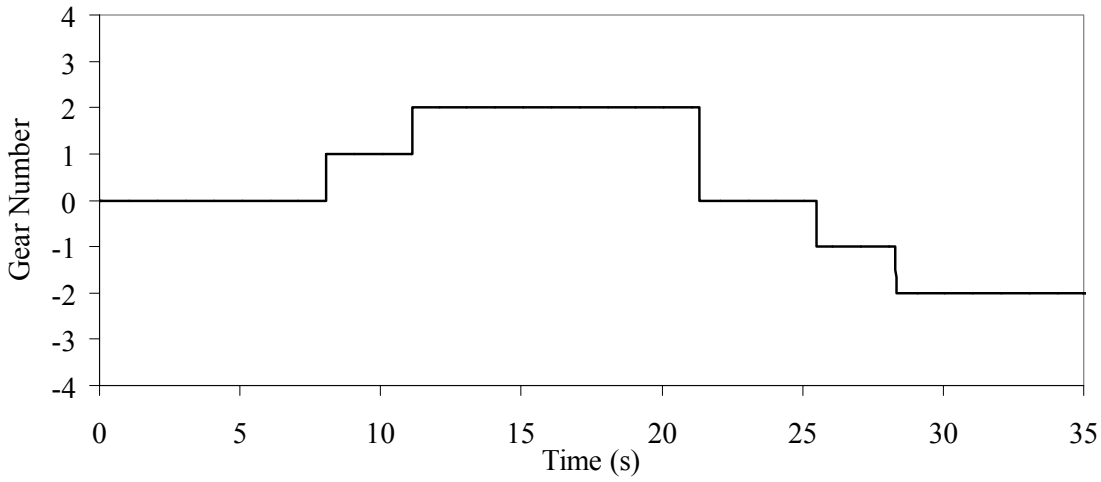

Figure 23. Gear Number for Acceleration Run 1

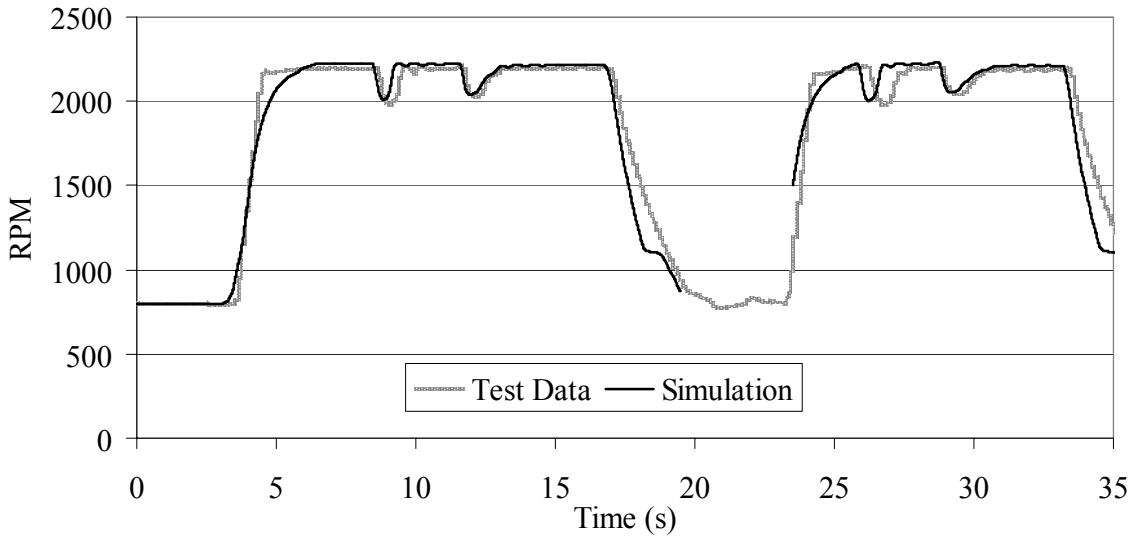

Figure 24. Engine RPM for Acceleration Run 1

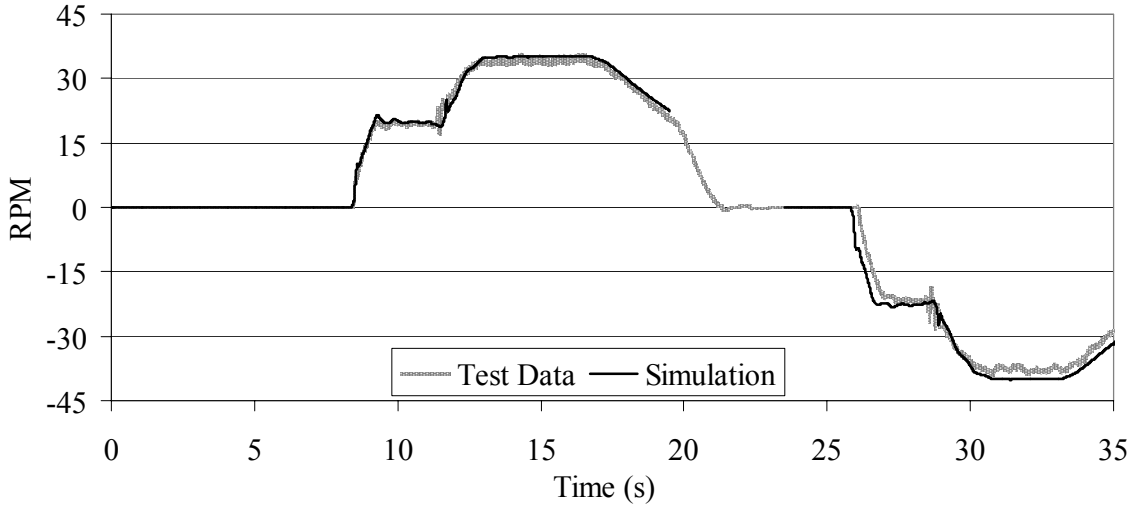

Figure 25. Front Right Wheel RPM for Acceleration Run 1

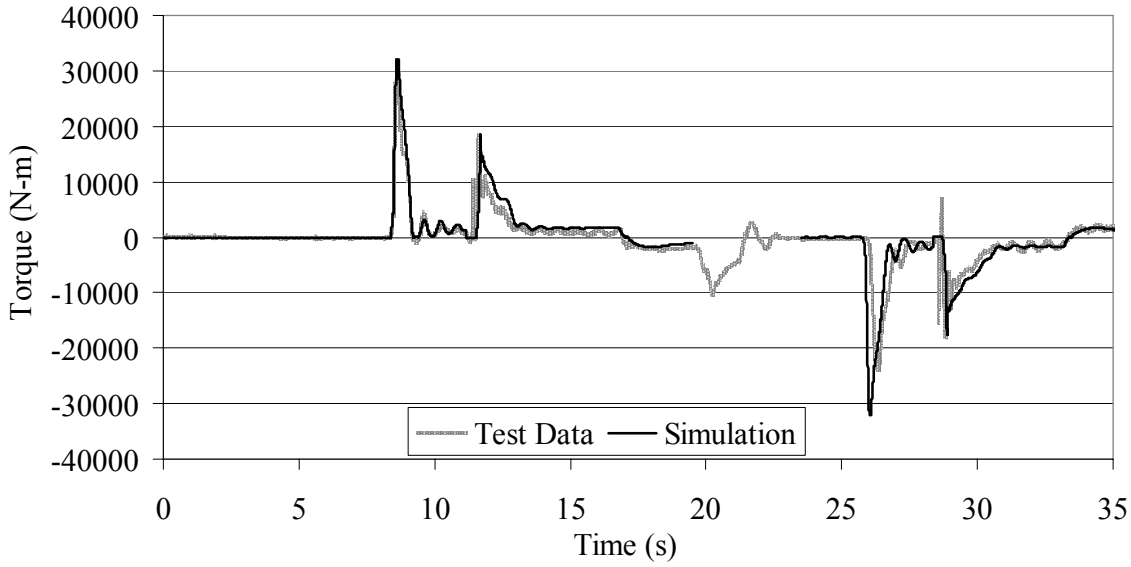

Figure 26. Total Axle Torque for Acceleration Run 1

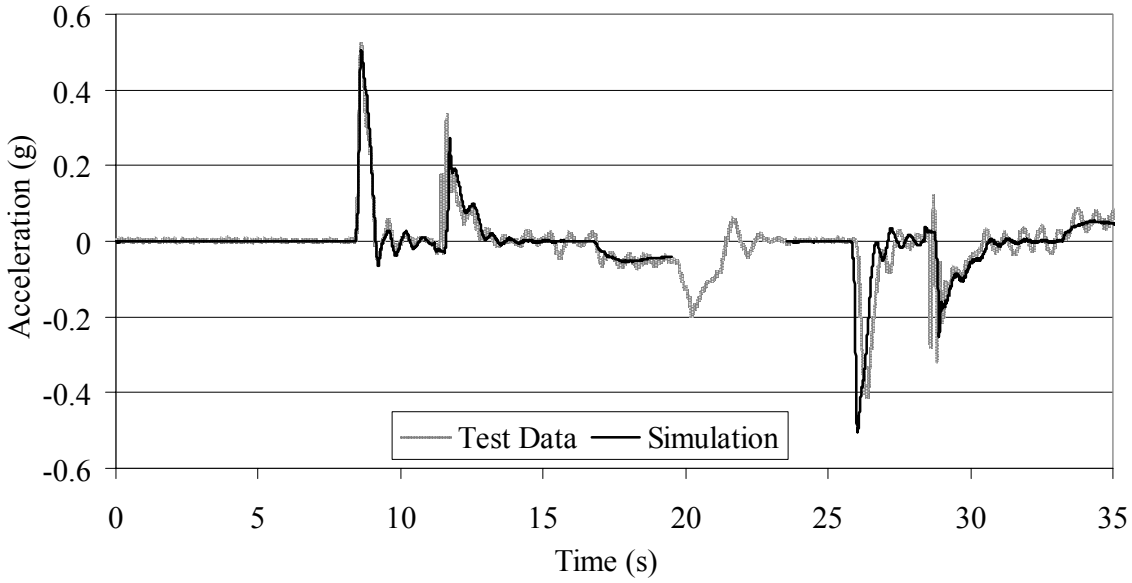

Figure 27. Fore/Aft Acceleration for Acceleration Run 1

Figure 22 shows the accelerator input, and Figure 23 shows the gear number. The simulated engine RPM in Figure 24 shows a good match for the measured engine RPM at idle and during shifts into first gear forward, second gear forward, and second gear reverse. The simulated engine RPM during the shift into first gear reverse leads the test results, but has a similar shape. This is due to the assumed clutch pressure curve, which is apparently a bit too responsive. The simulated front right wheel RPM shown in Figure 25 agrees reasonably well with the test data. Again, the effect of the over responsive clutch when shifting into first gear reverse is seen, where the simulated vehicle begins to move early.

Figure 26 compares the total axle torque. The simulation agrees well with the test data for the shift into first gear forward. The simulated maximum torque during the shift into second gear forward is similar to the recorded value; however the characteristic torque phase and inertial phase of the shift are not captured. This is because the off-going

clutch pressure curve is set to be very steep to avoid a tie-up condition when interfaced with the transmission ECM for the on-line simulation. The reason for doing this was discussed in detain in Section 7.2. The simulated axle torque for the shift into first gear reverse again indicates that the reverse clutch pressure curve is too steep and begins too early, leading the recorded axle torque and having a magnitude higher than recorded. The simulated and measured axle torque for the shift into second gear reverse may be compared along the same lines as was done for the shift into second gear forward. The fore/aft acceleration comparison shown in Figure 27 reflects the same behavior as the axle torque comparison. The largest discrepancy is during the sequential shifts at the 12 and 23 second times. The difference, as was discussed previously in reference to the axle torque figure, is due to the underrepresented clutch overlap.

The issues associated with the second gear reverse clutch pressure curve may be taken care of with some adjustment. The most notable deficiencies in the simulation involve the clutch pressure curves. These problems may be addressed in future projects by modeling the transmission hydraulic system. Overall the model appears to perform reasonably considering its intended purpose. Simulation results for Acceleration Run 2 and Acceleration Run 3 are shown in Appendix C.

10.4 Brakes Run 2

Two braking tests were conducted on the actual 980G by Caterpillar. The first brake run involves shifts into the first gears, both forward and reverse, and stops from top speed in these gears. The second brake run involves shifts into the second gears, both forward and reverse, and stops from top speed in these gears. The vehicle behavior when shifting into the first gears from a stationary position was already discussed in Section 10.3, so the second gear brake run is presented here for variety. The simulation comparison for the first gear brake run, Brake Run 1, is shown in Appendix C.

Figures 28 to 33 from Brake Run 2 are shown next. Figure 28 shows the accelerator pedal input to the model, and Figure 30 shows the brake pedal input to the model. These model inputs are the same as those measured during the actual test runs. Figure 29 shows the gear number.

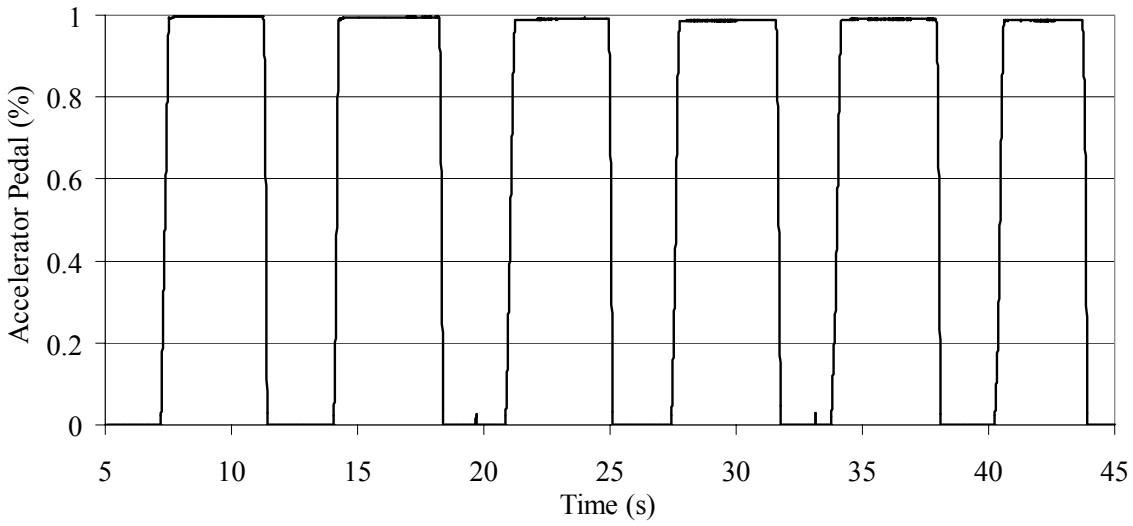

Figure 28. Accelerator Pedal Position for Brake Run 2

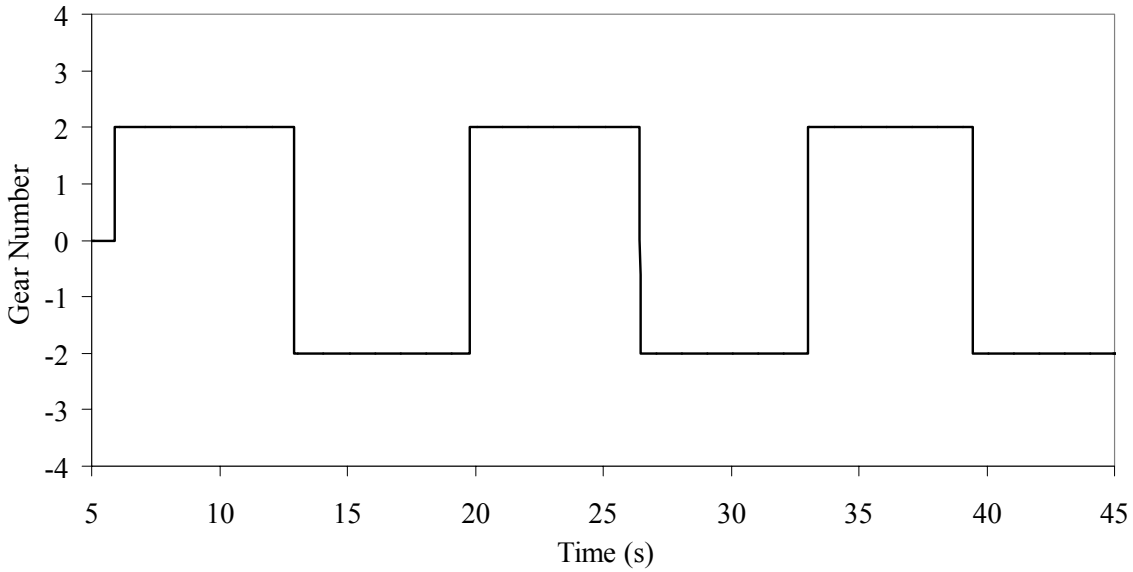

Figure 29. Gear Number for Brake Run 2

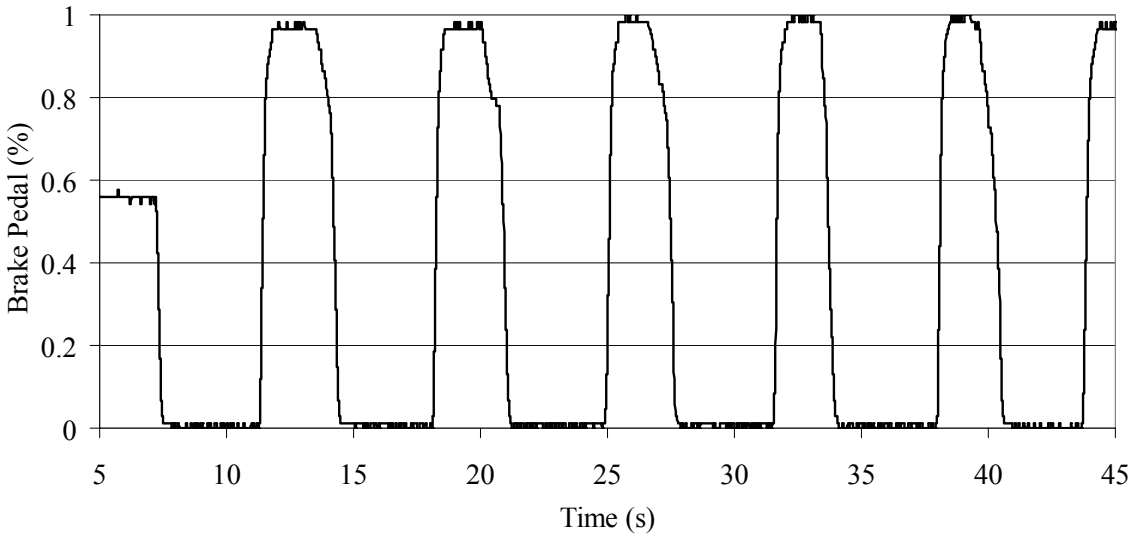

Figure 30. Brake Pedal Position for Brake Run 2

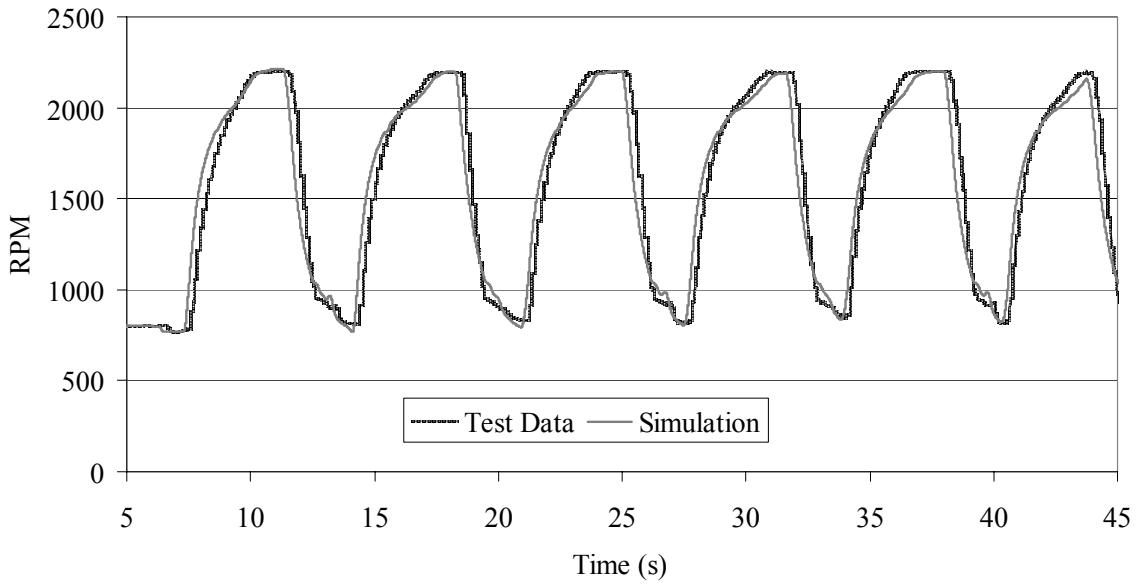

Figure 31. Engine RPM for Brake Run 2

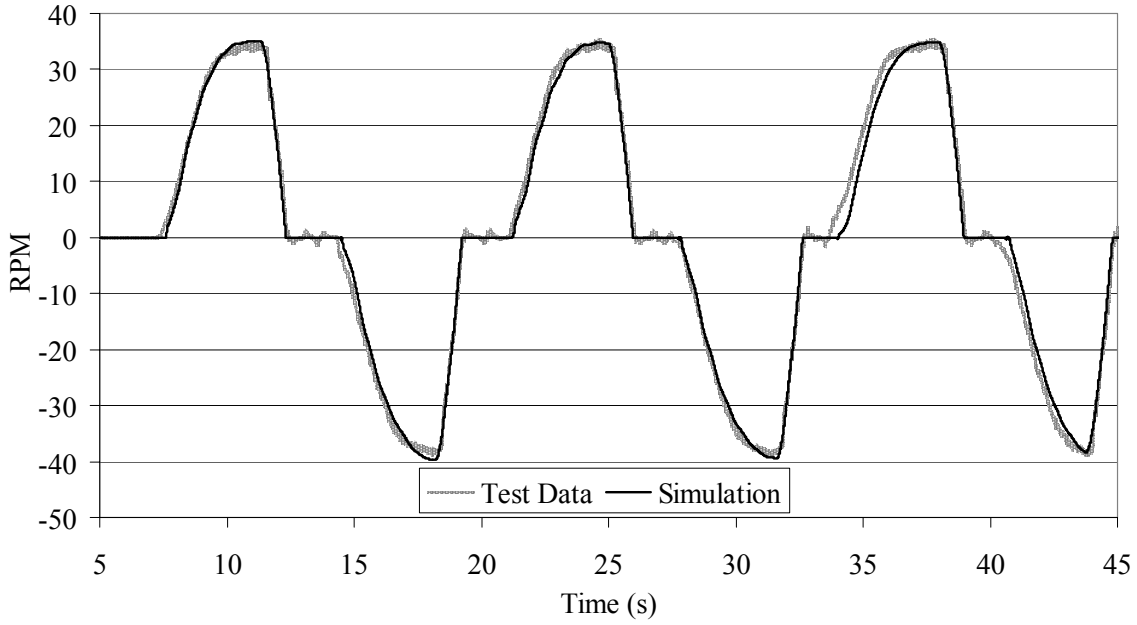

Figure 32. Front Right Wheel RPM for Brake Run 2

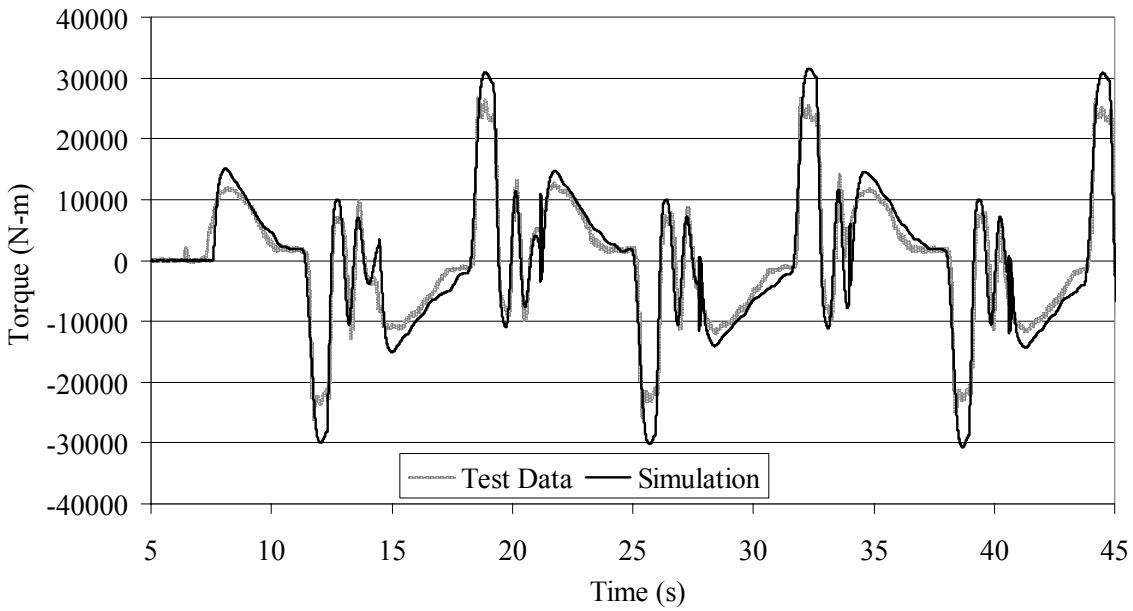

Figure 33. Total Axle Torque for Brake Run 2

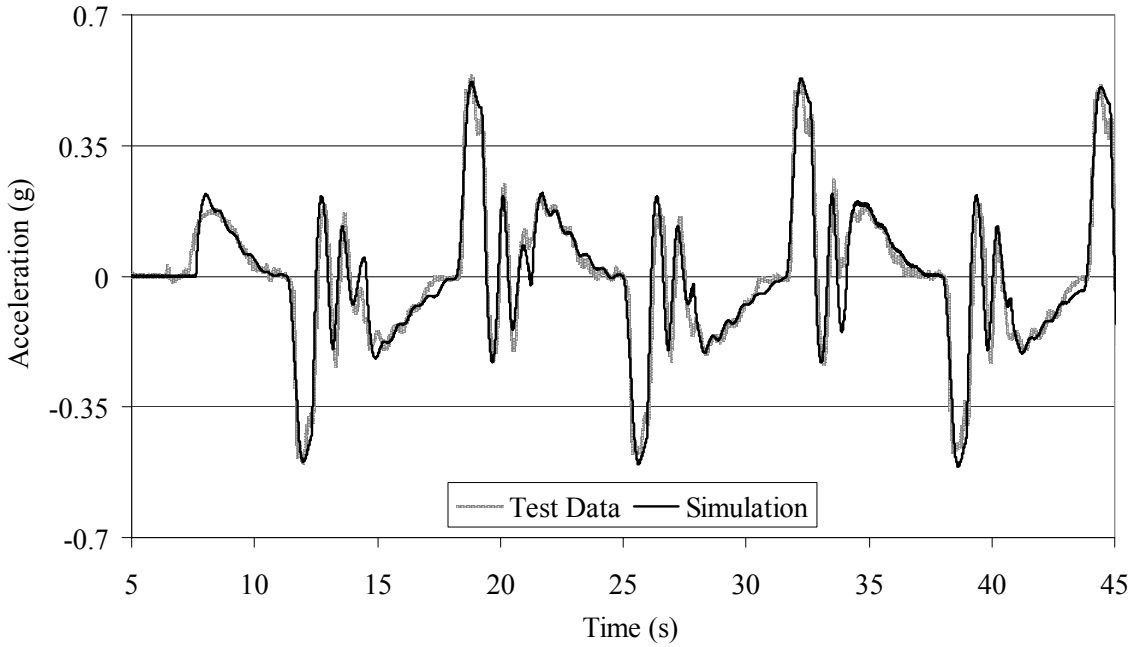

Figure 34. Fore/Aft Acceleration for Brake Run 2

Figure 31 compares the measured and simulated engine RPM. The model captures the shape and maximum/minimum RPM of the test well. The simulated engine RPM appears to lead the test results a bit. Figure 32 shows that the simulated front right wheel RPM compares reasonably well with the test data. The simulated wheel RPM has transitions which are more abrupt than the test data. Also it can be seen that the simulated wheel RPM does not oscillate after making a stop as the recorded wheel RPM does. This behavior is due to the logic that takes over when the wheels become locked. Figure 33 shows the total axle torques. The simulation appears to predict a brake torque which is higher than what was recorded during the test; however the fore/aft acceleration comparison in Figure 34 shows a good agreement between simulated and measured values.

10.5 Shift Reversal Run 1

This section compares the model simulation results with the measured vehicle behavior for a first gear shift reversal. Here the vehicle is given a full accelerator pedal command, shifted in to first gear forward, allowed to reach top speed, shifted into first gear reverse, allowed to reach top speed, and then shifted into first gear forward. One of the main goals of this current project was to determine if the NADS motion system was capable of simulating the large accelerations encountered in heavy construction equipment. In order to test whether the NADS motion system is capable of simulating these extreme accelerations, the vehicle model must be able to accurately reproduce these accelerations. The first gear shift reversal causes the largest accelerations of all engine and powertrain related driving maneuvers. Therefore, it is vital that the engine and powertrain models are able to reproduce the measured vehicle fore/aft acceleration for this particular driving maneuver. Figures 35 to 40 show the model inputs, and compare the simulated and recorded data for the first gear shift reversal. Comparisons for the second gear shift reversal are shown in Appendix C.

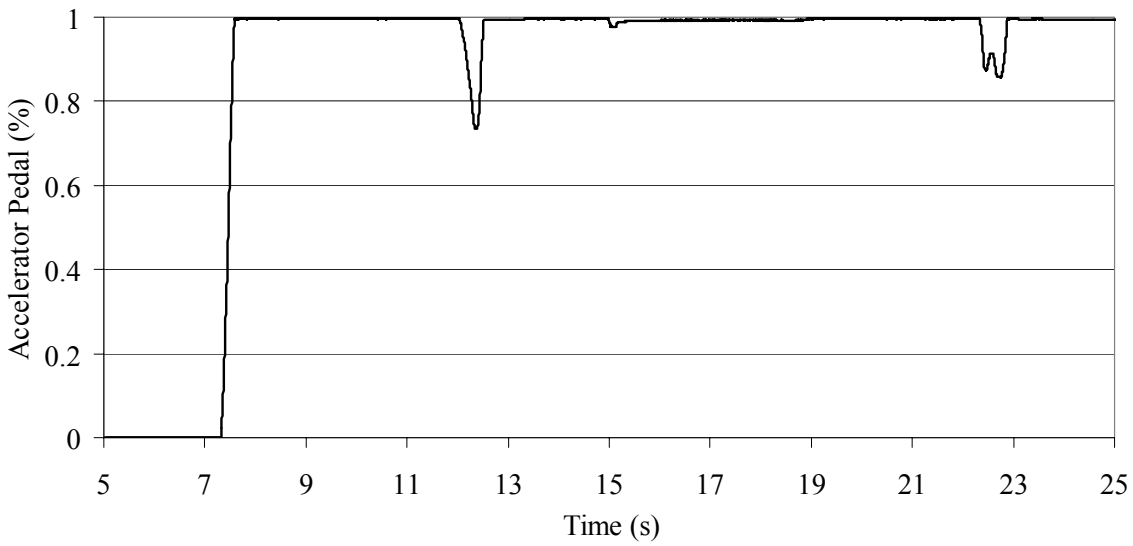

Figure 35. Accelerator Pedal Position for Reversal Run 1

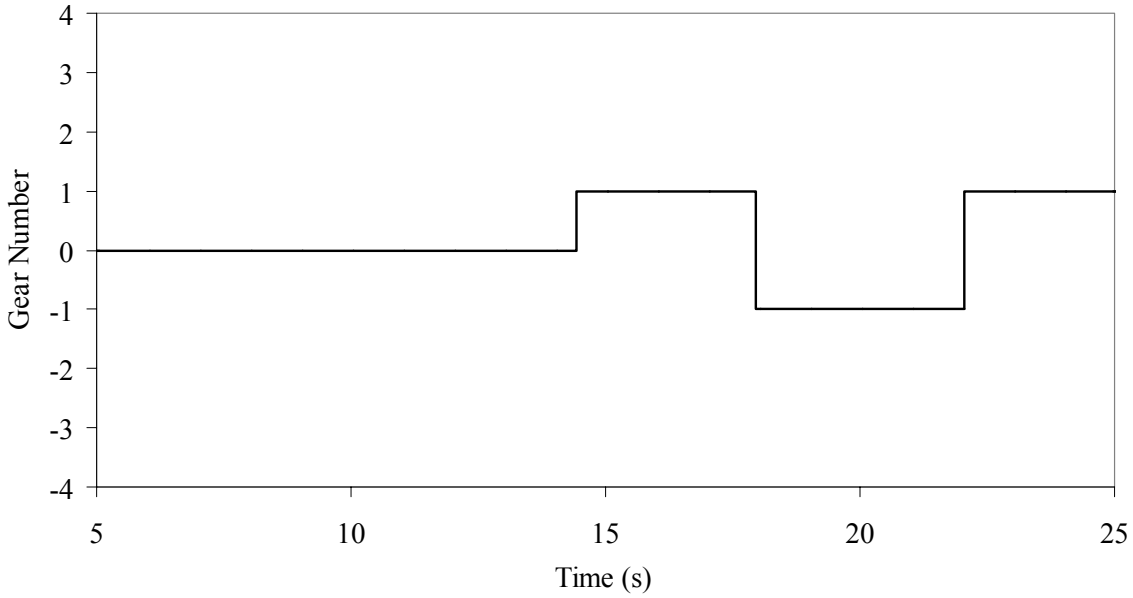

Figure 36. Gear Number for Reversal Run 1

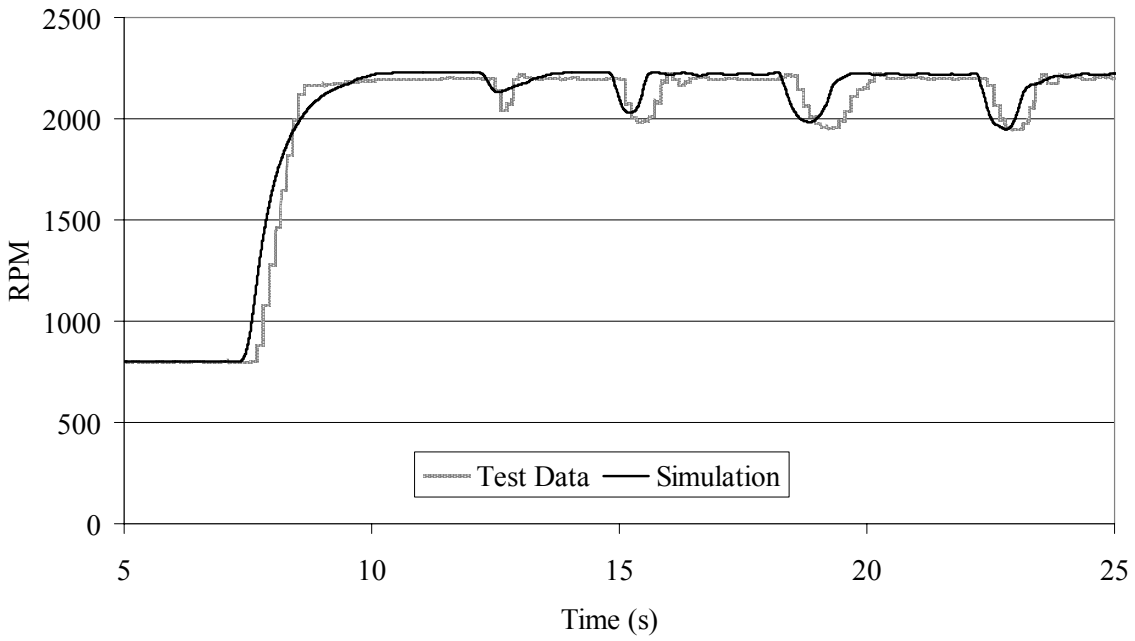

Figure 37. Engine RPM for Reversal Run 1

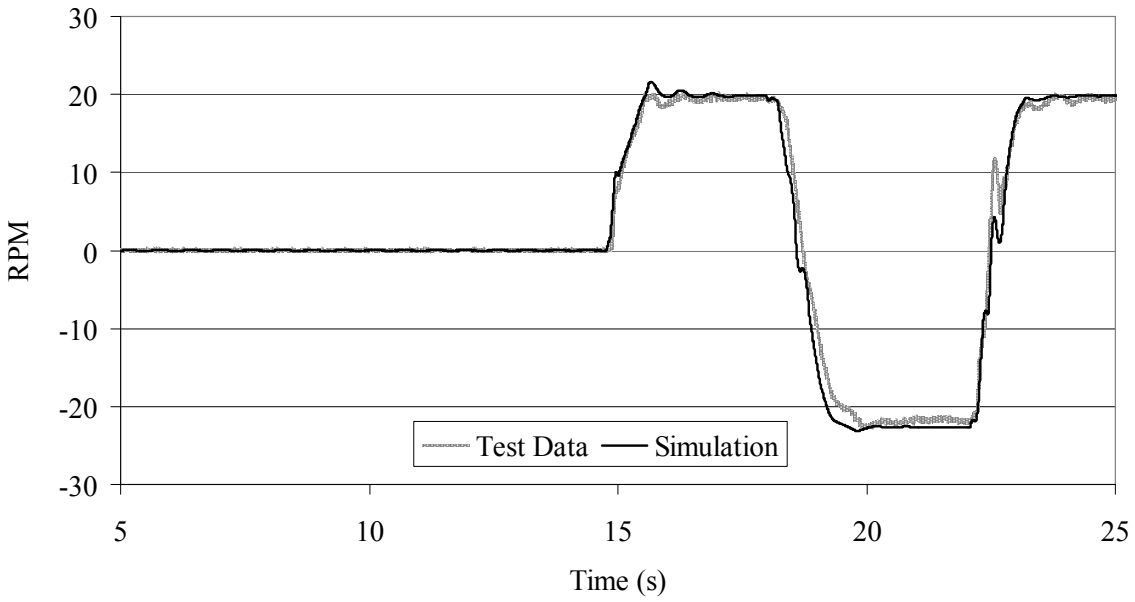

Figure 38. Front Right Wheel RPM for Reversal Run 1

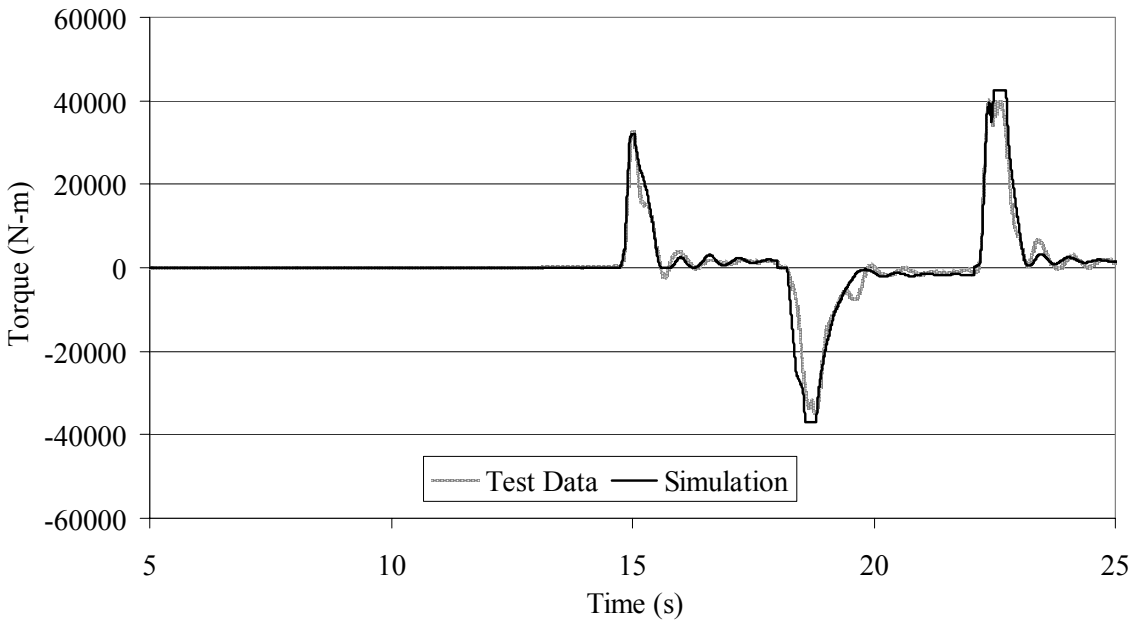

Figure 39. Total Axle Torque for Reversal Run 1

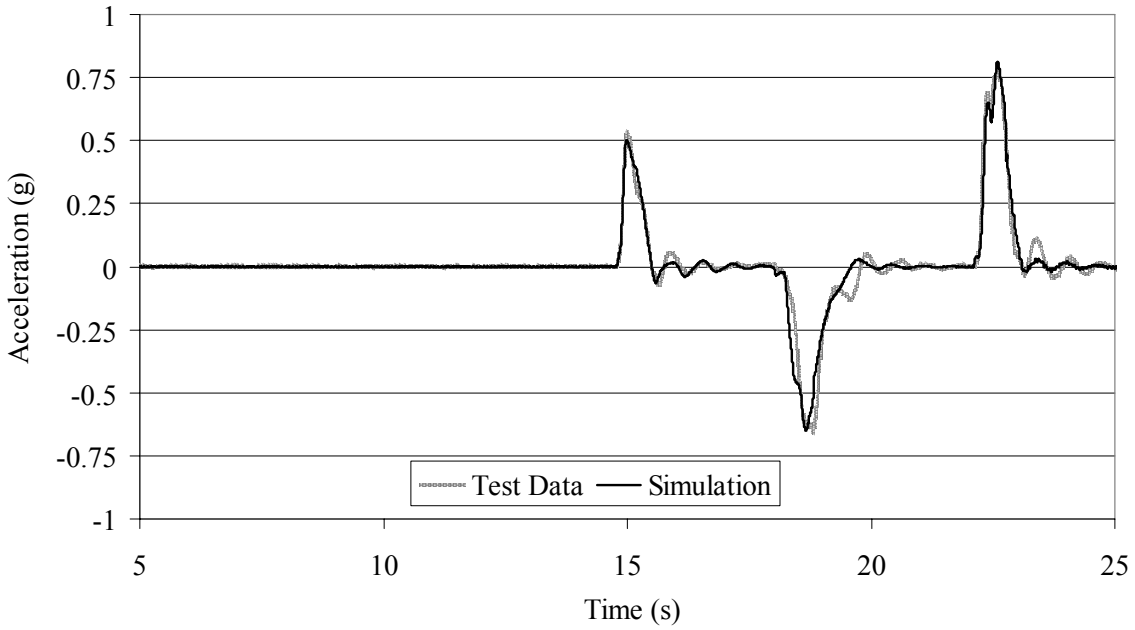

Figure 40. Fore/Aft Acceleration for Reversal Run 1

Figure 35 shows the accelerator pedal position, which is at its maximum value for the majority of the simulation. Figure 36 shows the gear number. No brake pedal position plot is included because the brakes were not used during this driving maneuver. The engine RPM comparison in Figure 37 is typical of the results for this model. The shape of the simulated engine RPM is similar to that of the recorded engine RPM, but the simulated engine RPM tends to lead the recorded RPM. Figure 38 compares the simulated front right wheel RPM to the measure value. The effect of the simulated reverse clutch being a bit too responsive is seen for the shift into first gear reverse. Here again, this may be taken care of with a more physical transmission hydraulic model, or for the purpose of the present study, by adjusting the pressure curve. A small spike is seen around the twenty two second mark in both the simulated and measured wheel RPM. This is due to wheel slip, and may also be partly due to a superimposed vehicle pitch (as the wheel RPM is measured relative to the chassis). In either case the simulation exhibits a behavior similar to the test measurements. Figure 40 compares the simulated fore/aft acceleration with the measured value. It is clear that the model is able to reproduce the level of acceleration experienced by the actual vehicle.

CHAPTER 11

SUMMARY AND CONCLUSIONS

In this thesis engine, powertrain, and brake models were described and the simulation results from the vehicle model, which included these models, were compared with test data. Different approaches to modeling an engine were discussed in Chapter 3. The engine model used was less complex than many of the engine models in use today. The simulation results indicate that the engine model is adequate for real-time simulation to reproduce the behavior of a stock 980G wheel loader. If future studies require the evaluation of different engine control strategies, then more engine subsystem models should be included—such as a turbocharger model, a fuel governor model, and intake and exhaust manifold models.

Dynamic and static torque converter models were discussed in Chapter 4. The main advantage the dynamic model has over the static model is that the effect of the fluid inertia is accounted for. The dynamic model was considered for this project because the transmission dynamics were modeled during shifts, as opposed to modeling shifts with a torque converter speed ratio blend function. Because the shift dynamics were modeled, the torque converter could experience fast speed changes and the inertia of the working fluid could have an impact on the simulation results. The drawbacks to the dynamic model are the complexity of the equations and the difficulty associated with determining the parameters needed to formulate the model. A method was outlined which solved these problems by using Hrovat and Tobler`s [13] calibration procedure to estimate the hard to find parameters, and using offline simulations of the dynamic model to determine time lags to apply to the on-line version of a static model. This method was not used in the present project because of problems encountered during the calibration procedure. The simulation results from Chapter 10 do not indicate that the static model limits the performance of the vehicle model as it pertains to the purpose of this study. However, the

effect the fluid inertia has on the turbine torque would be most evident at the beginning stages of a shift. Since the clutches will be slipping at this time, the turbine torque cannot be seen in the measured axle torques, so it is difficult to tell whether the torque response is too fast based on the measured test data. A few test simulations were run with time lags which covered the frequency range where inertia effects are reported to have influence. Including the lags did not appear to affect the simulation results.

In Chapter 5 the motivation for creating a new transmission model was discussed. A dynamic transmission model was needed for this study because shift reversals were to be simulated, and these cannot be simulated with blending functions. Chapter 6 presented methods for deriving the equations needed to model the transmission for all operating conditions. The model is based on the assumptions of infinite output shaft inertia and neglects the inertia of all but the input shaft body and one internal transmission body. The methods presented for deriving the transmission equations are not limited by these assumptions, and may be expanded for use in situations where these assumptions are not employed. Neglecting the smaller transmission bodies` inertias seems to be justifiable based on the comparisons in Chapter 10. However, the impact of the infinite output shaft inertia assumption should be investigated if this transmission model is to be used in a higher fidelity application.

Chapter 7 discussed the transmission model from the shift solenoid signals to the clutch pressure, and the clutch pressure to the clutch torque. Lack of information about the transmission hydraulics and ECM control method led to the use of predefined clutch pressure curves. In order to ensure the on-line simulation of shifts would be predictable, the off-going clutch pressure curves were set to be very steep so that clutch overlap was not captured. This is the largest limitation of the present transmission model, and is responsible for the discrepancies in the torques and accelerations from the test data during clutch-to-clutch shifts. Considering all of the models presented in this paper, the

most needed future work is the development of a physically representative transmission hydraulic model.

A clutch torque model which considers both hydrodynamic torque and asperity contact torque was qualitatively discussed in Section 7.3. The particular nature of the 980G clutches are such that the hydrodynamic contribution to the total clutch torque is assumed insignificant. If the hydrodynamic torque is required for the accurate simulation of a future vehicle transmission model, the simplified model by Berger et al. [25] is a good candidate because it hold potential for real-time applications.

Chapter 8 discussed an approximate transfer case model that can be used to model a locked transfer case with estimated drive shaft spring and damping values. This model functions very well under the present circumstances. However, if the accuracy of the simulation was to be improved from the present state, including the transmission output shaft/transfer case as an independent body is one of the first things to consider. This would require a reliable transmission output shaft/transfer case inertia value, and reliable drive shaft stiffness values.

Chapter 9 presented models for the differentials, final drives, service brakes, and parking brake. These models are fairly straight forward and appear to be adequate for the purpose of this study. The most needed work on the brake model has to do with the conditions for which the brakes lock, and this aspect of the brake model is located in the wheel body's model, which is not discussed in this paper.

Chapter 10 presented comparisons between the simulated vehicle model behavior and that measured from an actual 980G. The deviations between these data associated with the engine, powertrain, and brake models were discussed in the above paragraphs. In general, the simulated behavior for which the engine, powertrain, and brake models are responsible appear to be within the bounds for reasonably reproducing a realistic driving environment in the NADS.

In summary, the major contributions from this thesis involve the transmission, transfer case, and torque converter models. The transmission model presented in Chapter 6 is dynamically representative of the actual transmission, and as a result it can be used for a wide range of applications. This allowed for shift reversals to be simulated during this study. Also, the model was capable of interfacing directly with the vehicles` actual transmission controller. This has two advantages over programming the shift logic within the model. First, using the actual ECM ensures the shift logic will be identical to that experienced in the actual vehicle. Second, the full functionality of the transmission controller can be used. In the case of the 980G, the NADS could be run with the transmission in either automatic or manual mode. If future research leads to the creation of a hydraulic model to work with the dynamic model, NADS customers could use the simulator to test a driver`s feedback to different clutch solenoid modulation strategies using their own transmission hardware/software.

The approximate transfer case model presented in Chapter 8, though having limited fidelity, is very practical. If a locked transfer case must be modeled, and detailed vehicle information is not available (as is often the case), the approximate model is a good option to consider. The research gathered and method presented for modeling the transient behavior of the torque converter for real-time applications may be valuable in future studies. The other models used in this study were not particularly unique. However, they were implemented successfully and helped facilitate the 980G SII MWL simulation at the NADS.

APPENDIX A

HROVAT AND TOBLER TORQUE CONVERTER MODEL [13]

The four state equations, for positive axial flow are given in Equations 67-70 below. The subscripts $i, t,$ and s correspond to the impeller, turbine, and stator. The symbols used in these equations which are not either state variable or fundamental parameters are further broken down in Equations 71-82. Table A1 and Figure A1 identify the state variables and fundamental parameters.

State Equations

$$I_i\dot{\omega}_i + \rho S_i\dot{Q} = -\rho\left(\omega_i R_i^2 + R_i\frac{Q}{A}\tan[\alpha_i] - \omega_s R_s^2 - R_s\frac{Q}{A}\tan[\alpha_s]\right)Q + \tau_i \tag{67}$$

$$I_t\dot{\omega}_t + \rho S_t\dot{Q} = -\rho\left(\omega_t R_t^2 + R_t\frac{Q}{A}\tan[\alpha_t] - \omega_i R_i^2 - R_i\frac{Q}{A}\tan[\alpha_i]\right)Q + \tau_t \tag{69}$$

$$I_s\dot{\omega}_s + \rho S_s\dot{Q} = -\rho\left(\omega_s R_s^2 + R_s\frac{Q}{A}\tan[\alpha_s] - \omega_t R_t^2 - R_t\frac{Q}{A}\tan[\alpha_t]\right)Q + \tau_s \tag{69}$$

$$\begin{aligned}\rho\left(S_i\dot{\omega}_i + S_t\dot{\omega}_t + S_s\dot{\omega}_s\right) + \frac{\rho L_f}{A}\dot{Q} = \\ \rho\,\mathrm{sgn}[Q]\left(R_i^2\omega_i^2 + R_t^2\omega_t^2 + R_s^2\omega_s^2 - R_s^2\omega_i\omega_s - R_i^2\omega_t\omega_i - R_t^2\omega_s\omega_t\right) \\ +\omega_i\frac{Q}{A}\rho\left(R_i\tan[\alpha_i] - R_s\tan[\alpha_s]\right) + \omega_t\frac{Q}{A}\rho\left(R_t\tan[\alpha_t] - R_i\tan[\alpha_i]\right) \\ +\omega_s\frac{Q}{A}\rho\left(R_s\tan[\alpha_s] - R_t\tan[\alpha_t]\right) - p_L\end{aligned} \tag{70}$$

Fluid Geometric Parameters

$$S_i = \int_0^{Li} r\tan[\alpha]dl\,;\, S_t = \int_0^{Lt} r\tan[\alpha]dl\,;\, S_s = \int_0^{Ls} r\tan[\alpha]dl \tag{71,72,73}$$

$$L_f = \int_0^{L_i+L_t+L_s}\frac{dl}{\cos^2[\alpha]} \tag{74}$$

Fluid Loss Parameters

$$p_L = \frac{\rho}{2}\text{sgn}[Q]\left(C_{sh,i}V_{sh,i}^2 + C_{sh,t}V_{sh,t}^2 + C_{sh,s}V_{sh,s}^2\right) + \frac{\rho f}{2}\text{sgn}[Q]\left(V_s^{*2} + V_s^{*2} + V_s^{*2}\right) \quad (75)$$

$$V_i^* = V(1+\tan[\alpha_i]);V_t^* = V(1+\tan[\alpha_t]);V_s^* = V(1+\tan[\alpha_s]) \quad (76,77,78)$$

$$V_{sh,i} = R_s(\omega_s - \omega_i) + \frac{Q}{A}(\tan[\alpha_s] - \tan[\alpha_i']) \quad (79)$$

$$V_{sh,t} = R_i(\omega_i - \omega_t) + \frac{Q}{A}(\tan[\alpha_i] - \tan[\alpha_t']) \quad (80)$$

$$V_{sh,s} = R_i(\omega_t - \omega_s) + \frac{Q}{A}(\tan[\alpha_t] - \tan[\alpha_s']) \quad (81)$$

Table A1. Symbols for Hrovat and Tobler Model

Symbol	Description
ω	angular velocity
Q	axial flow volume, assumed spatially constant
τ	torque
V	axial torus flow velocity, assumed spatially constant
A	net flow area
r	radial coordinate
R	radius of design path at an element exit
I	combined polar moment of inertia of an element and the fluid within
ρ	mass density of fluid
α	element exit angles at design path
α'	element entrance angles at design path
α	blade angle along deign path (with no subscript)
L	length of axial projection of meridian line
C_{sh}	shock loss coefficients
f	fluid friction factor

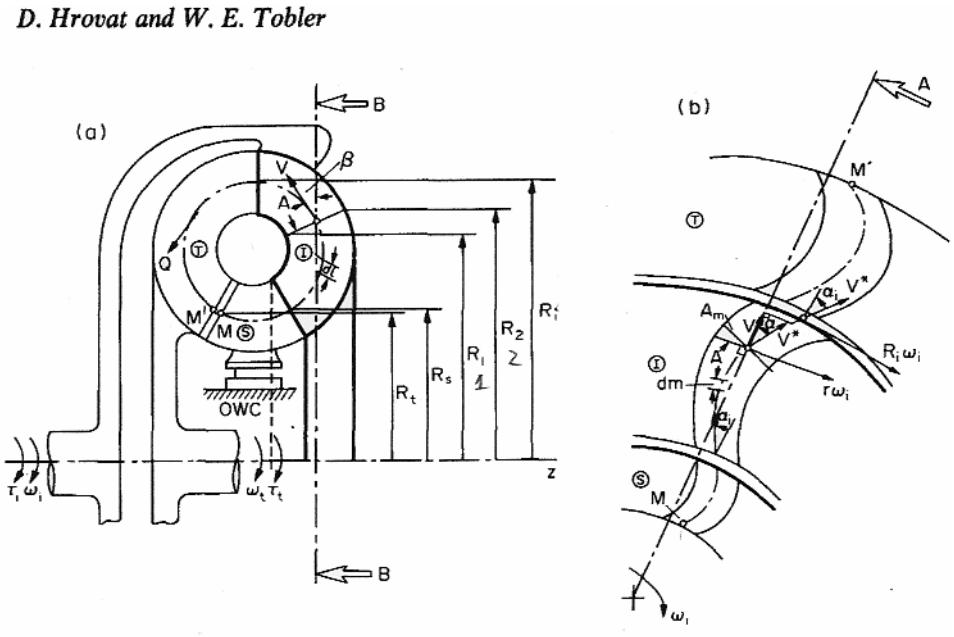

Figure A1. Torque Converter for Hrovat and Tobler Model [13]

Equations 67-69, the first three state equations, are all similar. Some insight into the nature of these equations may by examining the moment of momentum equation for the impeller. Using the relation $Q = VA$, Equation 67 may be rearranged as follows.

$$\underbrace{I_i\dot{\omega}_i + \rho S_i\dot{Q}}_{\substack{\text{Transient}\\ \text{Term}}} = \underbrace{R_s\underbrace{(\omega_s R_s + V\tan[\alpha_s])}_{\text{Total Velocity}}\rho Q}_{\substack{\text{Momentum}\\ \text{In}}} - \underbrace{R_i\underbrace{(\omega_i R_i + V\tan[\alpha_i])}_{\text{Total Velocity}}\rho Q}_{\substack{\text{Momentum}\\ \text{Out}}} + \underbrace{\tau_i}_{\substack{\text{Torque}\\ \text{In}}}$$

The fourth torque converter state equation, Equation 70, is found by application of a power balance on the torque converter system, shown in Equation 82 below.

$$\frac{dE}{dt} = P_{in} - P_{loss} \tag{82}$$

The energy, input power, and power loss given by Equations 83, 84, and 85.

$$E = \frac{1}{2}\left(I_i\omega_i^2 + I_t\omega_t^2 + I_s\omega_s^2 + \rho\frac{L_f}{A}Q^2 \right) + \rho Q\left(\omega_i S_i + \omega_t S_t + \omega_s S_s\right) \tag{83}$$

$$P_{in} = \tau_i\omega_i + \tau_t\omega_t + \tau_s\omega_s \tag{84}$$

$$P_{loss} = P_{Sh} + P_{Fl} \tag{85}$$

The power loss in Equation 85 is due to shock and friction losses, shown in Equations 86 and 87.

$$P_{Sh} = \frac{1}{2}\rho|Q|\left(C_{sh,i}V_{sh,i}^2 + C_{sh,t}V_{sh,t}^2 + C_{sh,s}V_{sh,s}^2\right) \tag{86}$$

$$P_{Fl} = \frac{1}{2}\rho|Q|f\left(V_i^{*2} + V_t^{*2} + V_s^{*2}\right) \tag{87}$$

The fourth state equation, Equation 70, can be derived by substituting the following into Equation 82: the time derivative of Equation 83, the combination of Equations 67-69 with Equation 84, and the combination of Equations 85-87.

The state equations given here represent the general case. When the stator is locked the following values will be used, as shown in Equation 88,

$$\begin{aligned} \dot{\omega}_s &= 0 \\ \omega_s &= 0 \end{aligned} \tag{88}$$

and when the stator is freewheeling, Equation 89 is used,

$$\tau_s = -\tau_{drag} \tag{89}$$

where τ_{drag} is the drag associated with the spinning of the one way clutch. For reverse flow, $Q < 0$, the equations will be similar but with the appropriate inlet and exit angles and radii interchanged.

APPENDIX B

EXAMPLE TRANSMISSION EQUATIONS USING EMBEDDING TECHNIQUE

B.1 The Embedding Technique

In this appendix the embedding technique is used to derive the transmission equations of motion—the output shaft torque equation plus one differential equation per degree of freedom—for the same cases presented in the text: mode 15, mode 9, and mode 4. The resultant equations are shown to be identical to those derived in the text. First the embedding technique equations are presented. Following this the constraint equations for the transmission are presented. Then the transmission equations for mode 15, 9, and 4 are calculated.

The embedding technique can be used to derive a minimum number of differential equations expressed in terms of the system's independent coordinates [33]. The embedding technique is useful when modeling systems with many interconnected parts, if the system degrees of freedom can be identified and the constraint forces are not required. Based directly on the formulation of Shabana [33], assuming mass centroidal body reference frames, the embedding technique equations summarized as follows. The independent accelerations are solved for as shown in Equation 90,

$$\ddot{\mathbf{q}}_{\mathrm{i}} = \overline{\mathbf{M}}_i^{-1}\overline{\mathbf{Q}}_i \tag{90}$$

where $\ddot{\mathbf{q}}_{\mathrm{i}}$ is the vector of independent accelerations and the first term on the right hand side of Equation 90 is given below in Equation 91,

$$\overline{\mathbf{M}}_i^{-1} = \mathbf{B}_i^{\mathrm{T}}\mathbf{M}\mathbf{B}_i \tag{91}$$

where $\mathbf{B}_i$ is the velocity transformation matrix and $\mathbf{M}$ is the mass matrix arranged with the independent coordinates occupying the lower rows. The velocity transformation matrix is constructed as shown in Equation 92,

$$\mathbf{B}_i = \begin{bmatrix} -\mathbf{C}_{\mathbf{q}d}^{-1}\mathbf{C}_{\mathbf{q}i} \\ \mathbf{I} \end{bmatrix} \tag{92}$$

where $\mathbf{C}_{\mathbf{q}d}$ and $\mathbf{C}_{\mathbf{q}i}$ are the dependent and independent sub matrices from the constraint Jacobian matrix. The matrix $\overline{\mathbf{Q}}_i$ is defined in Equation 93,

$$\overline{\mathbf{Q}}_i = \mathbf{B}_i^{\mathrm{T}}\mathbf{Q}_e - \mathbf{B}_i^{\mathrm{T}}\mathbf{M}\boldsymbol{\gamma}_i \tag{93}$$

where $\mathbf{Q}_e$ is the vector of generalized external forces, ordered such that the forces associated with the independent coordinates occupy the lower rows of the vector. The term $\boldsymbol{\gamma}_i$ is zero when the constraints are linear and not explicit function of time, which is the case here. Collecting all these equations, the independent coordinate acceleration vector is formulated as shown in Equation 94.

$$\ddot{\mathbf{q}}_i = \left[\begin{bmatrix} -\mathbf{C}_{\mathbf{q}d}^{-1}\mathbf{C}_{\mathbf{q}i} \\ \mathbf{I} \end{bmatrix}^{\mathrm{T}} \mathbf{M} \begin{bmatrix} -\mathbf{C}_{\mathbf{q}d}^{-1}\mathbf{C}_{\mathbf{q}i} \\ \mathbf{I} \end{bmatrix}\right]^{-1} \begin{bmatrix} -\mathbf{C}_{\mathbf{q}d}^{-1}\mathbf{C}_{\mathbf{q}i} \\ \mathbf{I} \end{bmatrix}^{\mathrm{T}} \mathbf{Q}e \tag{94}$$

In order to solve this equation for the independent coordinates, the constraint Jacobian must be set up and partitioned into dependent and independent parts, the mass matrix must be defined, and the vector of generalized external forces must be defined.

B.2 The General Transmission Equations

The general constraint equation for a planetary gear set is given in Equation 95,

$$\theta_S - \theta_C(1+e) + \theta_R e = 0 \tag{95}$$

where $\theta_S, \theta_C,$ and θ_R are the rotational coordinates of the sun gear, planet carrier, and ring gears respectively. The term e is the ratio of the number of teeth (or contact radius) on the ring gear to the number of teeth (or contact radius) on the sun gear. The gear set constraints for the 980G transmission are given below in Equations 96-100.

$$\theta_1 - \theta_2(1+e_1) + \theta_3 e_1 = Const \tag{96}$$

$$\theta_1 - \theta_3(1+e_2) + \theta_4 e_2 = Const \tag{97}$$

$$\theta_8 - \theta_3(1+e_3) + \theta_5 e_3 = Const \tag{98}$$

$$\theta_8 - \theta_5(1+e_4) + \theta_6 e_4 = Const \tag{99}$$

$$\theta_6 - \theta_8(1+e_5) + \theta_7 e_5 = Const \tag{100}$$

where the term $Const$ is used to represent an arbitrary constant value (there is no need to keep track of the angular displacement of the coordinates in this case). The vector of generalized coordinates may be ordered as shown in Equation 101.

$$\mathbf{q} = \begin{bmatrix} \theta_2 & \theta_4 & \theta_5 & \theta_6 & \theta_7 & \theta_3 & \theta_1 & \theta_8 \end{bmatrix}^{\mathrm{T}} \tag{101}$$

The mass matrix corresponding to this order is shown in Equation 102,

$$\mathbf{M} = \begin{bmatrix} J_2 & 0 & 0 & 0 & 0 & 0 & 0 & 0 \\ 0 & J_4 & 0 & 0 & 0 & 0 & 0 & 0 \\ 0 & 0 & J_5 & 0 & 0 & 0 & 0 & 0 \\ 0 & 0 & 0 & J_6 & 0 & 0 & 0 & 0 \\ 0 & 0 & 0 & 0 & J_7 & 0 & 0 & 0 \\ 0 & 0 & 0 & 0 & 0 & J_3 & 0 & 0 \\ 0 & 0 & 0 & 0 & 0 & 0 & J_1 & 0 \\ 0 & 0 & 0 & 0 & 0 & 0 & 0 & J_8 \end{bmatrix} \tag{102}$$

B.3 Equations for Mode 15

Considering first the case when no clutches are locked, there will be three degrees of freedom. Coordinates 1, 3, and 8 are selected to be independent. The vector of generalized external forces is shown in Equation 103.

$$\mathbf{Q}e = \begin{bmatrix} -T_{CL1}\,\mathrm{sgn}[\omega_{CL1}] \\ -T_{CL2}\,\mathrm{sgn}[\omega_{CL2}] \\ -T_{CL3}\,\mathrm{sgn}[\omega_{CL3}] \\ -T_{CL4}\,\mathrm{sgn}[\omega_{CL4}] - T_{CL5}\,\mathrm{sgn}[\omega_{CL5}] \\ -T_{CL6}\,\mathrm{sgn}[\omega_{CL6}] \\ 0 \\ T_{In} \\ -T_{Out} + T_{CL5}\,\mathrm{sgn}[\omega_{CL5}] \end{bmatrix} \tag{103}$$

For this transmission mode, no clutch constraints are imposed; only the gear set constraints active The constraint Jacobian can be constructed and partitioned as shown in Equation 104.

$$\mathbf{C}_{\mathbf{q}d}\delta\mathbf{q}_d + \mathbf{C}_{\mathbf{q}i}\delta\mathbf{q}_i = \begin{bmatrix} -(1+e_1) & 0 & 0 & 0 & 0 \\ 0 & e_2 & 0 & 0 & 0 \\ 0 & 0 & e_3 & 0 & 0 \\ 0 & 0 & -(1+e_4) & e_4 & 0 \\ 0 & 0 & 0 & 1 & e_5 \end{bmatrix} \begin{bmatrix} \delta\theta_2 \\ \delta\theta_4 \\ \delta\theta_5 \\ \delta\theta_5 \\ \delta\theta_7 \end{bmatrix} + \begin{bmatrix} e_1 & 1 & 0 \\ -(1+e_2) & 1 & 0 \\ -(1+e_3) & 0 & 1 \\ 0 & 0 & 1 \\ 0 & 0 & -(1+e_5) \end{bmatrix} \begin{bmatrix} \delta\theta_3 \\ \delta\theta_1 \\ \delta\theta_8 \end{bmatrix} = \mathbf{0} \tag{104}$$

Substituting the results from Equations 102-104 into Equation 94 will give the independent accelerations. If the inertias of bodies 2, 4, 5, 6, and 7 are set equal to zero, Equations 105-107 are obtained.

$$\begin{aligned} \ddot{\theta}_3 = \frac{1}{J_3}\Bigg(& -\frac{e_1}{1+e_1}T_{CL1}\,\mathrm{sgn}[\omega_{CL1}] - \frac{1+e_2}{e_2}T_{CL2}\,\mathrm{sgn}[\omega_{CL2}] - \frac{1+e_3}{e_3}T_{CL3}\,\mathrm{sgn}[\omega_{CL3}] \\ & - \frac{(1+e_3)(1+e_4)}{e_3e_4}T_{CL4}\,\mathrm{sgn}[\omega_{CL4}] - \frac{(1+e_3)(1+e_4)}{e_3e_4}T_{CL5}\,\mathrm{sgn}[\omega_{CL5}] \\ & + \frac{(1+e_3)(1+e_4)}{e_3e_4e_5}T_{CL6}\,\mathrm{sgn}[\omega_{CL6}]\Bigg) \end{aligned} \tag{105}$$

$$\ddot{\theta}_1 = \frac{1}{J_1}\left(T_{In} - \frac{1}{1+e_1}T_{CL1}\,\mathrm{sgn}[\omega_{CL1}] + \frac{1}{e_2}T_{CL2}\,\mathrm{sgn}[\omega_{CL2}]\right) \tag{106}$$

$$\begin{aligned} \ddot{\theta}_8 = \frac{1}{J_8}\Bigg(& -T_{Out} + \frac{1}{e_3}T_{CL3}\,\mathrm{sgn}[\omega_{CL3}] + \frac{1+e_3+e_4}{e_3e_4}T_{CL4}\,\mathrm{sgn}[\omega_{CL4}] \\ & + \frac{(1+e_3)(1+e_4)}{e_3e_4}T_{CL5}\,\mathrm{sgn}[\omega_{CL5}] - \frac{(1+e_3)(1+e_4)+e_3e_4e_5}{e_3e_4e_5}T_{CL6}\,\mathrm{sgn}[\omega_{CL6}]\Bigg) \end{aligned} \tag{107}$$

Equations 105 and 106 are the same as Equations 31 and 32 in Section 6.4.1. Assuming infinite output shaft inertia the acceleration of body 8 may be set equal to zero, Equation 107 may then be simplified and rearranged to yield Equation 33 from Section 6.4.1, which is shown again below.

$$T_{Out} = \frac{1}{e_3} T_{CL3}\,\mathrm{sgn}[\omega_{CL3}] + \frac{1+e_3+e_4}{e_3 e_4} T_{CL4}\,\mathrm{sgn}[\omega_{CL4}] + \frac{(1+e_3)(1+e_4)}{e_3 e_4} T_{CL5}\,\mathrm{sgn}[\omega_{CL5}] - \frac{(1+e_3)(1+e_4)+e_3 e_4 e_5}{e_3 e_4 e_5} T_{CL6}\,\mathrm{sgn}[\omega_{CL6}] \tag{34}$$

B.4 Equations for Mode 9

When clutch 1 is locked the rotational coordinate of body 1 and body 8 are the selected independent coordinates. The torque from clutch 1 is no longer considered in the generalized external force vector, because it is a constraint force. When clutch 1 is locked, body 2 is fixed to the transmission housing and the constraint $\theta_2 = Const$ is imposed. The generalized external force vector is shown in Equation 108, and the constraint Jacobian in partitioned form is shown in Equation 109.

$$\mathbf{Q}e = \begin{bmatrix} 0 \\ -T_{CL2}\,\mathrm{sgn}[\omega_{CL2}] \\ -T_{CL3}\,\mathrm{sgn}[\omega_{CL3}] \\ -T_{CL4}\,\mathrm{sgn}[\omega_{CL4}] - T_{CL5}\,\mathrm{sgn}[\omega_{CL5}] \\ -T_{CL6}\,\mathrm{sgn}[\omega_{CL6}] \\ 0 \\ T_{In} \\ -T_{Out} + T_{CL5}\,\mathrm{sgn}[\omega_{CL5}] \end{bmatrix} \tag{108}$$

$$\mathbf{C}_{\mathbf{q}d}\delta\mathbf{q}_d + \mathbf{C}_{\mathbf{q}i}\delta\mathbf{q}_i =$$
$$\begin{bmatrix} -(1+e_1) & 0 & 0 & 0 & 0 & e_1 \\ 0 & e_2 & 0 & 0 & 0 & -(1+e_2) \\ 0 & 0 & e_3 & 0 & 0 & -(1+e_3) \\ 0 & 0 & -(1+e_4) & e_4 & 0 & 0 \\ 0 & 0 & 0 & 1 & e_5 & 0 \\ 1 & 0 & 0 & 0 & 0 & 0 \end{bmatrix} \begin{bmatrix} \delta\theta_2 \\ \delta\theta_4 \\ \delta\theta_5 \\ \delta\theta_6 \\ \delta\theta_7 \\ \delta\theta_3 \end{bmatrix}$$
$$+ \begin{bmatrix} 1 & 0 \\ 1 & 0 \\ 0 & 1 \\ 0 & 1 \\ 0 & -(1+e_5) \\ 0 & 0 \end{bmatrix} \begin{bmatrix} \delta\theta_1 \\ \delta\theta_8 \end{bmatrix} = \mathbf{0} \tag{109}$$

Substituting the results from Equations 102, 108, and 109 into Equation 94 will give the independent accelerations. If the inertias of bodies 2, 4, 5, 6, and 7 are set equal to zero, Equations 110 and 111 result.

$$\ddot{\theta}_1 = \frac{e_1}{e_1^2 J_1 + J_3}\left(e_1 T_{In} + \frac{1+e_1+e_2}{e_2} T_{CL2}\,\mathrm{sgn}[\omega_{CL2}] + \frac{1+e_3}{e_3} T_{CL3}\,\mathrm{sgn}[\omega_{CL3}] \right.$$
$$+ \frac{(1+e_3)(1+e_4)}{e_3 e_4} T_{CL4}\,\mathrm{sgn}[\omega_{CL4}] + \frac{(1+e_3)(1+e_4)}{e_3 e_4} T_{CL5}\,\mathrm{sgn}[\omega_{CL5}] \tag{110}$$
$$\left. - \frac{(1+e_3)(1+e_4)}{e_3 e_4 e_5} T_{CL6}\,\mathrm{sgn}[\omega_{CL6}] \right)$$

$$\ddot{\theta}_8 = \frac{1}{J_8}\left(-T_{Out} + \frac{1}{e_3} T_{CL3}\,\mathrm{sgn}[\omega_{CL3}] + \frac{1+e_3+e_4}{e_3 e_4} T_{CL4}\,\mathrm{sgn}[\omega_{CL4}] \right.$$
$$\left. + \frac{(1+e_3)(1+e_4)}{e_3 e_4} T_{CL5}\,\mathrm{sgn}[\omega_{CL5}] - \frac{(1+e_3)(1+e_4)+e_3 e_4 e_5}{e_3 e_4 e_5} T_{CL6}\,\mathrm{sgn}[\omega_{CL6}] \right) \tag{111}$$

Equation 110 is the same as Equation 37 from Section 6.4.2. Assuming infinite output shaft inertia the acceleration of body 8 may be set equal to zero, Equation 111 may then be simplified and rearranged to yield equation 33 from Section 6.4.1, remembering that the output shaft torque equation is the same for mode 15 and mode 9.

B.5 Equations for Mode 4

When clutch 1 and clutch 6 are locked the rotational coordinate of body 8 is the selected independent coordinate. The torque from clutch 1 and clutch 6 are no longer considered in the generalized external force vector and the clutch constraints $\theta_2 = Const$ and $\theta_7 = Const$ are imposed. The generalized external force vector is given in Equation 112, and the partitioned constraint Jacobian is shown in Equation 113.

$$\mathbf{Q}e = \begin{bmatrix} 0 \\ -T_{CL2}\,\mathrm{sgn}[\omega_{CL2}] \\ -T_{CL3}\,\mathrm{sgn}[\omega_{CL3}] \\ -T_{CL4}\,\mathrm{sgn}[\omega_{CL4}] - T_{CL5}\,\mathrm{sgn}[\omega_{CL5}] \\ 0 \\ 0 \\ T_{In} \\ -T_{Out} + T_{CL5}\,\mathrm{sgn}[\omega_{CL5}] \end{bmatrix} \tag{112}$$

$$\mathbf{C}_{\mathbf{q}d}\delta\mathbf{q}_d + \mathbf{C}_{\mathbf{q}i}\delta\mathbf{q}_i = \begin{bmatrix} -(1+e_1) & 0 & 0 & 0 & 0 & e_1 & 1 \\ 0 & e_2 & 0 & 0 & 0 & -(1+e_2) & 1 \\ 0 & 0 & e_3 & 0 & 0 & -(1+e_3) & 0 \\ 0 & 0 & -(1+e_4) & e_4 & 0 & 0 & 0 \\ 0 & 0 & 0 & 1 & e_5 & 0 & 0 \\ 1 & 0 & 0 & 0 & 0 & 0 & 0 \\ 0 & 0 & 0 & 0 & 1 & 0 & 0 \end{bmatrix} \begin{bmatrix} \delta\theta_2 \\ \delta\theta_4 \\ \delta\theta_5 \\ \delta\theta_6 \\ \delta\theta_7 \\ \delta\theta_3 \\ \delta\theta_1 \end{bmatrix}$$

$$+ \begin{bmatrix} 0 \\ 0 \\ 1 \\ 1 \\ -(1+e_5) \\ 0 \\ 0 \end{bmatrix} \begin{bmatrix} \delta\theta_8 \end{bmatrix} = \mathbf{0} \tag{113}$$

Substituting the results from Equations 102, 112, and 113, into Equation 95 will give the independent accelerations. If the inertias of bodies 2, 4, 5, 6, and 7 are set equal to zero the following equation results.

$$\begin{aligned}\ddot{\theta}_8 = &\left(\frac{(1+e_3)^2(1+e_4)^2}{((1+e_3)(1+e_4)+e_3e_4e_5)^2(e_1^2J_1+J_3)+(1+e_3)^2(1+e_4)^2J_8}\right)\\ &\left(-T_{Out}-\frac{e_1((1+e_3)(1+e_4)+e_3e_4e_5}{(1+e_3)(1+e_4)}T_{In}\right.\\ &-\frac{(1+e_2+e_3)((1+e_3)(1+e_4)+e_3e_4e_5)}{e_2(1+e_3)(1+e_4)}T_{CL2}\,\mathrm{sgn}[\omega_{CL2}]\\ &\left.-\frac{1+e_4(1+e_5)}{1+e_4}T_{CL3}\,\mathrm{sgn}[\omega_{CL3}]-(1+e_5)T_{CL4}\,\mathrm{sgn}[\omega_{CL4}]-e_5T_{CL5}\,\mathrm{sgn}[\omega_{CL5}]\right)\end{aligned} \tag{114}$$

Assuming infinite output shaft inertia the acceleration of body 8 may be set equal to zero, Equation 114 may then be simplified and rearranged to yield Equation 42 from Section 6.4.3. Equation 42 is repeated below.

$$\begin{aligned}T_{Out} = &-\frac{e_1((1+e_3)(1+e_4)+e_3e_4e_5)}{(1+e_3)(1+e_4)}T_{In}\\ &-\frac{(1+e_1+e_2)((1+e_3)(1+e_4)+e_3e_4e_5)}{e_2(1+e_3)(1+e_4)}T_{CL2}\,\mathrm{sgn}[\omega_{CL2}]\\ &-\frac{1+e_4(1+e_5)}{1+e_4}T_{CL3}\,\mathrm{sgn}[\omega_{CL3}]-(1+e_5)T_{CL4}\,\mathrm{sgn}[\omega_{CL4}]-e_5T_{CL5}\,\mathrm{sgn}[\omega_{CL5}]\end{aligned} \tag{42}$$

APPENDIX C

FURTHER SIMULATION COMPARISONS

C.1 Acceleration Run 2

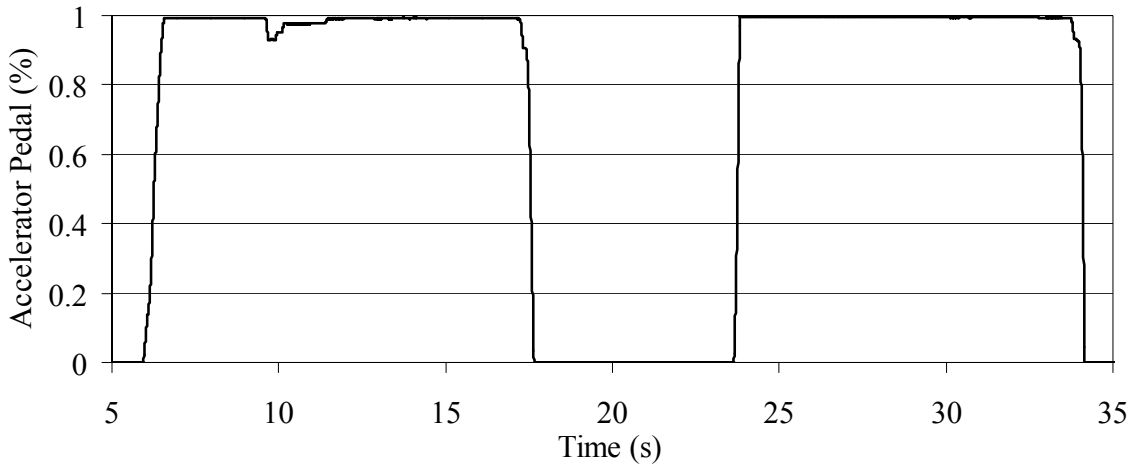

Figure C1. Accelerator Pedal Position for Acceleration Run 2

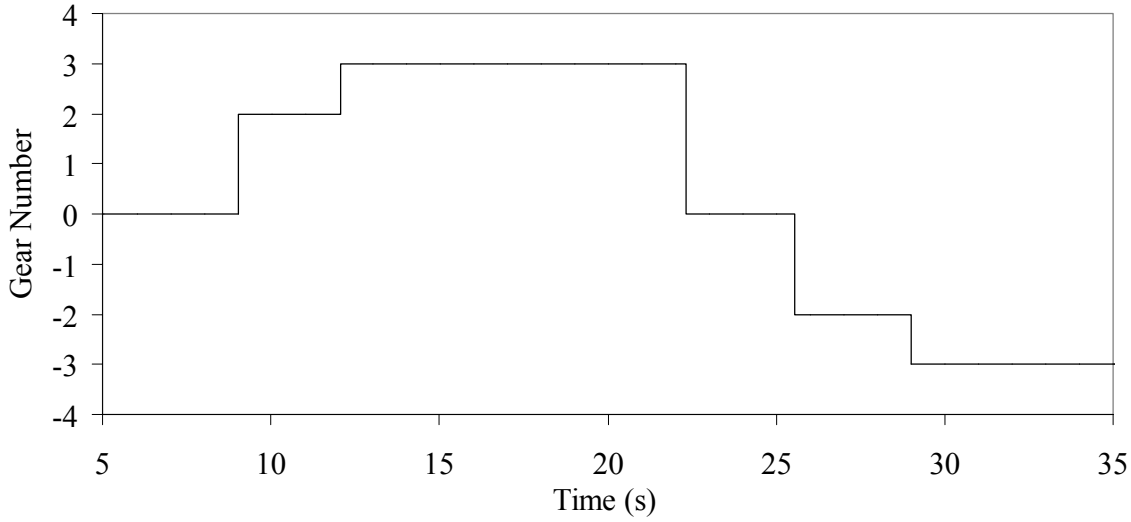

Figure C2. Gear Number for Acceleration Run 2

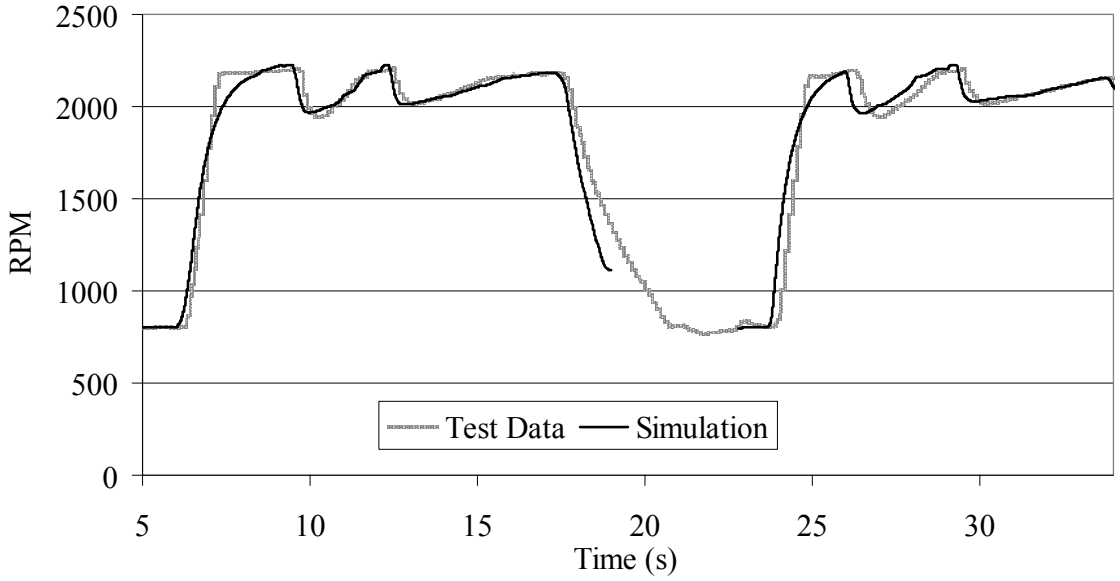

Figure C3. Engine RPM for Acceleration Run 2

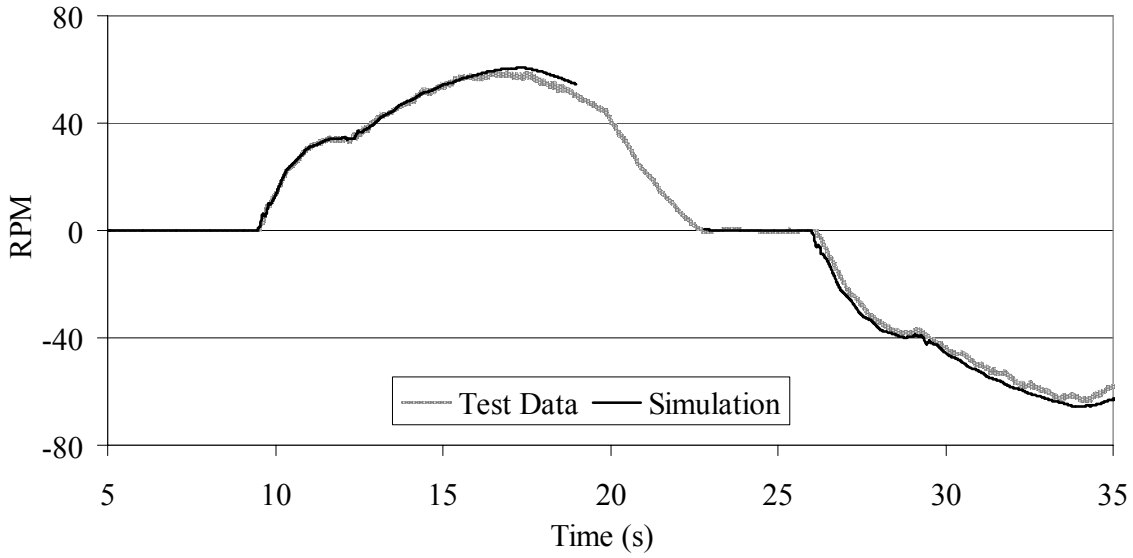

Figure C4. Front Right Wheel RPM for Acceleration Run 2

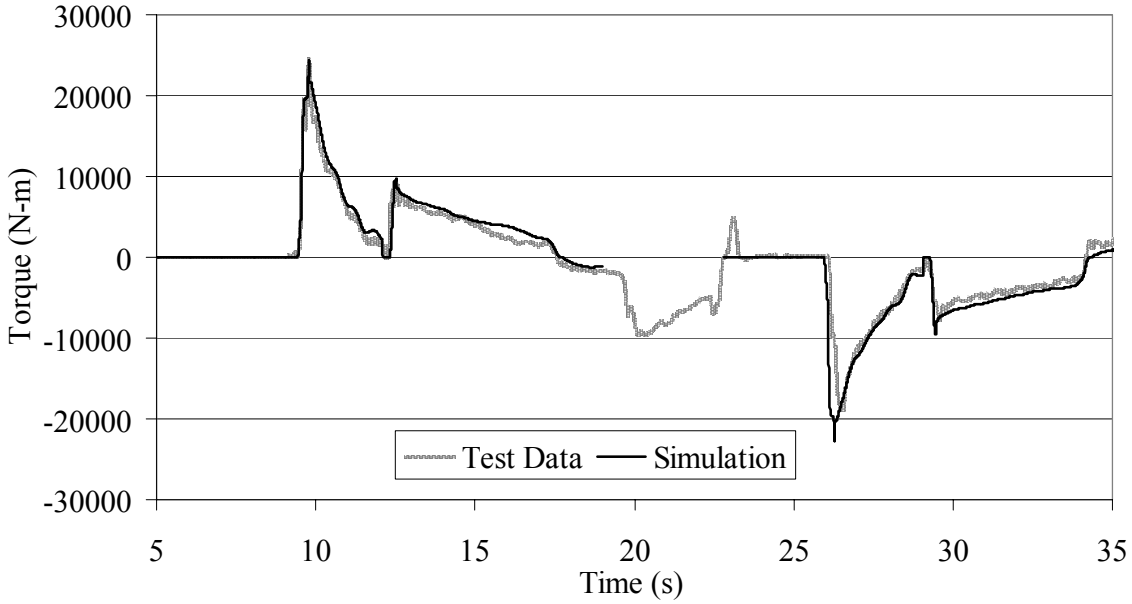

Figure C5. Total Axle Torque for Acceleration Run 2

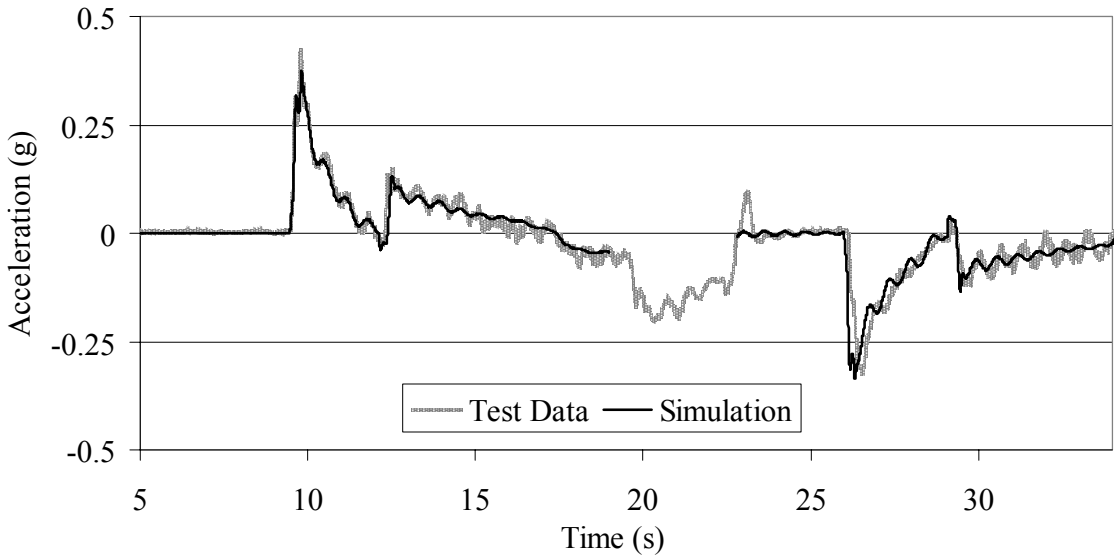

Figure C6. Fore/Aft Acceleration for Acceleration Run 2

C.2 Acceleration Run 3

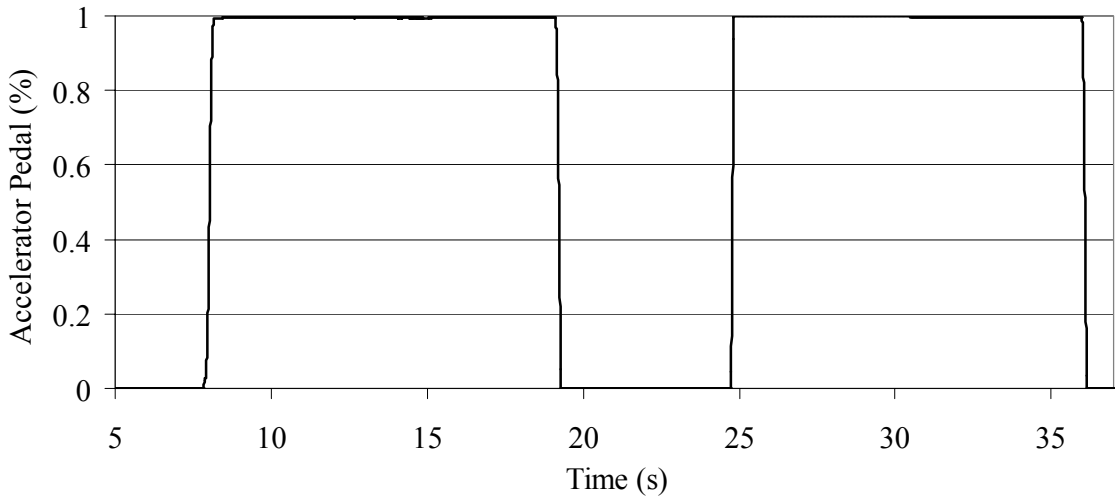

Figure C7. Accelerator Pedal Position for Acceleration Run 3

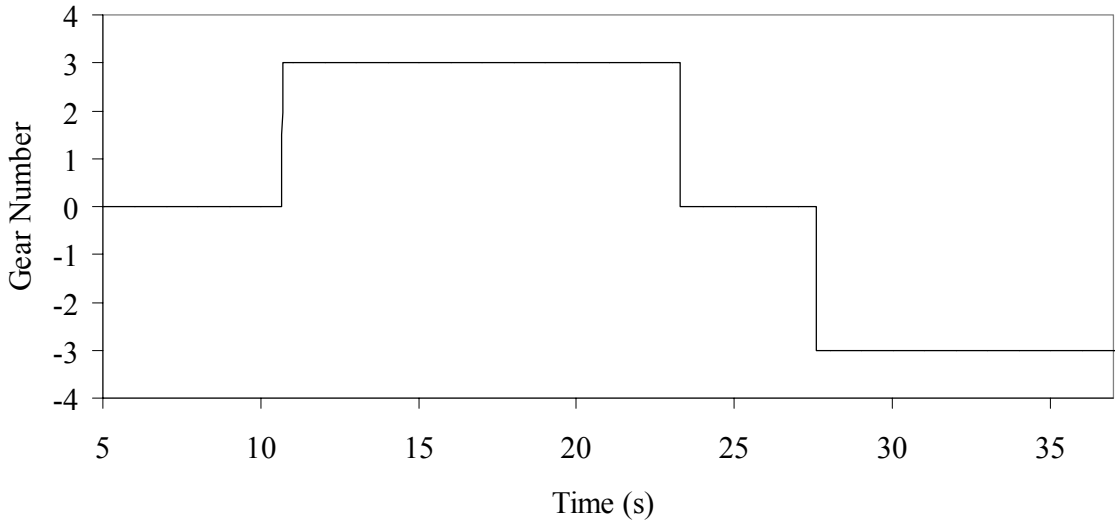

Figure C8. Gear Number for Acceleration Run 3

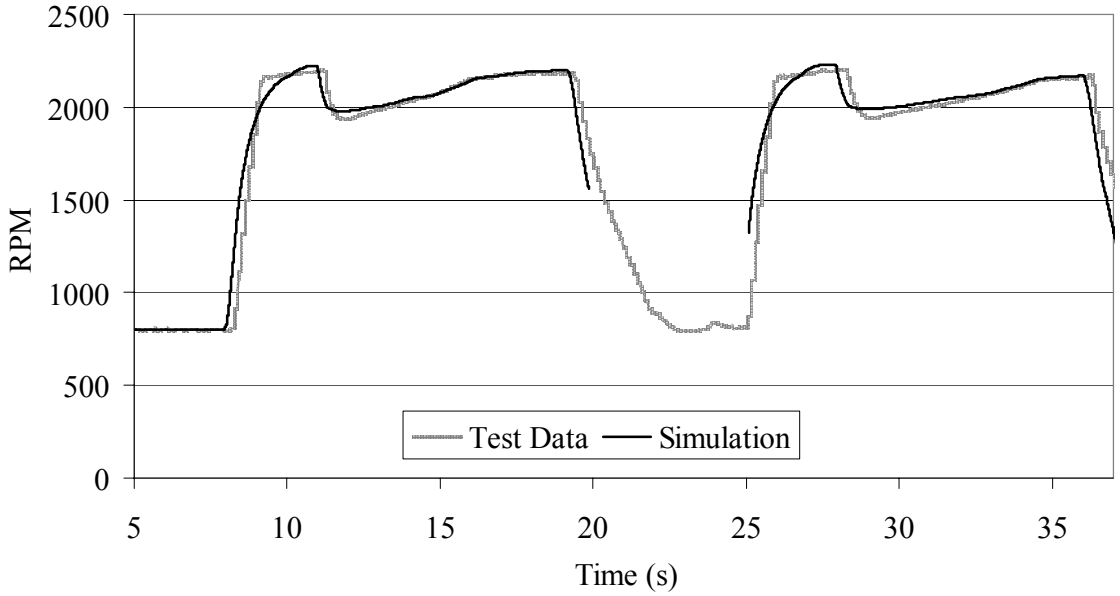

Figure C9. Engine RPM for Acceleration Run 3

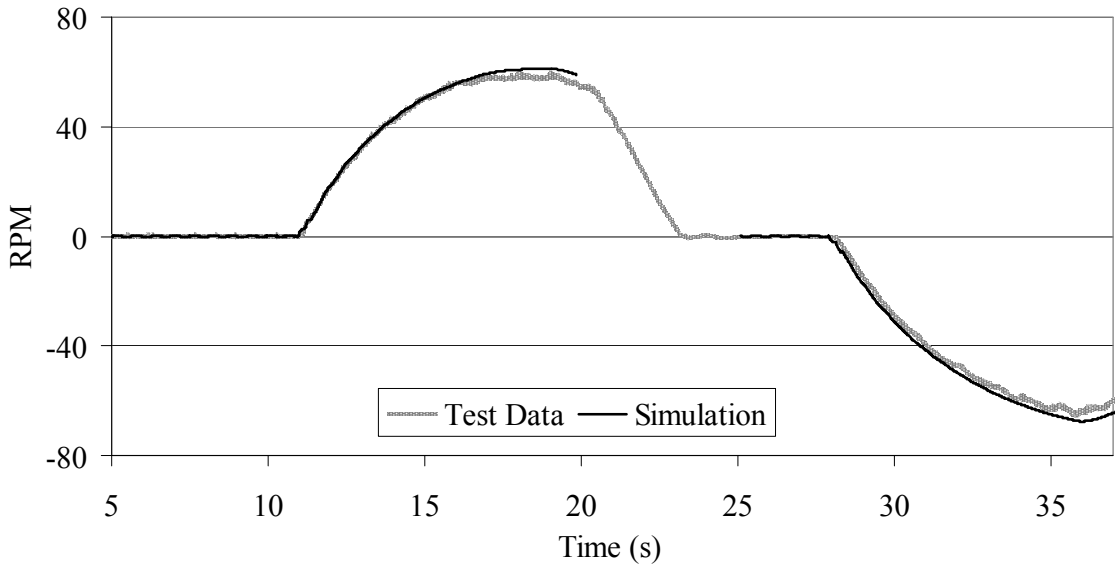

Figure C10. Front Right Wheel RPM for Acceleration Run 3

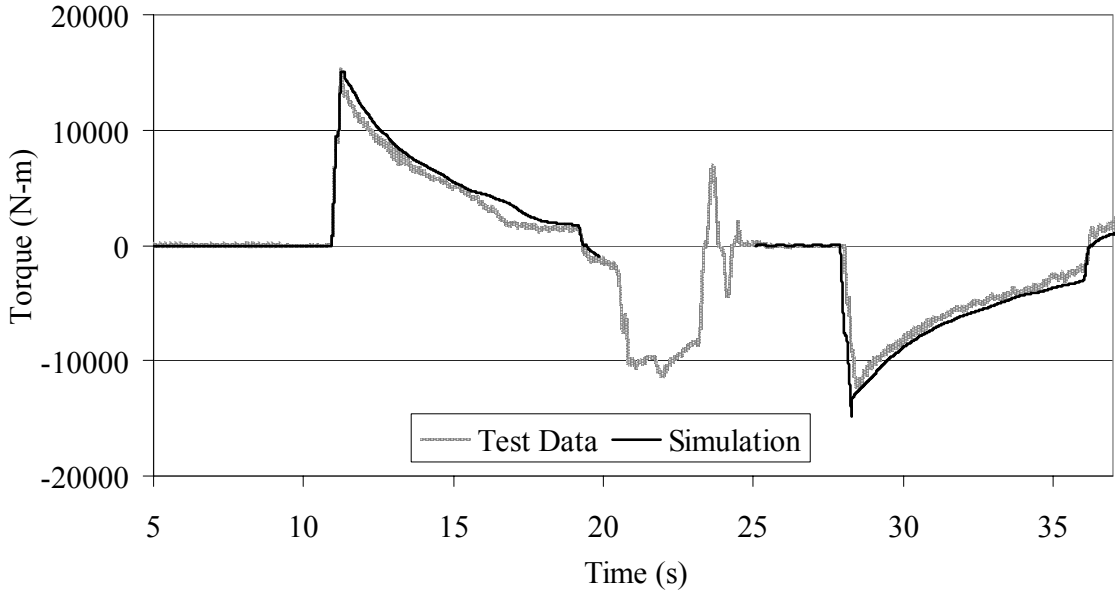

Figure C11. Total Axle Torque for Acceleration Run 3

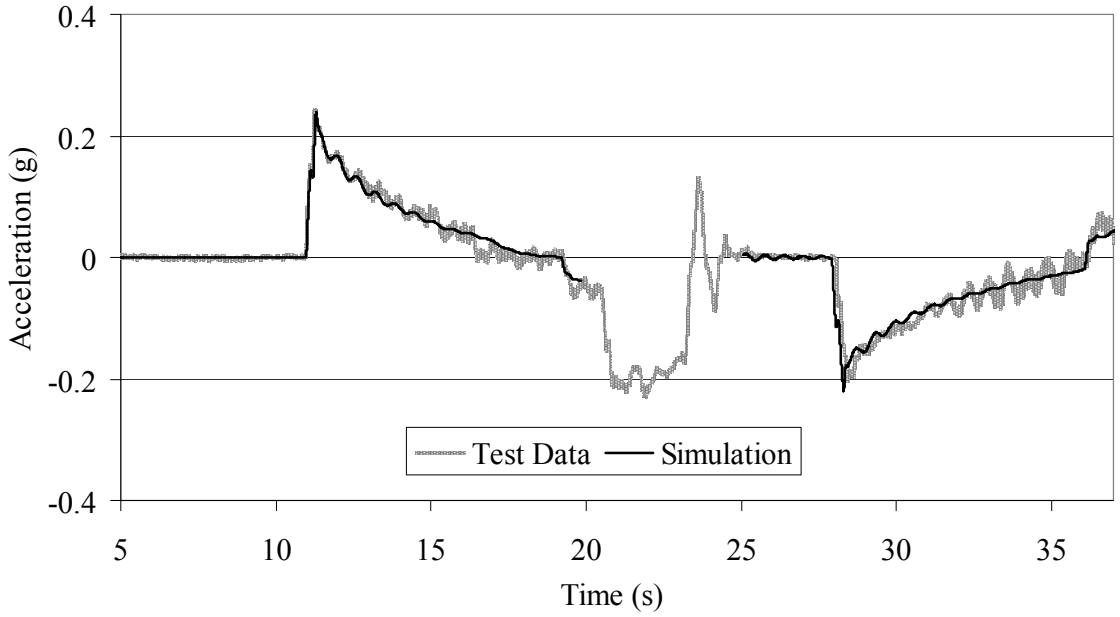

Figure C12. Fore/Aft Acceleration for Acceleration Run 3

C.3 Brake Run 1

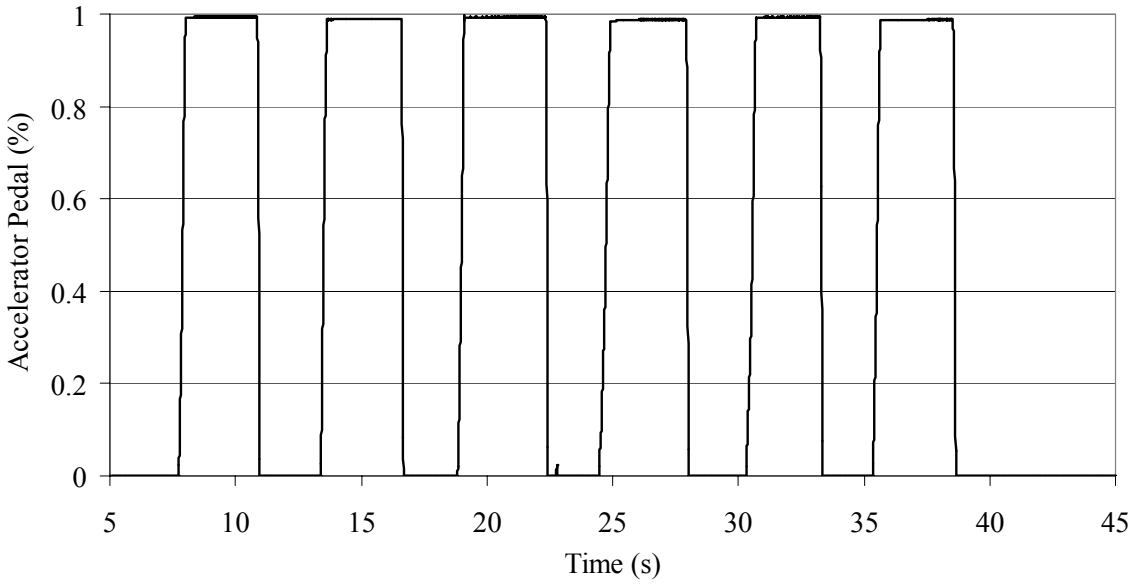

Figure C13. Accelerator Pedal Position for Brake Run 1

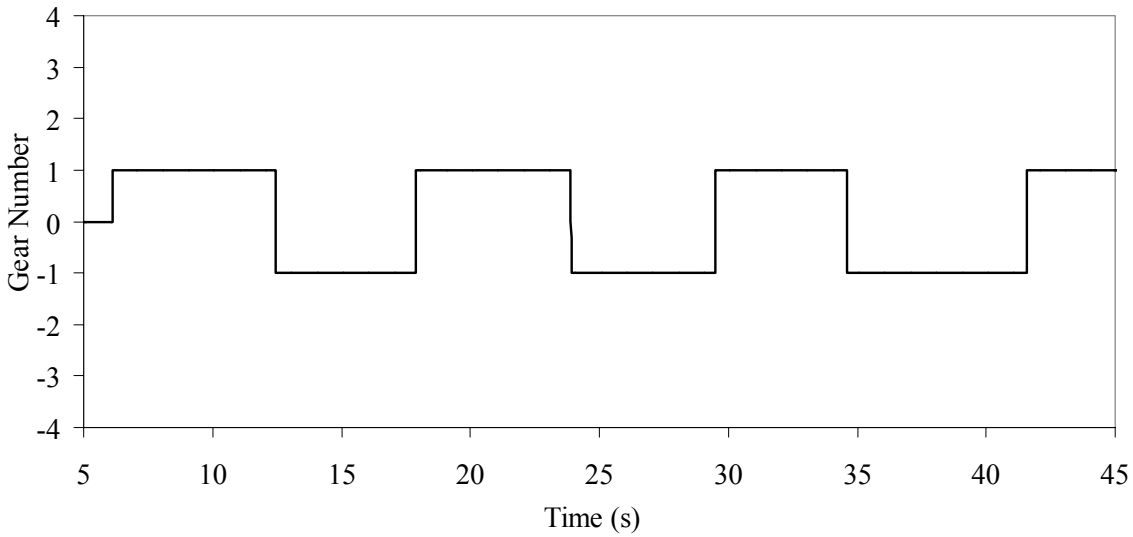

Figure C14. Gear Number for Brake Run 1

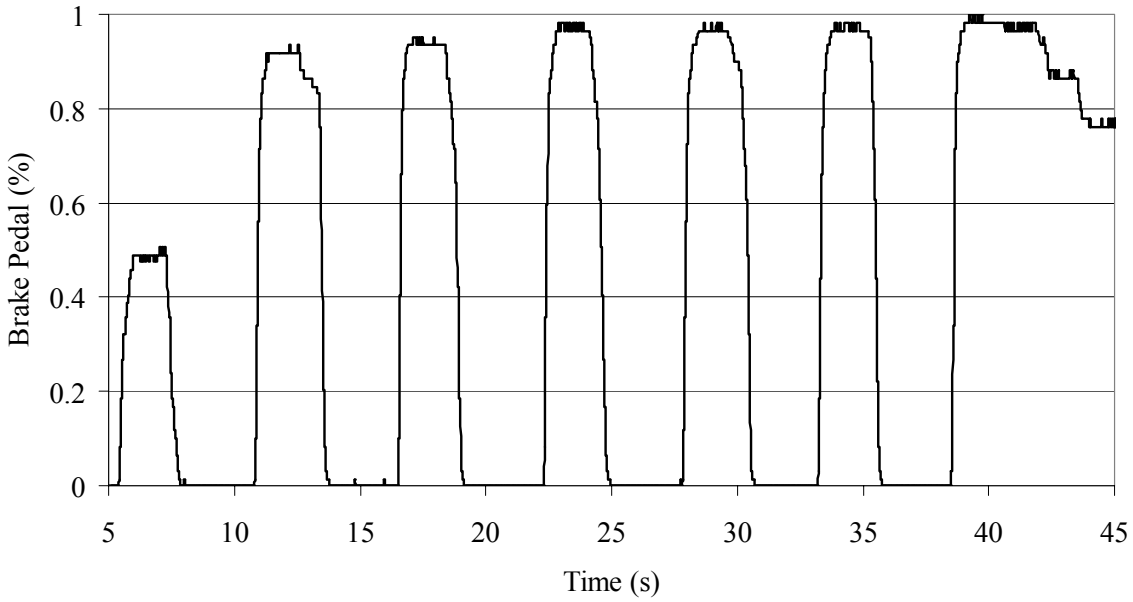

Figure C15. Brake Pedal Position for Brake Run 1

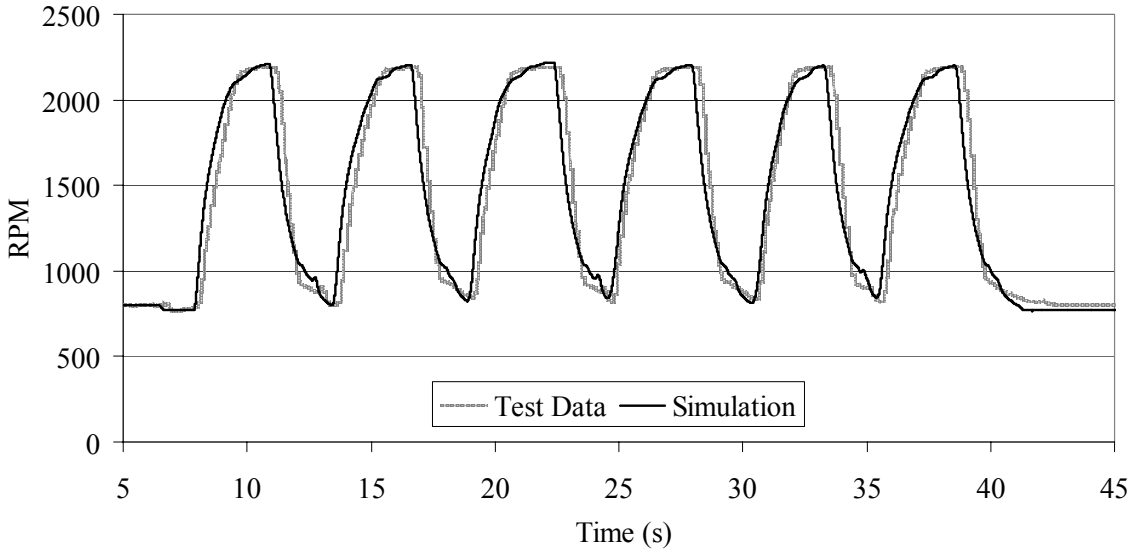

Figure C16. Engine RPM for Brake Run 1

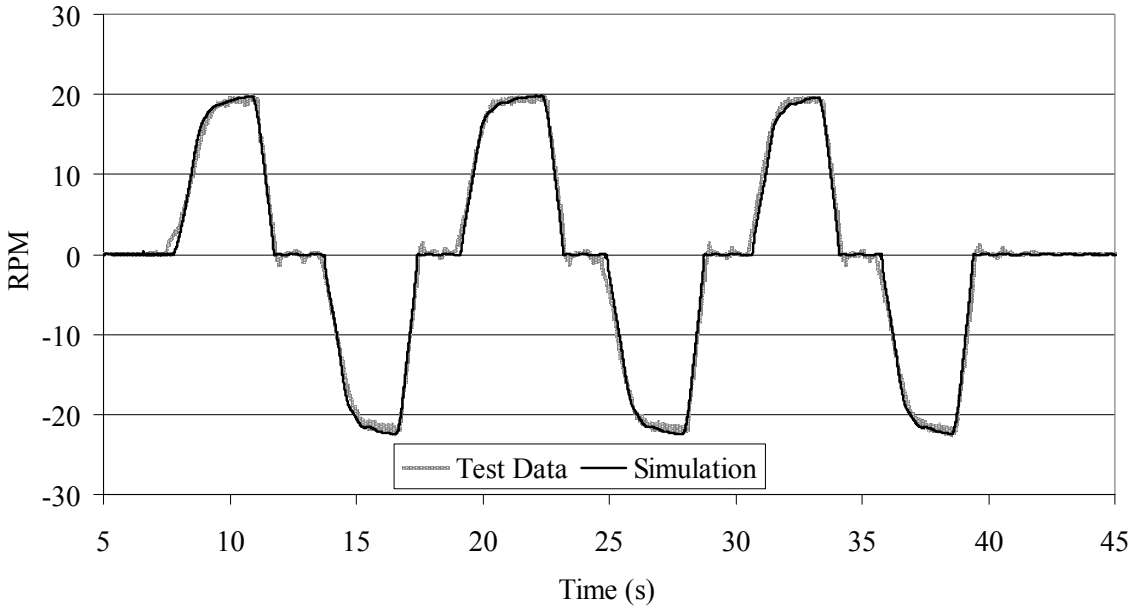

Figure C17. Front Right Wheel RPM for Brake Run 1

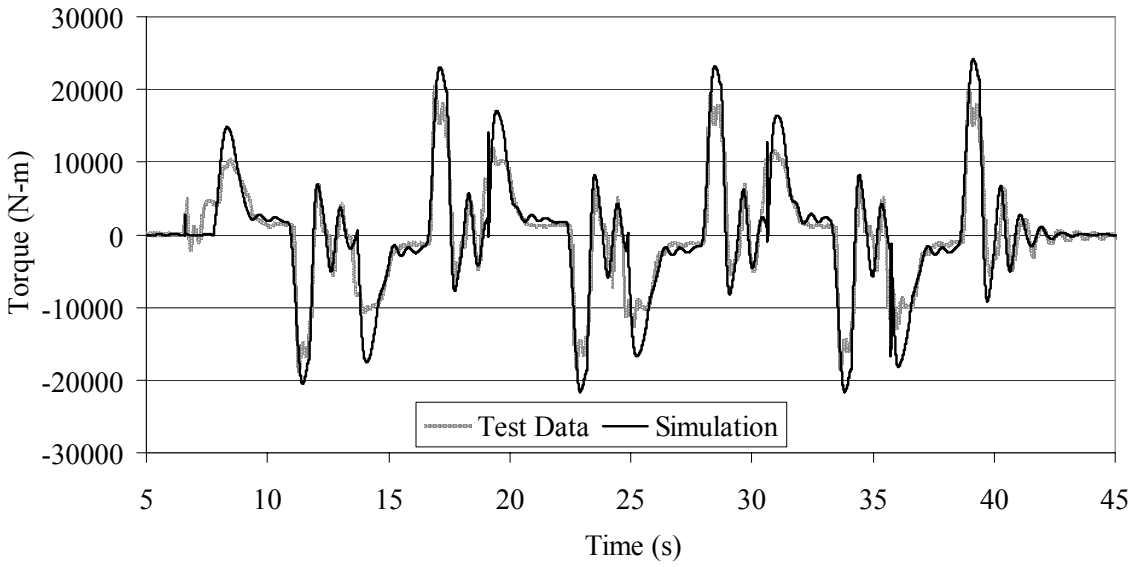

Figure C18. Total Axle Torque for Brake Run 1

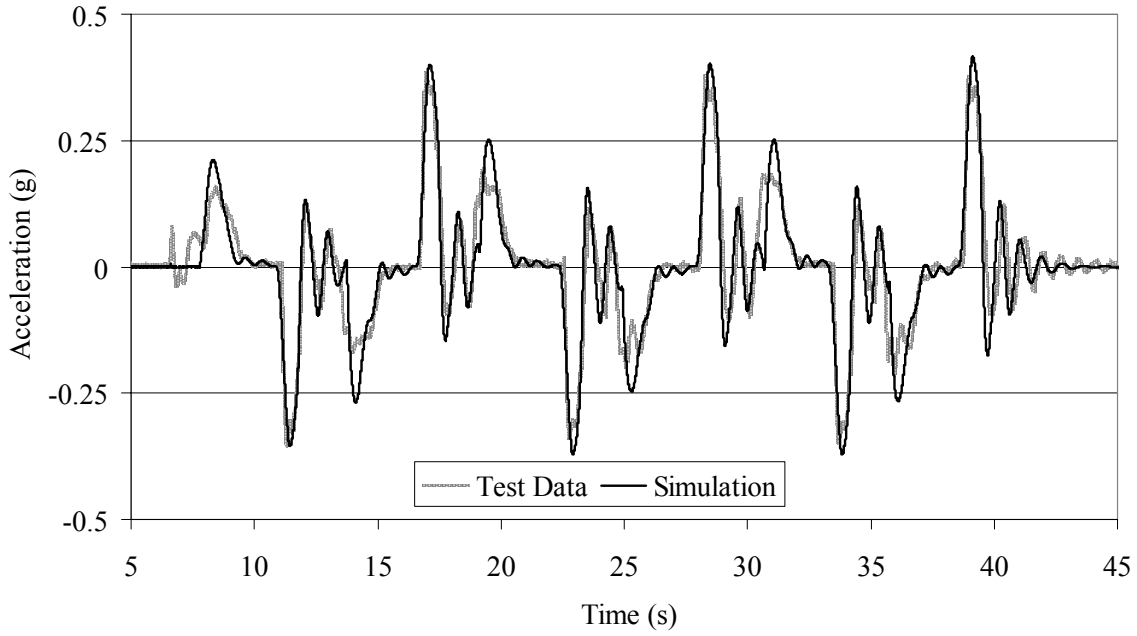

Figure C19. Fore/Aft Acceleration for Brake Run 1

C.4 Shift Reversal Run 2

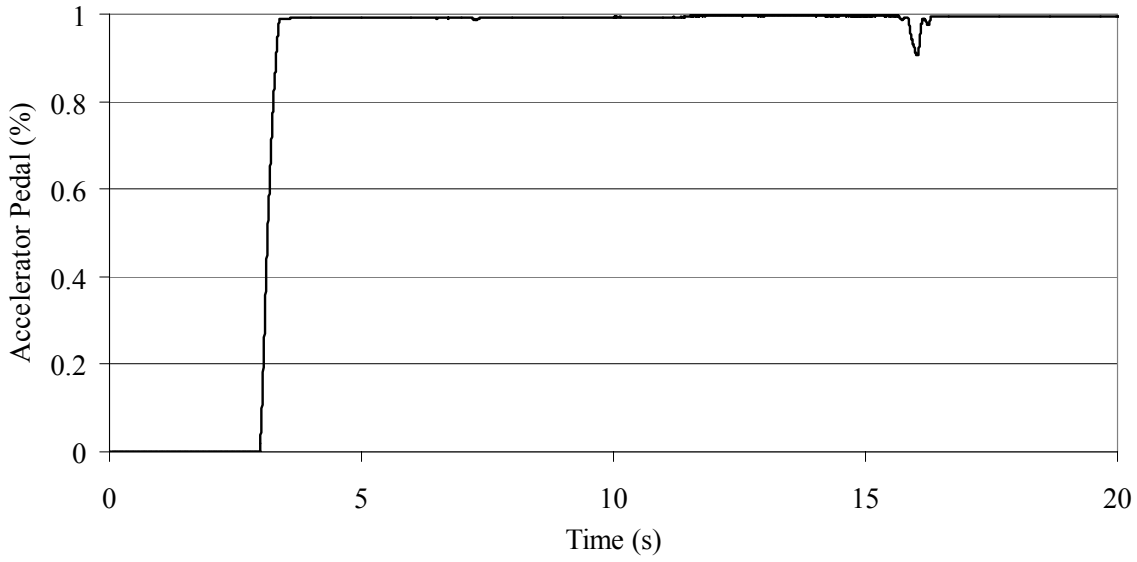

Figure C20. Accelerator Pedal Position for Reversal Run 2

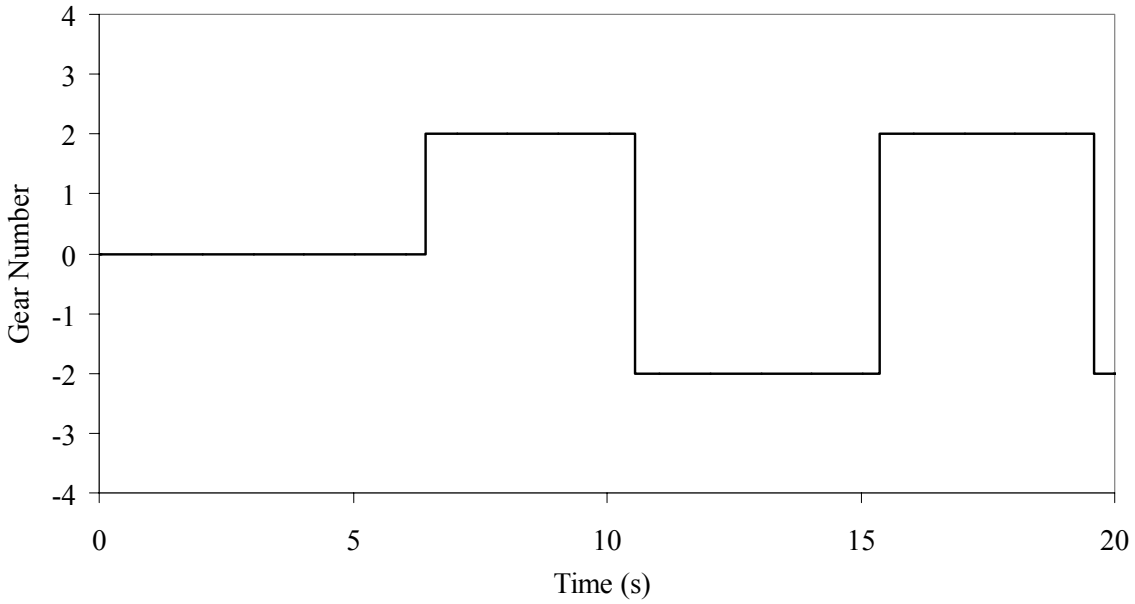

Figure C21. Gear Number for Reversal Run 2

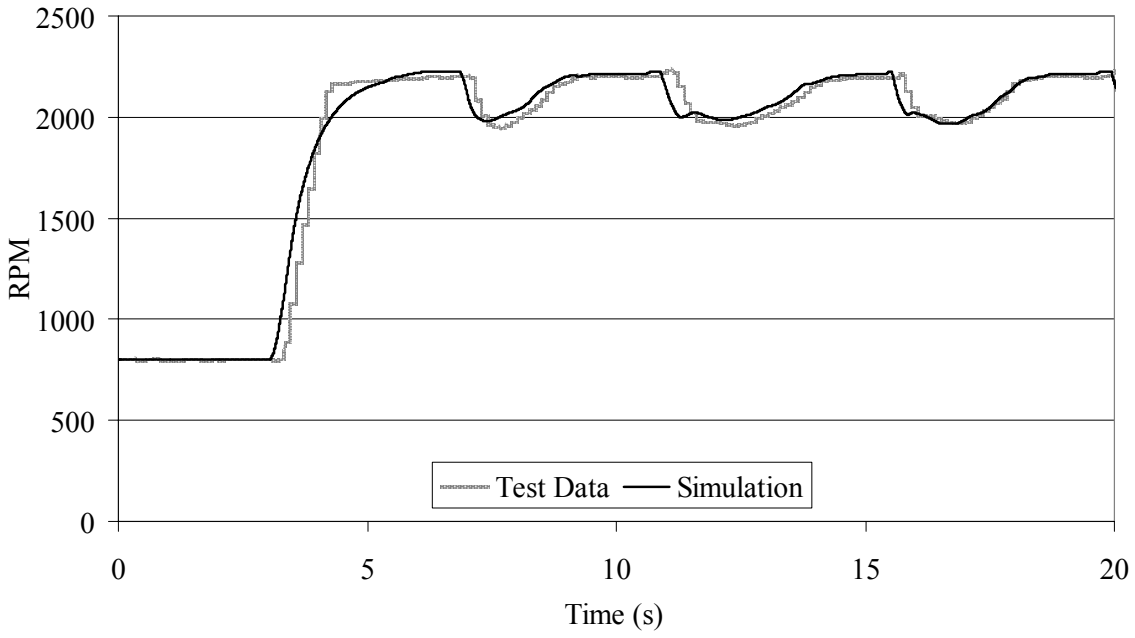

Figure C22. Engine RPM for Reversal Run 2

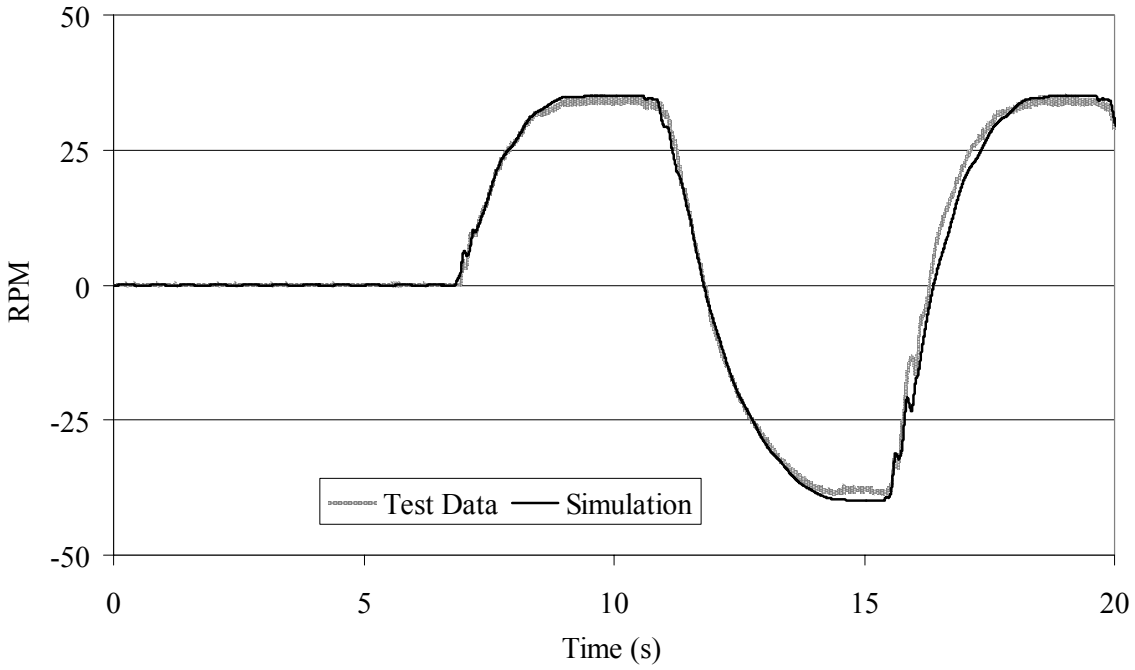

Figure C23. Front Right Wheel RPM for Reversal Run 2

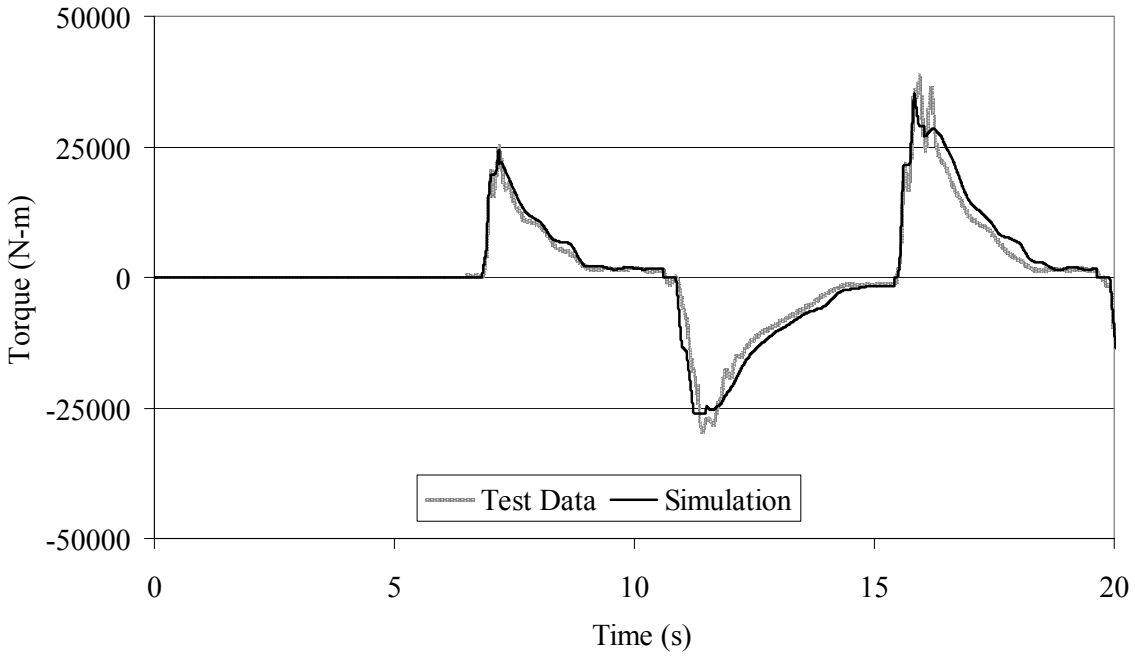

Figure C24. Total Axle Torque for Reversal Run 2

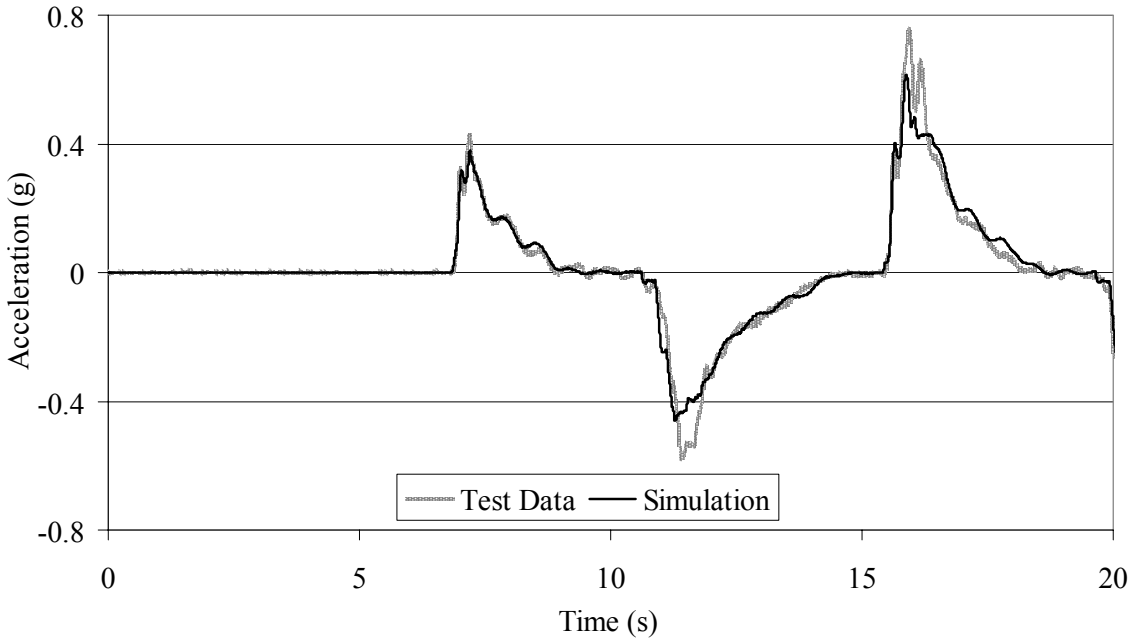

Figure C25. Fore/Aft Acceleration for Reversal Run 2

REFERENCES

1. *NADS Downloadable Images.* http://www.nads-sc.uiowa.edu/media/cg_renderings/interior/malibu_bay_01q4.jpg (accessed March 3, 2006).

2. Ferguson, C.R.; Kirkpatrick, A.T. Internal Combustion Engines, 2nd ed.; John Wiley & Sons, Inc.: New York, 2001.

3. Assanis, D.; Bryzik, W.; Chalhoub, N.; Filipi, Z.; Henein, N.; Jung, D.; Liu, X.; Louca, L.; Moskwa, J.; Munns, S.; Overholt, J. Papalambros, P.; Riley, S.; Rubin, Z.; Sendur, P.; Stein, J.; Zhang, G. "Integration and Use of Diesel Engine, Driveline and Vehicle Dynamics Models for Heavy Duty Truck Simulation", *SAE Technical Paper Series*, 1999-01-0970, 1999.

4. German, H.C. "Real-Time Vehicle Subsystem Modeling and Simulation", M.S. Thesis, The University of Iowa, 2000.

5. Jamzadeh, F.; Hsieh, T.; Struthers, K. "Dynamic Simulation Modeling For Heavy Duty Automatic Transmission Control Development", *SAE Technical Paper Series*, 92241, 1992.

6. Ciesla, C.R.; Jennings, M.J. "A Modular Approach to Powertrain Modeling and Shift Quality Analysis", *SAE Technical Paper Series*, 950419, 1995.

7. Tsangarides, M.C.; Tobler, W.E. "Dynamic Behavior of a Torque Converter with Cetrifugal Bypass Clutch", Design Practices: Passenger Car Automatic Transmissions, 3rd ed.; SAE Transmission/Axle/Driveline Forum Committee, Comp.; Society of Automotive Engineers, Inc.: Warrendale, PA, 1994; pp 137-152.

8. Center of Computer-Aided Design Researchers; Moskwa, J.; Bernard, J. NADS Vehicle Dynamics Software: Powertrain Subsystem Software Specification, NADSdyna Release 4.0.; Center of Computer-Aided Design, The University of Iowa, 1995.

9. Qualman, J.W.; Egbert, E.L. "Fluid Couplings", Design Practices: Passenger Car Automatic Transmissions, 3rd ed.; SAE Transmission/Axle/Driveline Forum Committee, Comp.; Society of Automotive Engineers, Inc.: Warrendale, PA, 1994; pp 38.

10. Dong, Y.; Korivi, V.; Attibele, P.; Yuan, Y. "Torque Converter CFD Engineering Part I: Torque Ratio and K Factor Improvement Through Stator Modifications", *SAE Technical Paper Series*, 2002-01-0883, 2002.

11. Upton, E.W. "Application of Hydrodynamic Drive Units to Passenger Car Automatic Transmissions", Design Practices: Passenger Car Automatic Transmissions, 3rd ed.; SAE Transmission/Axle/Driveline Forum Committee, Comp.; Society of Automotive Engineers, Inc.: Warrendale, PA, 1994; pp 60.

12. Jandasek, V.J. "Design of Single-Stage Three-Element Torque Converter", Design Practices: Passenger Car Automatic Transmissions, 3rd ed.; SAE Transmission/Axle/Driveline Forum Committee, Comp.; Society of Automotive Engineers, Inc.: Warrendale, PA, 1994; pp 81.

13. Hrovat, D.; Tobler, W.E. "Bond Graph Modeling and Computer Simulation of Automotive Torque Converters", *Journal of the Franklin Institute*, Pergamon Press Ltd., 0016-0032, 1985; pp 93-114.

14. Pan, C.; Moskwa, J. "Dynamic Modeling and Simulation of the Ford AOD Automobile Transmission", *SAE Technical Paper Series*, 950899, 1995.

15. Ishihara, T.; Emori, R.I. "Torque Converter as a Vibration Damper and Its Transient Characteristics", Society of Automotive Engineers Mid-Year Meeting, Detroit, Michigan, June, 1966; 660368, pp. 501-512.

16. Shindo, Y.; Ito, H.; Ishihara, T. "A fundamental Consideration on Shift Mechanism of Automatic Transmission", *SAE Technical Paper Series*, 790043, 1979.

17. Tugcu, A.K.; Hebbale, K.V.; Alexandridis, A.A.; Karmel, A.M. "Modeling and Simulation of the Powertrain Dynamics of Vehicles Equipped with Automatic Transmission", Proceedings of ASME Symposium on Simulation of Ground Vehicles and Transportation Systems, ASME Winter Annual Meeting, Anaheim, CA, 1984.

18. Goering, C.E.; Stone, M.L.; Smith, D.W.; Tumquist, P.K. Off-Road Vehicle Engineering Principles, American Society of Agricultural Engineers, St. Joseph, MI, 2003; pp 320.

19. Parts Manual: 980G Series II Wheel Loader, Shin Caterpillar Mitsubishi Ltd., Printed in Japan, 2003.; XEBP7540.

20. Munns, S., "Computer Simulation of Powertrain Components with Methodologies for Generalized System Modeling", M.S. Thesis, The University of Wisconsin-Madison, 1996.

21. Benford, H.L.; Leising, M.B. "The Lever Analogy: A New Tool in Transmission Analysis", SAE, 810102, 1981.

22. Koch, L.G. "Power Train-Vehicle Modeling to Simulate Shifting Transients of Off-Highway Vehicles", SAE, 720044, 1972.

23. Yang, Y.; Lam, R.C.; Fujii, T. "Prediction of Torque Response During The Engagement of Wet Friction Clutch", *SAE Technical Paper Series*, 981097, 1998.

24. Berger, E.J.; Sadeghi, F.; Krousgrill, C.M. "Finite Element Modeling of Engagement of Rough and Grooved Wet Clutches", *ASME Journal of Tribology*, 118, January, 1996; pp 137-146.

25. Berger, E.J.; Sadeghi, F.; Krousgrill, C.M. "Analytical and Numerical Modeling of Engagement of Rough, Permeable, Grooved Wet Clutches", *ASME Journal of Tribology*, 119, January, 1997; pp 143-148.

26. Patir, N.; Cheng, H.S. "An Average Flow Model for Determining Effects of Three-Dimensional Roughness on Partial Hydrodynamic Lubrication", *ASME Journal of Tribology*, 100, January, 1978; pp 12-17.

27. Patir, N.; Cheng, H.S. "Application of Average Flow Model to Lubrication Between Rough Sliding Surfaces", *ASME Journal of Tribology*, 101, April, 1979; pp 220-230.

28. Beavers, G.S.; Joseph, D.D. "Boundary Conditions at a Naturally Permeable Wall", Journal of Fluid Mechanics, 30, 1967; pp 197-207.

29. Davis, C.L.; Sadeghi, F.; Krousgrill, C.M. *A Simplified Approach to Modeling Thermal Effects in Wet Clutch Engagement: Analytical and Experimental Comparison*, *ASME Journal of Tribology*, 122, January, 2000; pp 110-118.

30. Personal Communication with Viabhav Shah, engineer in Power System Analysis, Technology and Solutions Division, Caterpillar Inc. on 8/9/2005.

31. Personal communication with transmission repair technician 7/2005.

32. Caterpillar, Inc. "980G Series II Wheel Loader", AEHQ5462 (12-01), Caterpillar, U.S.A., 2001.

33. Shabana, A.A. Computational Dynamics, 2nd ed.; John Wiley & Sons, Inc.: New York, 2001.